

In-situ spectroscopic and electrochemical studies related to liquid-phase heterogeneous catalysis

Citation for published version (APA):

Gootzen, J. F. E. (1997). *In-situ spectroscopic and electrochemical studies related to liquid-phase heterogeneous catalysis*. [Phd Thesis 1 (Research TU/e / Graduation TU/e), Chemical Engineering and Chemistry]. Technische Universiteit Eindhoven. <https://doi.org/10.6100/IR498164>

DOI:

[10.6100/IR498164](https://doi.org/10.6100/IR498164)

Document status and date:

Published: 01/01/1997

Document Version:

Publisher's PDF, also known as Version of Record (includes final page, issue and volume numbers)

Please check the document version of this publication:

- A submitted manuscript is the version of the article upon submission and before peer-review. There can be important differences between the submitted version and the official published version of record. People interested in the research are advised to contact the author for the final version of the publication, or visit the DOI to the publisher's website.
- The final author version and the galley proof are versions of the publication after peer review.
- The final published version features the final layout of the paper including the volume, issue and page numbers.

[Link to publication](#)

General rights

Copyright and moral rights for the publications made accessible in the public portal are retained by the authors and/or other copyright owners and it is a condition of accessing publications that users recognise and abide by the legal requirements associated with these rights.

- Users may download and print one copy of any publication from the public portal for the purpose of private study or research.
- You may not further distribute the material or use it for any profit-making activity or commercial gain
- You may freely distribute the URL identifying the publication in the public portal.

If the publication is distributed under the terms of Article 25fa of the Dutch Copyright Act, indicated by the "Taverne" license above, please follow below link for the End User Agreement:

www.tue.nl/taverne

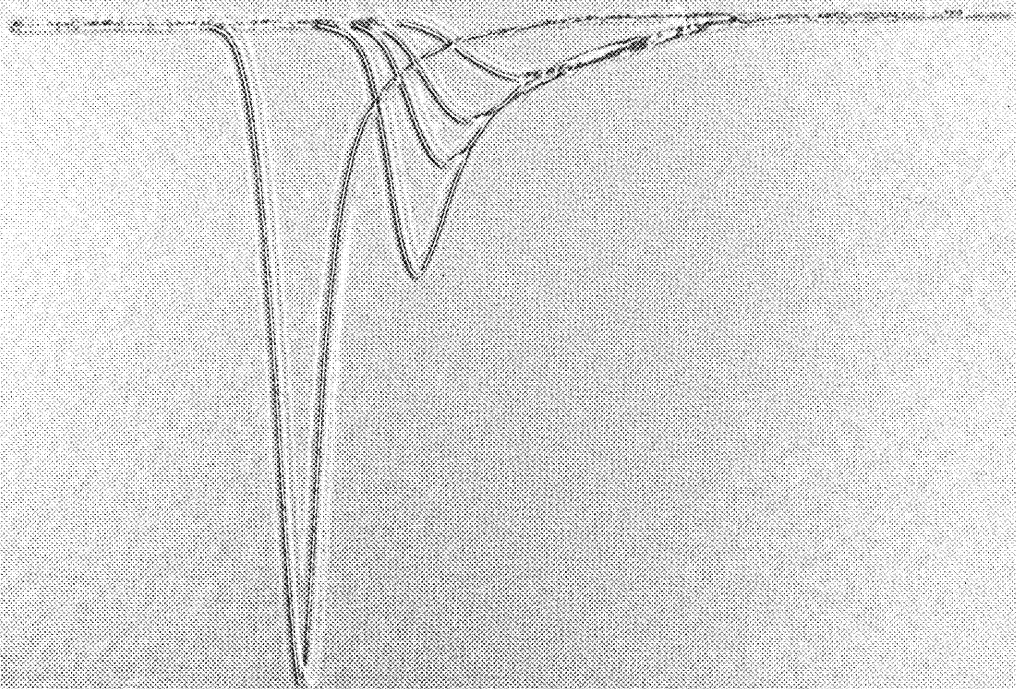
Take down policy

If you believe that this document breaches copyright please contact us at:

openaccess@tue.nl

providing details and we will investigate your claim.

In-situ spectroscopic and electrochemical studies related to liquid phase heterogeneous catalysis



J.F.E. Gootzen

In-situ spectroscopic and electrochemical studies
related to
liquid-phase heterogeneous catalysis

Proefschrift

ter verkrijging van de graad van doctor aan de
Technische Universiteit Eindhoven, op gezag van de
Rector Magnificus, prof.dr. M. Rem, voor een
commissie aangewezen door het College voor
Promoties in het openbaar te verdedigen
op donderdag 27 november 1997 om 16.00 uur

door

J.F.E. Gootzen

geboren te Maasbracht

Dit proefschrift is goedgekeurd door de promotoren:

prof. dr. J.A.R. van Veen

en

prof. dr. R.A. van Santen

Copromotor:

dr. W.H.M. Visscher

printed at the Universiteitsdrukkerij, Eindhoven University of Technology

CIP DATA TECHNISCHE UNIVERSITEIT EINDHOVEN

Gootzen, J.F.E.

In-situ spectroscopic and electrochemical studies related to liquid phase heterogeneous catalysis / J.F.E. Gootzen. - Eindhoven : Technische Universiteit Eindhoven, 1997.

Proefschrift. -

ISBN 90-386--0838-1

NUGI 813

Trefw.: heterogene katalyse / elektrochemie / oppervlakte-onderzoek ; infraroodspectroscopie

Subject headings: catalysis / electrochemical analysis / surface reaction / reflection IR spectroscopy

The work described in this thesis was carried out at the Schuit Institute of Catalysis, Laboratory of Inorganic Chemistry and Catalysis, Eindhoven University of Technology. Financial support has been supplied by SON/STW under the auspices of the Netherlands Organization for Scientific Research (NWO).

Contents:

Chapter 1	Introduction	1
Chapter 2	Experimental Methods	7
Chapter 3	The characterization of ethanol and 1,2-ethanediol adsorbates on platinized platinum with FTIRS and DEMS	17
Chapter 4	The adsorption of C3 alcohols, 1-butanol and ethene on platinized platinum as studied with FTIRS and DEMS	33
Chapter 5	On the adsorbates formed during the platinum catalyzed (electro)oxidation of ethanol, 1,2-ethanediol and methyl- α -D-glucopyranoside at high pH.	55
Chapter 6	The study of NO adsorbate layers on platinized platinum in the liquid phase with cyclic voltammetry, DEMS and FTIRS.	81
Chapter 7	The electrocatalytic reduction of NO_3^- on Pt, Pd and Pt-Pd electrodes activated with germanium.	97
Chapter 8	A DEMS and cyclic voltammetry study of NH_3 oxidation on platinized platinum	121
Summary		139
Samenvatting		142
List of publications		145
Dankwoord		146
Curriculum Vitae		147

Chapter 1

Introduction

1.1 Catalysis

Catalysis is highly relevant to chemical industry as the majority of chemical products is nowadays produced with the aid of catalysts. There are several reasons that explain the importance of catalysis. First of all, the rate of a chemical reaction is greatly enhanced in the presence of a catalyst making reactions possible that would otherwise be far too slow. Catalysis also contributes to environment-friendly production methods as waste production is considerably lower for catalyzed reactions than for non-catalyzed stoichiometric reactions.

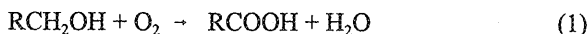
In heterogeneous catalysis the catalyst and the reactants are present in a different phase; whereas the catalyst is typically a solid, the reactants are present in the gas or liquid phase. The catalyzed reactions, which consist of the breaking and formation of chemical bonds, occur at the surface of the catalyst, which is reactive because the surface atoms are coordinatively unsaturated which implies that they have less neighbouring atoms than atoms in the bulk of the material. The specific role of the catalyst in terms of energy is to lower the activation energies of the dissociative and associative reactions by the formation of a stabilizing bond between the reacting fragments and the catalyst surface.

The recent progress in the study of heterogeneous catalysis has relied on spectroscopic techniques that can provide in-situ or ex-situ information of the events that occur on the catalyst surface. In fundamental catalysis research the focus has been on the solid/gas interface because a wide variety of characterization techniques is available. Most of the powerful techniques that have been developed at the the solid/gas interface need vacuum conditions, like X-ray Photoelectron Spectroscopy (XPS), Thermal Desorption Spectrometry (TDS) and Electron Energy Loss Spectroscopy (EELS), and it is questioned whether these low pressure results can be translated to realistic high pressure conditions. In contrast to the solid/gas interface, only very few spectroscopic techniques are available to study the solid/liquid interface. The vacuum techniques can now only be used ex-situ, requiring transfer of the catalyst after use to a vacuum chamber. However, the gap between UHV and liquid phase is very large and the question arises whether the structure of the metal/liquid interface is perturbed or not, either by transfer to UHV

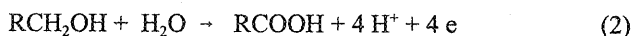
or by contamination during transfer. Therefore, it would be preferable to have spectroscopic methods available to study the catalytic surface in the liquid phase in-situ.

1.2 An electrochemical approach to liquid phase heterogeneous catalysis

An electrochemical approach to liquid phase heterogeneous catalysis offers interesting possibilities to obtain more insight into the nature of the reactions involved. Catalytic liquid phase oxidations or hydrogenations can be carried out electrochemically by application of a potential difference between the electrode and the solution. The advantage of this approach is that hydrogen and oxygen, which both have a low solubility, can be omitted as a reactant. Problems in kinetic studies that relate to mass transfer of these gases are avoided in this way. For instance, the catalytic oxidation of alcohols with molecular oxygen on platinum, according to:



can also be performed electrochemically, without using molecular oxygen but by applying an electrochemical potential on the platinum electrode, at which the reaction takes place:



By using an electrochemical approach it becomes possible to use in situ surface spectroscopy in the liquid phase. Recently developed combined in-situ electrochemical and spectroscopic techniques can help to generate a molecular picture of electrocatalytic reactions. This thesis describes the use of two of such techniques that were developed during the last two decades and which consist of combinations of electrochemical tools and respectively reflection-absorption Fourier Transform IR spectroscopy and mass spectrometry.

The IR technique makes use of a thin layer cell which enables the collection of spectra from the electrode surface while this is in contact with the solution phase. An additional feature of the thin layer cell is that reactants or products in the liquid phase near the electrode can also be detected. The effect of the electrode potential can easily be studied. The mass spectrometry technique enables the detection of volatile products that are formed at the electrode while this is present in the liquid phase. It stands to reason that these two techniques have had an important impact on the field of electrocatalysis as well as on more fundamental aspects of electrochemistry like the adsorption of electrolyte anions and understanding of the nature of the double layer. Whereas earlier, chemical information could only be obtained in a rather indirect way from current-potential relations, now in-situ spectroscopic information is available that provides identification of the products of a particular electrochemical reaction and that can clarify the structure of the

adsorbates on the catalytic surface in action.

In addition to these modern combinations of spectroscopic and electrochemical techniques also pure electrochemical techniques like cyclic voltammetry and coulometry can still be used to generate useful information.

For this thesis it has been preferred to study pure metal electrodes rather than carbon supported electrodes. Firstly, the reflection FTIRS technique is restricted to pure metal electrodes because of the need of a IR reflective surface. Secondly, this thesis aims to perform a quantitative analysis of the electrocatalytic reactions of interest. Therefore unsupported electrodes are favoured because the determination of charges in cyclic voltammetric and DEMS experiments can be performed with higher accuracy. To ensure this, rough electrodes are used that possess a high surface area. Finally, the preparation of surface-alloy electrodes is more convenient on unsupported electrodes.

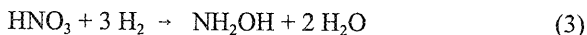
At first sight electrochemistry and catalysis seem two completely different research disciplines. Whereas catalysis is related with adsorption, desorption, associative and dissociative reactions on a surface, electrochemistry is mainly associated with redox reactions that are based on electron transfer across the surface. However, in the field of electrocatalysis the two disciplines meet, combining the characteristics given above and this thesis shows that in the liquid phase they can be strongly related. According to Trasatti and Parsons [1] a liquid phase heterogeneous catalytic system where a charged interphase is formed between the solid and liquid should also be considered as an electrochemical system. This implies that heterogeneous liquid phase catalysis cannot be dealt with without considering electrochemical parameters. In spite of this the links between electrochemistry and liquid phase heterogeneous catalysis are not pronounced in the literature. They can roughly be divided into two groups [2]; (i) studies concerning the similarity or sometimes even the equivalence of liquid phase heterogeneous catalysis and electrocatalysis and (ii) studies that use electrochemical tools for characterization and modification of the catalysts or to study elementary adsorption steps.

Several electrocatalytic reactions are described in this thesis; (i) the electrocatalytic oxidation of alcohols, (ii) the reduction of nitrate and related to that the redox behaviour of NO adlayers and (iii) the oxidation of ammonia.

The platinum catalyzed oxidation of alcohols with molecular oxygen might be an attractive route for the production of intermediates for the pharmaceutical and food industry [3]. Typical substances that have been studied are for example D-glucose, methyl- α -D-glucopyranoside, L-sorbose and cinnamyl alcohol. These oxidations can be performed at mild conditions, typically between 20 and 90^o C at atmospheric pressure and mild pH. Still a major problem of the catalytic alcohol oxidation is the deactivation of the catalyst, for which several causes have been proposed in the literature; (i) particle growth, (ii) oxidation/corrosion of the active metal and (iii) deposition of carbonaceous residue. Different views can be encountered in the literature on the preferred process conditions, either the oxygen diffusion limited regime is preferred or the kinetic

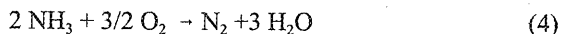
regime in the absence of mass transfer limitations.

The catalytic hydrogenation of concentrated nitrate solutions with hydrogen gas is industrially performed in fosforic acid on carbon supported platinum-palladium catalysts activated with germanium [4,5].



The desired product hydroxylamine (NH_2OH) is used as an intermediate in the production of caprolactam, which is an intermediate in the formation of nylon-6. The selectivity for NH_2OH is about 80%, the side products being NH_4^+ , N_2O and N_2 . Until now no electrochemical investigations of the nitrate reduction have been carried out on this or any other alloy system. Some work has been done on non-activated platinum, palladium and rhodium electrodes, although no information of reaction products is available. The low reaction rates found in these cases convincingly demonstrates the necessity of an activator on platinum and palladium to enhance the rate for nitrate reduction.

The platinum catalyzed oxidation of ammonia with oxygen to gaseous nitrogen is of current industrial interest.



The recent interest in environmental issues has increased the effort in end-of-pipe treatments such as the cleaning of nitrate, nitrite and ammonia containing waste water. Of course N_2 is the desired product in all these reactions and a catalytic instead of electrochemical treatment would be favoured [6]. Nevertheless, as argued above, electrochemical studies can generate useful information. Whereas for the reduction of nitrate and nitrite at neutral pH palladium-copper catalysts have been shown to be the most suitable system to obtain a high N_2 selectivity, still no effective catalyst is available for the oxidation of ammonia. In the 1960's several studies have been carried out concerning the ammonia oxidation on platinum in relation to the development of fuel cells. However after that period, only minor attention has been given to this reaction, leaving the development of new alloy catalysts almost completely unexplored.

1.3 Outline of this thesis

Chapter 2 describes the experimental techniques that will be used throughout the following chapters. Chapters 3 and 4 discuss the composition of the irreversible adsorbates that are formed from small alcohol molecules on platinumized platinum at low pH. The kinetics of the adsorption of primary alcohols has been studied earlier by de Bruijn [7]. Not only primary, but also

secondary alcohols and polyols have been included in the study. High surface area electrodes were used to ensure high quality data and the combination of Fourier Transform IR Spectroscopy (FTIRS), Differential Electrochemical Mass Spectrometry (DEMS) and adsorption and oxidation charge data obtained with coulometry and cyclic voltammetry has led to conclusive results on the composition of the alcohol adsorbates on platinized platinum.

Chapter 5 deals with the composition of the irreversible adsorbates of both small primary alcohols and methyl- α -D-glucopyranoside at high pH. Moreover, this chapter discusses experimental evidence for (i) the equivalence of electrochemical and catalytic alcohol oxidation, (ii) the composition of the catalytic surface in action and (iii) the causes for catalyst deactivation. Concerning (ii) and (iii) a subdivision is made into the oxygen diffusion limited regime and the kinetic regime.

Chapter 6 deals with the composition of NO adlayers, which is closely related with the question of the mechanism of N_2O formation. The findings contrast with the classic picture of N_2O formation in which adsorbed NOH intermediates play an important role.

Chapter 7 discusses the effect of the catalyst surface composition of platinum / palladium surface alloys activated with germanium on the activity and the selectivity of the electrocatalytic reduction of nitrate. Special attention is given to the mechanism of the reaction.

Chapter 8 discusses the electrocatalytic oxidation of ammonia to gaseous nitrogen. This chapter is concerned with (i) the surface composition of the catalyst in action, (ii) the mechanism of N_2 formation and (iii) the deactivation of the catalyst.

- [1] S. Trasatti, R. Parsons, *Pure Appl. Chem*, 58, 437, 1986.
- [2] G. Horányi, *Catal. Today* 19, 285, 1994.
- [3] T. Mallat, A. Baiker, *Catal. Today* 19, 247, 1994.
- [4] C.G.M. van de Moesdijk, *PhD Thesis* Eindhoven University of Technology 1978.
- [5] C.G.M. van de Moesdijk in J.R. Kosak (ed), *Catalysis of Organic Reactions in Chemical Industries*, Marcel Dekker, New York, 18, 379, 1984.
- [6] L. Marinčić, F.B. Leitz, *J. Appl. Electrochem.* 8, 333, 1978.
- [7] F.A. de Bruijn, *PhD Thesis* Eindhoven University of Technology 1996.

Experimental Methods

2.1 Cyclic Voltammetry

Cyclic voltammetry is among the most popular electrochemical techniques and it can be used to study the redox behaviour of compounds that remain in the liquid phase, but also to characterize the surface of the electrode or the redox behaviour of irreversibly adsorbed species. The fundamentals of cyclic voltammetry have been well documented for redox reactions without adsorption [1,2]. However, for electrocatalytic reactions, which involve strongly adsorbed species, no strong theoretical basis exists. A short description of the technique will be given here. Electrochemical measurements are performed with a three electrode configuration; (i) a working electrode, which is the electrode of interest, (ii) a counter electrode and (iii) a reference electrode, which possesses a constant potential. In acid electrolytes the Hg/Hg₂SO₄ (MSE) reference electrode was used whereas in basic electrolyte the Hg/HgO electrode was used. All potentials will be given with respect to the Reversible Hydrogen Electrode (RHE). To generate a cyclic voltammogram the potential of the working electrode is varied periodically with respect to the reference electrode by a potentiostat, as shown in Figure 1, and the current response is recorded. A cyclic voltammogram of a noble metal like platinum or palladium in aqueous acid or alkali

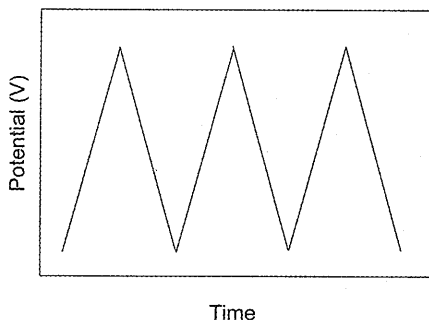


Figure 1: Potential program used for cyclic voltammetry.

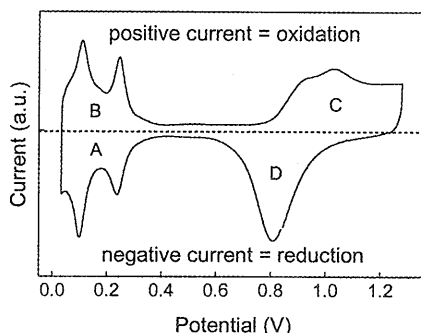


Fig2. : Cyclic voltammogram of platinumized platinum in 0.5 M H₂SO₄ electrolyte. Scan rate 2 mV/s. For the explanation of symbol A, B, C and D see text.

electrolyte possesses several pronounced features, which we will discuss here. The potential window that can be accessed is limited by the decomposition of water into hydrogen at 0 V and oxygen at 1.5 V vs RHE. Figure 2 shows a cyclic voltammogram for platinum in 0.5 M H_2SO_4 . In region A two reduction peaks are present, indicated by convention by a negative current, which both originate from the reduction of a proton to form adsorbed hydrogen. The different positions of the two reduction peaks at 0.1 and 0.23 V reflect the different adsorption energies for hydrogen, which are correlated with the surface structure. Studies on single crystal electrodes have shown that the position of the hydrogen peaks depend strongly on the structure of the surface. Region B concerns the opposite reactions of region A: the oxidation of adsorbed hydrogen to protons. In the potential region between B and C, which is called the double layer region, only a small current is observed that originates from charging of the surface. In region C water is oxidized and as a result platinum-oxides are formed, a process which is believed to result at lower potentials in PtOH adspecies and for higher potentials in successively PtO and PtO_2 . Region D corresponds to the reduction of the platinumoxide species to water.

The charges involved in the formation of adsorbed hydrogen or oxygen can be used to determine the area of a particular electrode. This is important in order to be able to compare the performance of different electrodes. In the case of platinum, the charge involved in the oxidation of a monolayer of hydrogen, Q_H , is used, assuming the stoichiometry Pt : H = 1 and $Q_H = 215 \mu C/cm^2$ [3] for polycrystalline platinum. This charge density corresponds with an atom density for surface platinum of 2.23 nmol/cm². For palladium this procedure is not possible because the adsorption/desorption peaks for adsorbed hydrogen coincide with those for the dissolution of hydrogen in the bulk of palladium. Alternatively, the surface area can be determined from the charge involved in the oxide reduction peak, taking a Pd:O ratio of 1 : 0.8 for the end potential of 1.4 V in the cyclic voltammogram, or by oxidation of a CO covered surface, assuming a ratio of Pd:CO of 1 : 0.65 in analogy with UHV measurements [4].

From a perspective of catalysis it is plausible to expect oxidations or hydrogenations to occur in

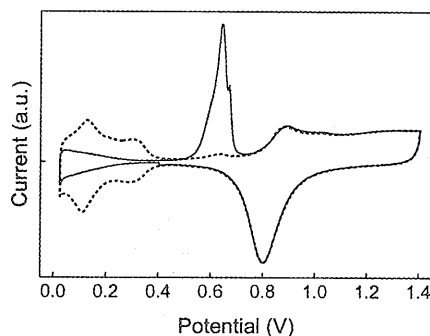


Fig. 3: Cyclic Voltammogram of adsorbed CO on platinumized platinum in 0.5 M $HClO_4$. Scan rate 5 mV/s. First cycle (—) and second cycle (---).

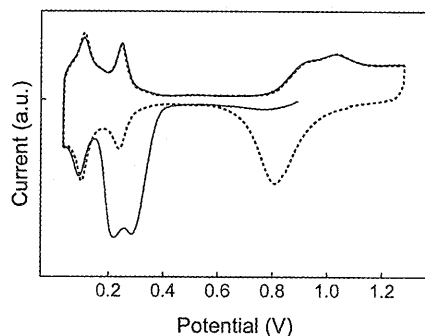


Fig. 4: Cyclic Voltammogram of adsorbed NO on platinumized platinum in 0.5 M H_2SO_4 . Scan rate 2 mV/s. First cycle (—) and second cycle (---).

the potential region where oxygen and hydrogen adspecies respectively are formed. However, unfortunately this is not so simple. Figure 3 and 4 show cyclic voltammograms for the oxidation and reduction respectively of monolayers CO and NO on a platinum electrode. CO was adsorbed while the potential was kept at 0.4 V. After that the scan was started in the negative potential direction, indicated by the full line. The hydrogen adsorption/desorption peaks below 0.4 V are fully blocked by adsorbed CO, with respect to the second cycle indicated by the dashed line. It is clear that the oxidation of CO at 0.6 V occurs in a potential region where formation of platinum-oxides, which starts at 0.8 V, has not yet started. Figure 4 shows the cyclic voltammogram recorded after adsorption of dissolved NO at equilibrium potential. After adsorption the scan is started in the negative potential direction, indicated by the full line. The reduction of NO starts at 0.4 V, whereas formation of adsorbed hydrogen starts at 0.3 V.

It is well known for the oxidation of alcohols like methanol and ethanol that the maximum current density is observed at a potential where oxide formation starts, indicating that oxides block the surface instead of taking part in the reaction. These observations certainly raise questions concerning the mechanism of these reactions. It has been suggested by some that these oxidations occur by reaction with an adsorbed water molecule instead of the initial formation of an O or OH adspecies, which are involved in reaction. For reductions it is also questionable whether reaction occurs with an adsorbed hydrogen atom or with a proton from the solution. From this, one can conclude that it is not so much the presence of adsorbed oxides or hydrogen species, but the electrode potential that is the key factor in driving the various reactions.

2.2 Reflection Fourier Transform IR Spectroscopy (FTIRS)

2.2.1 Theoretical considerations

Infrared spectroscopy is a very common tool for chemists. The technique provides information on the vibrational properties of molecules and is based on the interaction between infrared radiation and the dipole active vibration modes of molecules. Chemical information can be obtained from the wavelengths at which these infrared absorptions occur. The technique that is used in this thesis, reflection infrared spectroscopy, is a variant of the common technique that enables the detection of infrared active species adsorbed on a reflective metal surface. It was originally developed for application in the gas phase and vacuum, but has recently been adapted by Bewick and coworkers [4,5] for the use in the liquid phase by combination with electrochemical tools. In this section we will give a summary of the theoretical backgrounds of the technique and we will discuss the design of the experimental setup.

The fundamental characteristics of reflection of infrared radiation on a reflective metallic surface has certain implications for the technique [6,7]; (i) only vibrations with a dipole moment perpendicular to the surface can be detected, (ii) the incident infrared beam should be reflected

at the surface at near grazing incidence and (iii) a single reflection can be used, which simplifies the experimental setup considerably. We will briefly explain these issues here.

To understand why only vibrations perpendicular to the surface can be observed it is necessary to explain the difference in the reflection characteristics of light with different polarisation directions. The electric field of the incident infrared beam can be described by two components, one with the electric field vector in the plane of incidence (p-polarized) and the other with the electric field perpendicular to the plane of incidence (s-polarized). S-polarized light undergoes a phase shift of 180° upon reflection for almost all angles of incidence, which results in destructive interference of the incident and reflected rays at the surface. It is for this reason that s-polarized IR radiation is unsuited to detect vibrations of adsorbed species. However, IR active molecules that reside further away from the surface in the liquid can be detected. With respect to the reflecting surface the p-polarized light can be divided in parallel and perpendicular components. The parallel component also undergoes a phase shift of 180° resulting in destructive interference whereas the perpendicular component of the p-polarized radiation does not suffer a phase shift of 180° and the incident and reflective beam interfere constructively. It follows from this argumentation that the IR beam can only have interaction with molecules that have a dipole active vibration perpendicular to the surface, since there is no electric field parallel to the surface due to destructive interference. This phenomenon is indicated in the literature as the surface selection rule.

The phenomena described above also explain why a high angle of incidence is necessary in reflection absorption infrared spectroscopy, since the component of the electric field that is perpendicular to the surface increases with increasing angle of incidence. In addition to this, the metal surface area that is irradiated by the IR beam increases for increasing angle of incidence implying that the number of molecules over which the field is exerted also increases. In practice, angles between 80 and 85° are used in the gas phase and between 60 and 70° in the liquid phase. In IR spectroscopy the intensity of an absorption is expressed as the reflectivity change $\Delta R/R_0$ ($\Delta R=R_0-R_1$), where R_0 and R_1 are the sample and the reference spectrum respectively. For transition metals a single reflection already yields a ΔR that is close to the optimum value [7] and therefore the simpler single reflection mode is used instead of a multiple reflection setup.

2.2.2 Description of the experimental setup

In the early designs of the so-called the Electrochemically Modulated IR Spectroscopy (EMIRS) developed by Bewick and coworkers, a dispersive IR spectrometer was used and the electrochemical cell was placed in the sample room of the infrared spectrometer [4,5]. However, this setup is rather inconvenient and nowadays a Fourier Transform IR spectrometer is used and the electrochemical cell is positioned on top of the sample room so that the nitrogen purge of the sample room remains intact upon operation of the cell. A schematic representation of the experimental setup, that was built in our own laboratory after a design from Iwasita and Vielstich

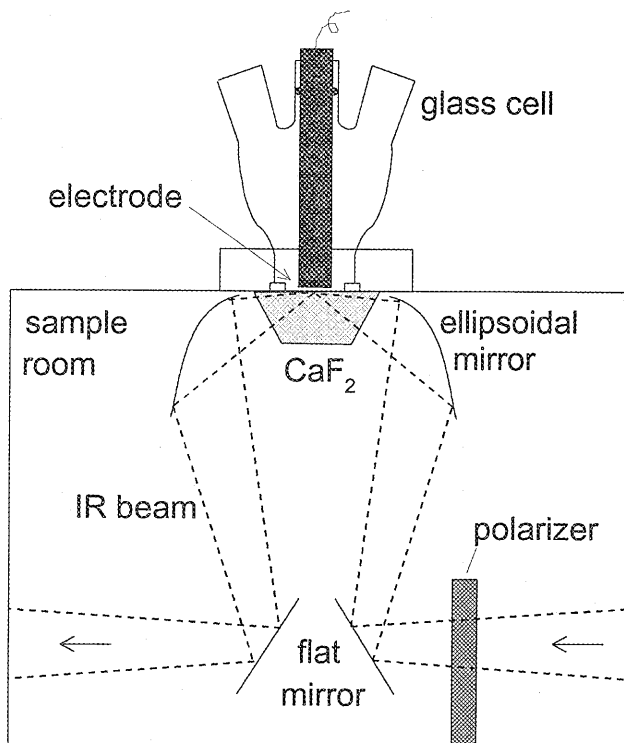


Figure 5: Schematic overview of the experimental setup of the reflection FTIR technique.

[8], is given in Figure 5. We received help from dr. ir. G.M.W. Kroesen of the laboratory of Particle-Physics in the Department of Physical Technology of the Eindhoven University of Technology. In this study a Biorad FTS 40A IR spectrometer, equipped with a liquid nitrogen cooled MCT detector, was used.

The bottom of the cell consists of a CaF_2 prism that is transparent for infrared radiation between 1000 cm^{-1} and 4000 cm^{-1} and is resistant to both acid and alkali electrolytes. The prism is cut at both sides at an angle of 65° and is placed in a holder that rests on the top of the spectrometer's sample room. In the early designs by Bewick no prism was used but a flat CaF_2 disk instead. However, in this construction high angles of incidence cannot be used because the IR radiation will reflect at the gas/ CaF_2 interface. By using the prism, the IR beam comes in perpendicular to the CaF_2 surface, causing no reflection losses. Higher angles of incidence than 70° cannot be used, because reflection of the IR beam at the CaF_2 /water interface will be dominant. We have explained in the previous section that a high angle of incidence increases the effectiveness of the technique.

The electrochemical cell, which is constructed completely of glass, can be screwed in the prism-holder and is sealed by a silicone rubber ring between the prism and the glass cell. The cell is provided with in- and outlet tubes for gases and electrolyte. This construction enables exchange

of the electrolyte while the system is kept under argon. The working electrode consists of a platinum disk connected at the back side to a copper screw. The electrode can be placed in a holder that consists of a metal interior embedded in teflon, which is resistant to both acid and alkali electrolytes.

A polarizer is used to remove the s-polarized component of the IR radiation. As explained in the previous section, the s-polarized component is inactive for the detection of adsorbate vibrations. Without the use of a polarizer, the beam is too intense for the detector, causing its overexcitation. By using the polarizer, the intensity of the reflected beam is reduced such that it fits the sensitivity of the detector.

2.2.4 Measurement procedure

It is important that both the metal and the CaF_2 window are flat and therefore they have to be polished with Al_2O_3 powder regularly. To conduct a measurement, the electrode is pushed against the CaF_2 window in a planparallel way and as a result a thin electrolyte layer of approximately 2-5 μm remains present between the electrode and the CaF_2 window. This layer is thin enough to prevent complete absorption of the IR radiation by the water layer and thick enough for the metal to be a 'real' electrode.

In the case of adsorption studies the electrode was pushed against the CaF_2 window after the adsorption and electrolyte exchange, whereas in other experiments IR measurements were done in the presence of a particular reactant in the solution. After the electrode has been positioned against the window a certain period is necessary for the system to stabilize. Mechanical instabilities in the thin layer lead to large changes in the water absorption that will appear in the spectrum.

To obtain useful IR spectra it is essential to remove the absorption bands of water and the electrolyte-anion such as chlorate and sulfate from the spectrum. This can only be accomplished by the subtraction $R_0 - R_1$ of the two single beam spectra R_0 and R_1 that were recorded successively after a potential excursion. The infrared spectra will be given throughout this thesis as $(R_0 - R_1)/R_0$. In the case of an adsorption study, the first IR spectrum is recorded at the adsorption potential, followed by a potential scan to oxidize or reduce the adsorbate followed by a second IR spectrum. Subtracting both spectra removes the water and electrolyte anion contributions.

The occurrence of an electrochemical current in the thin liquid layer during the IR measurement has some important consequences for the concentration of ions in this layer. For instance, in the oxidation of a monolayer CO a corresponding amount of electrons is transferred to the metal according to:



Simultaneously, two protons are formed per CO_2 molecule. In the case of perchloric acid

electrolyte, the oxidation current between the working and the counter electrode is carried by protons migrating out of the thin layer and chlorate anions migrating into the thin layer. Since the ionic conductivity λ_0 for protons is considerably higher than for chlorate, $\lambda_0(\text{H}^+) = 349.8$ and $\lambda_0(\text{ClO}_4^-) = 68 \text{ cm}^2 \Omega^{-1}$ [9], the current is carried for 84% by protons and for 16% by chlorate anions. The amount of protons that migrates out of the thin layer is somewhat smaller than the amount of protons formed in the CO oxidation and therefore the proton concentration in the thin layer increases and the water concentration decreases. The perchlorate concentration in the thin layer also increases after CO oxidation. For a plain platinum electrode, the proton concentration can be calculated to increase with 2.2 mM for a 3 μm thick liquid layer upon formation of a monolayer platinumoxide in perchloric acid electrolyte. As a result of these concentration changes the IR bands for ClO_4^- , H_3O^+ and H_2O appear in the subtract IR spectrum. Whereas ClO_4^- is characterized by a single band at 1140 cm^{-1} , the IR absorption properties of H_3O^+ are more diverse, in accordance to those of H_2O . Whereas water displays broad bands at 1645 , 2140 and 3180 cm^{-1} , H_3O^+ displays broad bands at 1800 and 2700 cm^{-1} . The argumentation presented above also holds for reduction reactions, the concentration changes in the thin layer being opposite. The appearance of IR bands of H_3O^+ , H_2O and ClO_4^- or HSO_4^- in the spectrum certainly forms a drawback of this technique, especially when one is looking for vibrations in the wave number region corresponding to the species mentioned above. This is for instance the case for the vibration of adsorbed NO molecules on Pt which coincide with those of water and protons. This problem can be circumvented in the case of adsorbed CO and NO by making use of the Stark effect to obtain IR spectra. The Stark effect represents a shift of the CO and NO vibrations as a function of the electrode potential. This is due to a change of the charge that is located in the orbitals of the adsorbate, which results in a change of the C-O or N-O bond strength. For adsorbed CO this shift is known to be approximately $30 \text{ cm}^{-1}/\text{V}$. As a result in the subtract spectrum R_0 - R_1 a bipolar adsorbate vibration arises. When the potentials E_0 and E_1 are chosen in the double layer region hardly any current flows in going from E_0 to E_1 and the appearance of H_3O^+ , H_2O and ClO_4^- or HSO_4^- vibrations in the subtract spectrum are avoided.

2.3 Differential Electrochemical Mass Spectrometry (DEMS)

The DEMS technique is a combination of cyclic voltammetry and mass spectrometry; it enables the simultaneous monitoring of the electrochemical current and the mass response while scanning the potential. Only gaseous or volatile compounds can be detected. The technique was originally developed by Bruckenstein and Gadde [10] and was further improved by Heitbaum et al [11,12]. The equipment was built in our own laboratory [13] and a schematic representation of the experimental setup is given in Figure 6.

Of crucial importance is the barrier between the liquid phase and the vacuum chamber. The

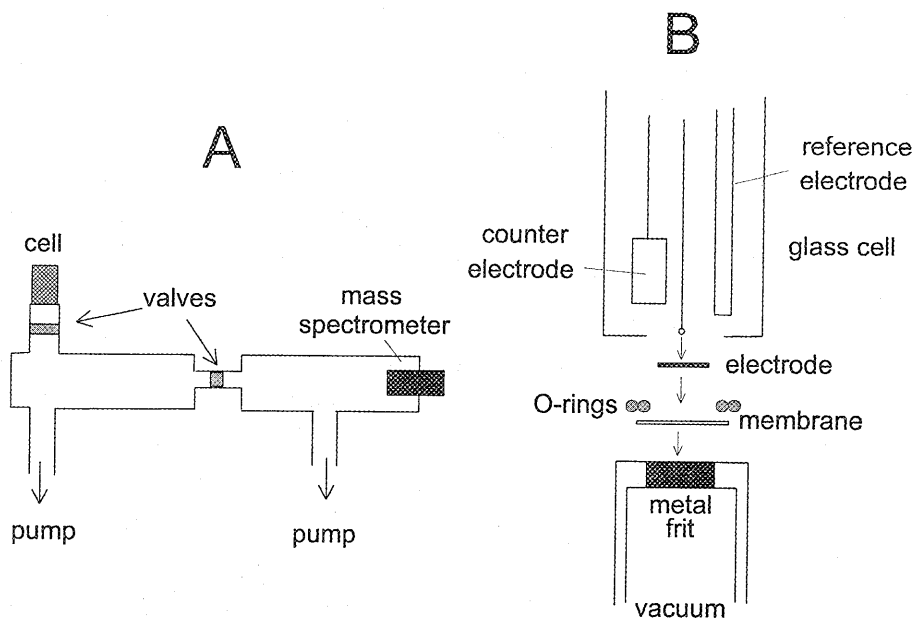


Figure 6: Schematic overview of the experimental setup for Differential Electrochemical Mass Spectrometry (DEMS); vacuum system(A) and electrochemical cell (B).

bottom of the electrochemical cell is formed by a 3 mm thick stainless steel metal grid (pore size 40 μm) on top of which a thin teflon membrane (Schleicher and Schüll, pore size 0.02 μm) is placed. The bottom of the cell is sealed by two viton rings that are placed between the glass cell and the metal grid. The working electrode is flat platinized platinum gauze that lies directly on top of the teflon membrane and is contacted with a gold wire. The working electrode is contacted with a polymer coated gold wire.

By this construction gaseous products formed at the working electrode can reach the Leybold Quadruvac PGA 100 mass spectrometer by passing the teflon membrane of which the pore size is small enough to prevent the liquid to reach the vacuum. Nevertheless, a considerable water pressure of approximately 10^{-5} mbar can build up in the inlet chamber, which is too high for the mass spectrometer to operate. Therefore, the system is differentially pumped by 2 Leybold turbomolecular pumps to prevent the pressure in the ionization chamber to become too high. In this setup, the ionization chamber is connected to the inlet chamber via a small tube that can be opened by a pneumatic valve. The pressure in the ionization chamber can be adjusted by the tunable valve between the turbomolecular pump and inlet chamber. Usually the valve is adjusted such that the pressure is $5 \cdot 10^{-6}$ mbar in the ionization chamber.

The gases that are formed at the electrode surface have to diffuse through the liquid before the vacuum can be entered. This results in a typical time delay of 2-5 seconds with which the mass spectrometer detects those gases. By using a gauze as working electrode the mass response is influenced by tailing, due to the presence of a concentration gradient toward the bulk solution. The electrochemical cell, which is entirely constructed of glass, contains inlet tubes for removal and admission of gases and electrolyte, such that exchange of electrolyte can be carried out while keeping the system under argon atmosphere.

References:

- [1] A.J. Bard, L.J. Faulkner, *Electrochemical Methods*, John Wiley and Sons, New York, 1980.
- [2] The Southampton Electrochemistry group, *Instrumental Methods in Electrochemistry*, Ellis Horwood Limited, Chichester, 1985.
- [3] T. Biegler, D.A.J. Rand, R. Woods, *J. Electroanal. Chem.* 29, 269, 1971.
- [4] R. Gómez, A. Rodes, J.M. Pérez, J.M. Feliu, A. Aldaz, *Surf. Sci.* 344, 85, 1995.
- [5] A. Bewick, K. Kunimatsu, B.S. Pons, *Electrochim. Acta* 25, 465, 1980.
- [6] A. Bewick, K. Kunimatsu, *Surf. Sci.* 101, 131, 1980.
- [7] R.G. Greenler, *J. Chem. Phys.* 44, 310, 1966.
- [8] Y.J. Chabal, *Surf. Sci. Rep.* 8, 211, 1988.
- [9] T. Iwasita, W. Vielstich, *Adv. in Electrochem. Sci. and Eng.*, Ed. H. Gerischer, C.W. Tobias, VCH Weinheim, 1990.
- [10] D.A. MacInnes, *The principles of Electrochemistry*, Dover, New York 1961, p. 342.
- [11] S. Bruckenstein, R.R. Gadde, *J. Am. Chem. Soc.* 93, 793, 1971.
- [12] O. Wolter, J. Heitbaum, *Ber. Bunsenges. Phys. Chem.* 88, 6, 1984.
- [13] J. Willsau, O. Wolter, J. Heitbaum, *J. Electroanal. Chem.* 185, 181, 1985.
- [14] T. Frelink, PhD Thesis Eindhoven University of Technology 1995.

Chapter 3

The characterisation of ethanol and 1,2-ethanediol adsorbates on platinized platinum with FTIRS and DEMS

Abstract

The irreversible adsorption of ethanol and 1,2-ethanediol on platinised platinum have been studied with Fourier Transform IR spectroscopy (FTIRS) and Differential Electrochemical Mass Spectrometry (DEMS) in perchloric acid electrolyte. The adsorption was found to be C-C(OH) dissociative for both ethanol and 1,2-ethanediol. During adsorption 1,2-ethanediol is completely dehydrogenated to adsorbed CO. For ethanol it was concluded that carbon species are formed in addition to adsorbed CO. Part of this residue is hydrogenated at low potential to methane.

3.1 Introduction

The electrochemical oxidation of 1,2-ethanediol and particularly ethanol on platinum are of considerable interest because of their role as model compounds for the study of the adsorption and electrooxidation behaviour of organic species on platinum. Electrochemical studies can also provide useful information with respect to the platinum catalyzed oxidation of alcohols with molecular oxygen in the liquid phase.

The electro-oxidation of ethanol over platinum yields carbondioxide, acetic acid and acetaldehyde [1 - 6], as was found with spectroscopic methods. Several studies have been conducted to elucidate the structure of the irreversibly adsorbed species that are present on platinum after removal of the ethanol solution. The results are rather contradictory and can be divided in three categories. (i) Dissociation of the carbon-carbon bond occurs during adsorption, leading to the formation of adsorbed CO. This was suggested on the basis of DEMS [7] and voltammetry [8 - 11]. (ii) C-C(OH) dissociative as well as non-dissociative adsorption was proposed on the basis of ECTDMS [2] and FTIRS [12,13]. (iii) Only non-dissociative adsorption occurs leaving the carbon-carbon bond intact. This conclusion was based on DEMS measurements [1]. The formation of adsorbed CO was also observed during bulk electrooxidation of ethanol with FTIR spectroscopy [3 - 6, 14] and potential modulated reflectance spectroscopy [15]. EMIRS [16] data suggested that in the presence of bulk ethanol C-C(OH) dissociative as well as non-dissociative adsorption occurs.

The electrooxidation of 1,2-ethanediol over platinum gives glycolic acid and carbondioxide as bulk products in acid medium as found with spectroscopic methods [17]. The formation of adsorbed CO in the presence of bulk 1,2-ethanediol has been observed with FTIRS [6, 17] and EMIRS [18].

It is remarkable that the possible presence of CH_x groups next to adsorbed CO has only been mentioned by a few authors [7, 9, 15]. In this chapter we therefore investigate the irreversibly formed adsorbate of ethanol and 1,2-ethanediol with FTIR spectroscopy and DEMS to establish if adsorbed CH_x groups are formed by C-C(OH) dissociative adsorption. Also some experiments with dichloromethane and ethane were conducted to study the possible formation of CH_x groups from these compounds.

3.2 Experimental Section

Infrared measurements were performed with a Biorad FTS 45A spectrometer, equipped with a liquid nitrogen cooled MCT detector. All spectra were recorded with 4 cm^{-1} resolution. The electrochemical cell, made of glass, was placed on top of the sample room and is equipped

with a CaF_2 prism with 65° beveled edges, to obtain a high reflection angle. The electrode consist of a platinum disk of 9 mm diameter attached to a copper screw, by which it is connected to the electrode holder consisting of a copper interior embedded in PTFE. The infrared beam is focused on the electrode by one flat and one ellipsoidal mirror, with which the optimal spot size could be obtained. A polarizer is placed in the sample room to obtain p-polarized light.

DEMS measurements were performed with a Leybold Quadruvac PGA 100 mass spectrometer. The experimental setup is similar to the one described previously [19]. The products were examined for CO_2 (CO_2^+ ; $m/e=44$), CH_4 (CH_3^+ ; $m/e=15$) and C_2H_6 (C_2H_4^+ ; $m/e=28$).

Electrochemical measurements were performed with an Autolab PGSTAT 20 computer controlled potentiostat. A $\text{Hg}/\text{Hg}_2\text{SO}_4$ electrode was used as a reference-electrode. All potentials will be referred to RHE. All measurements were performed with platinised platinum, that was prepared by electrodeposition in $0.05 \text{ M H}_2\text{PtCl}_6 + 0.01 \text{ M HCl}$ on smooth platinum. A deposition current of $10 \text{ mA}/\text{cm}^2$ was used on a substrate of 2.5 cm^2 . Before deposition the substrate was cleaned in a gas-oxygen flame at 1000° C . Platinised platinum was chosen since the high area enables accurate assessment of both the charges involved in redox processes and the amount of product detected with the mass spectrometer. The electrode area was determined from the charge involved in the oxidation of adsorbed hydrogen of a cyclic voltammogram obtained in 0.5 M HClO_4 .

Different electrodes were used for DEMS, FTIRS and cyclic voltammetry as indicated in the text. Before each measurement potential cycling between 0 and 1.5 V was carried out until a stable voltammogram was obtained. Electrolytes were prepared using ultrapure water ($18.2 \text{ M}\Omega$) obtained with an Elga water purification system. In the infrared experiments 0.1 M HClO_4 was used and for cyclic voltammetry and the DEMS measurements 0.5 M HClO_4 was used. Oxygen was removed from the electrolyte with Argon.

Adsorption was carried out at 0.4 V for 10 minutes in ethanol (Merck p.a.) or 1,2-ethanediol (Merck p.a.) containing solutions. In the case of dichloromethane (Merck p.a.) $100 \mu\text{l}$ was added to the blank electrolyte. Ethane (Hoek Loos, purity 2.6) and CO (Hoek Loos, purity 4.7) were adsorbed at 0.4 V for 10 minutes by bubbling through the solution. After adsorption the electrolyte was replaced by blank electrolyte, while the electrode was kept at the adsorption potential.

3.3 Results

3.3.1 Cyclic Voltammetry

A cyclic voltammogram of the ethanol adsorbate, formed at 0.40 V from 1 mM containing electrolyte, is shown in Figure 1. The dashed curve represents the blank electrolyte. If the anodic scan is started at the adsorption potential, referred to as 'direct' oxidation, a peak is present at 0.641 V with a shoulder at 0.679 V. This peak resembles the oxidation peak of adsorbed CO[20]. A broad wave is present in the oxide region, that is not terminated at the reverse potential. The amount of charge associated with oxidation of adsorbate in a second cycle is only very small. If the oxidation is performed after first cycling through the hydrogen region, referred to as 'indirect oxidation', a reduction wave is observed at potentials below 0.20 V. The subsequent oxidation peak at low potential has narrowed and shifted to 0.633 V with a shoulder at 0.667 V. The broad oxidation wave at higher potential has decreased. The total oxidation charge, including the peak at low potential as well as the broad wave at higher potential, has decreased from 229 $\mu\text{C}/\text{cm}^2$ for the 'direct' oxidation to 186 $\mu\text{C}/\text{cm}^2$ for 'indirect' oxidation. The platinum area was established from the oxidation charge of adsorbed hydrogen in a cyclic voltammogram obtained in blank electrolyte.

The charge involved in the reduction, Q_{red} , can be determined by subtracting the charge involved in the anodic part of the scan below 0.40 V from the charge involved in the cathodic part of the scan below 0.40 V. The cathodic part of the scan consists of both reduction of adsorbate and formation of adsorbed hydrogen from solution protons on uncovered platinum sites. The anodic part of the scan only consists of oxidation of adsorbed hydrogen. Subtracting both values gives the charge involved in reduction; $Q_{\text{red}} = 50 \mu\text{C}/\text{cm}^2$. The charge involved in the oxidation of adsorbed hydrogen has decreased to 20% of the value in the voltammogram of the blank electrolyte. This means that after reduction below 0.20 V still

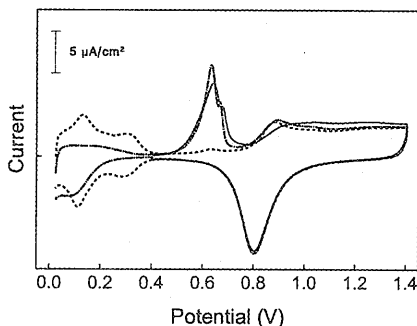


Fig. 1: C.V. of ethanol adsorbate; 'direct' oxidation (—), 'indirect' oxidation (---) and blank (----). Adsorption at 0.4 V in 1 mM ethanol. Electrolyte 0.5 M HClO_4 . Scan rate 5 mV/s. Real area 177 cm^2 .

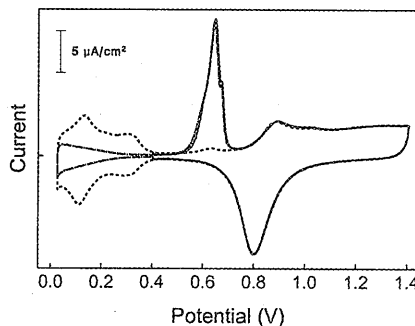


Fig. 2: C.V. of 1,2-ethanediol adsorbate; 'direct' oxidation (—), 'indirect' oxidation (---) and blank (----). Adsorption at 0.4 V in 1 mM 1,2-ethanediol. Electrolyte 0.5 M HClO_4 . Scan rate 5 mV/s. Real area 177 cm^2 .

80% of the platinum sites are covered with ethanol adsorbate. Note that hydrogen that is liberated during adsorption by C-H bond breaking is immediately oxidised to H^+ at the adsorption potential of 0.4 V and is thus not involved in the reactions described here.

The voltammogram of 1,2-ethanediol adsorbate formed at 0.4 V from 1 mM 1,2-ethanediol shows only an oxidation wave at 0.643 V with a shoulder at 0.670 V as shown in Figure 2. Again the anodic peak resembles the oxidation of adsorbed CO but it is less broad than in the case of ethanol. In contrast with ethanol no reduction can be observed at low potential and no broad oxidation wave is present at high potential. The total oxidation charge is $218 \mu\text{C}/\text{cm}^2$ and from the anodic part of the scan below 0.40 V it follows that 87% of the platinum sites are covered with 1,2-ethanediol adsorbate.

3.3.2 IR Experiments

Infrared spectra were obtained by subtracting the single beam spectra measured before (R_0) and after (R_1) oxidation of the adsorbate. The first single beam spectrum was obtained at the adsorption potential, the second was obtained at a potential of 0.75 V or at the adsorption potential after an excursion to 1.4 V. The IR spectrum of the ethanol adsorbate is shown in Figure 3, and is given as $\Delta R/R_0$ ($\Delta R=R_0-R_1$). Besides the positive-going ClO_4^- vibration at 1120 cm^{-1} [21] a negative-going CO vibration at 2044 cm^{-1} [22] and a positive-going band of CO_2 at 2344 cm^{-1} are observed. The negative going band at 1650 cm^{-1} is due to a uncompensated H_2O bending mode. Upon enhancement of the spectrum a small band is observed at 1805 cm^{-1} , that can be assigned to bridge bonded CO [22]. No C-H bands were observed within the detection limit of 0.01 %T (T =Transmission) in the particular wavenumber region.

The spectrum of the 1,2-ethanediol adsorbate is virtually the same as for the ethanol adsorbates. Figure 4 compares the spectra of adsorbed CO as obtained in the case of ethanol,

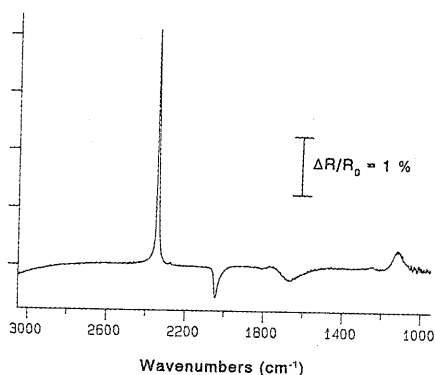


Fig. 3: IR spectrum of ethanol adsorbate, obtained after adsorption at 0.4 V in 1 mM ethanol. Electrolyte 0.1 M HClO_4 . Resolution 4 cm^{-1} , reference potential 0.4 V after scan to 1.4 V.

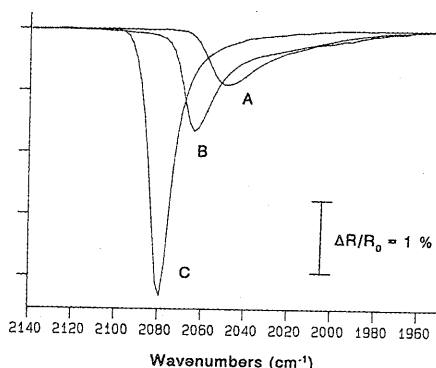


Fig. 4: CO IR vibrations obtained after adsorption of 1 mM ethanol (A), 1 mM 1,2-ethanediol (B) and CO (C) in 0.1 M HClO_4 . Resolution 4 cm^{-1} . Reference potential 0.75 V.

Table 1: Vibration frequencies and integrated absorbance of CO obtained after the adsorption of ethanol, 1,2-ethanediol and CO; the absorbance of CO is taken as unity.

	Frequency (cm ⁻¹)	Frequency (cm ⁻¹)	Integrated Absorbance (a.u.)
	1 mM	1 M	1 mM
ethanol	2044	2048	0.43
1,2-ethanediol	2054	2060	0.64
CO	2080	2080	1

1,2-ethanediol and gaseous CO. For both alcohols the amount of adsorbed CO formed during adsorption is lower than for gaseous CO. Concurrently the vibrations are shifted to lower wavenumbers as expected for lower coverages. The vibration frequency and integrated absorbance data are given in Table 1. The data suggest a considerable amount of adsorbed CO formed for both alcohols, with 1,2-ethanediol generating a higher amount than ethanol. The increase of the alcohol concentration from 1 mM to 1 M results in a small shift of the vibration frequency to higher wavenumbers. The small shift shows that the CO coverage increases only to a small extent in going from 1 mM to 1 M. It has been found that at a concentration of 1 mM ethanol a nearly maximal adsorbate coverage is obtained [23].

The calculation of the CO coverage from the integrated absorbance is difficult, since it is known from FTIRS studies in Ultra High Vacuum on single crystals [24-28] that the integrated absorbance is not linearly related to the CO coverage. The relation between the integrated absorbance and the CO coverage for polycrystalline platinum would have to be established in separate experiments. Moreover, it is uncertain whether coadsorbates are present in the case of ethanol and 1,2-ethanediol that might influence the vibrational properties of CO.

The formation of the adsorbed species from 1 M ethanol was studied in situ with FTIRS by raising the electrode potential from 0.05 V to 0.30 V and to 0.40 V, recording a spectrum at

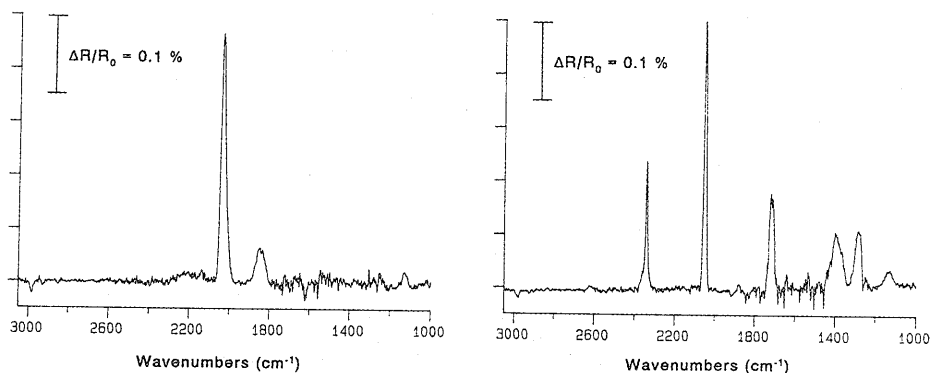


Figure 5: IR spectra obtained at 0.3 V (left spectrum) and 0.4 V (right spectrum) in 1M ethanol. Resolution 4 cm⁻¹. Reference potential 0.05 V.

each potential. At 0.05 V no chemisorption of ethanol occurs as shown by the absence of an anodic current when the ethanol solution is contacted with the platinum electrode; hence the spectrum recorded at 0.05 V can be used as reference spectrum. The results are shown in Figure 5 and the vibrations at 2040 cm^{-1} from linear CO and 1845 cm^{-1} from bridge bonded CO [22] indicate that ethanol adsorption occurs at 0.3 V. No other positive going bands are observed. At 2984 cm^{-1} a negative going C-H band [4] is observed indicative of the disappearance of ethanol from the solution.

At 0.40 V the vibration at 2053 cm^{-1} implies further formation of linear CO. The bands that appear at 1717, 1395 and 1285 cm^{-1} are indicative of acetic acid formation [4]. At 0.40 V a positive going band at 2343 cm^{-1} is observed that demonstrates the formation of CO_2 . Again the disappearance of a C-H vibration at 2984 cm^{-1} is observed.

Attempts to observe the hydrogenation products formed at potentials below 0.25 V did not succeed; no C-H vibrations or other vibrations could be found within the detection limit of 0.01 %T, probably due to the low concentration of hydrogenation products (approximately 2×10^{-4} M) in the thin layer and a low IR absorption of the C-H bands.

3.3.3 Differential Electrochemical Mass Spectrometry (DEMS)

Figure 6 shows the mass signals of CO_2 and CH_4 for the oxidation of ethanol adsorbate. When 'indirect' oxidation is performed, a small amount of methane is detected at potentials below 0.25 V. No ethane could be detected. The amount of carbondioxide formed in the 'indirect' oxidation is somewhat lower than in the 'direct' oxidation. The number of electrons, n_{ox} , liberated per formed CO_2 molecule can be calculated from the DEMS measurements. This requires calibration of the mass spectrometer for CO_2 ; this is carried out by measuring the oxidation of adsorbed CO to CO_2 in a reference experiment. This yields the calibration factor K_{CO} :

$$K_{\text{CO}} = \left(\frac{Q_{\text{ox}}}{Q_{\text{mass}}} \right)_{\text{CO}} \quad (1)$$

with Q_{ox} is the coulometric charge involved in the oxidation of CO to CO_2 and Q_{mass} represents the integrated mass current $\int i_{\text{mass}} dt$. The n_{ox} value for ethanol can then be obtained from the value $Q_{\text{ox}}/Q_{\text{mass}}$ measured for the alcohol oxidation according to:

$$n_{\text{ox}} = \left(\frac{Q_{\text{ox}}}{Q_{\text{mass}}} \right)_{\text{ethanol}} \frac{1}{K_{\text{CO}}} n_{\text{ox}}^{\text{CO}} \quad (2)$$

with $n_{\text{ox}}^{\text{CO}} = 2$ electrons per CO_2 molecule. The n_{ox} values were found to be 2.5 for the 'direct' oxidation of the ethanol adsorbate and 2.2 for the 'indirect' oxidation. The margin of error of these n_{ox} values is estimated to be 0.1.

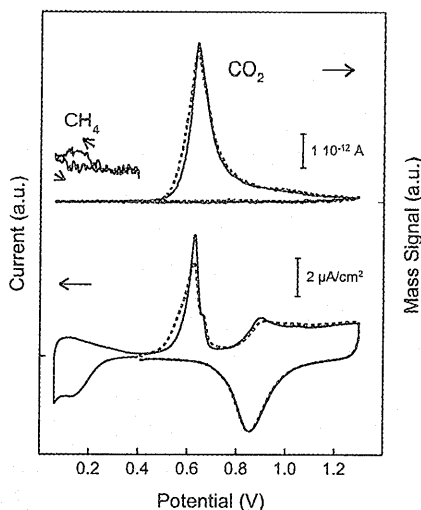


Fig. 6: DEMS measurement obtained after adsorption at 0.4 V in 1 mM ethanol. Electrolyte 0.5 M HClO₄. 'Direct' (----) and 'indirect' oxidation (—). Scan rate 2 mV/s, $m/e = 44$ (CO₂), $m/e = 15$ (CH₄). Real area 79 cm².

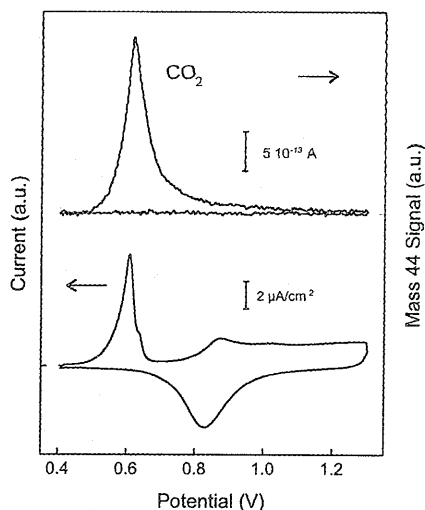


Fig. 7: DEMS measurement obtained after adsorption at 0.4 V in 1 mM 1,2-ethanediol. Electrolyte 0.5 M HClO₄. Scan rate 2 mV/s, $m/e = 44$ (CO₂). Real area 79 cm².

Figure 7 shows the DEMS results for adsorbed 1,2-ethanediol, that generates a higher amount of carbondioxide than adsorbed ethanol. A value of 2.1 electrons per CO₂ molecule was found. No hydrogenation products such as methane or ethane could be detected.

DEMS results for the irreversible adsorbates of dichloromethane and ethane are shown in Figure 8 and 9. Because of the low solubility of both dichloromethane and ethane only low adsorbate coverages were found. The n_{ox} values for dichloromethane and ethane were found to be respectively 3.2 and 3.3 electrons per CO₂ molecule.

3.3.4 Coulometry

The charge Q_{ads} , liberated during the adsorption, was determined at 0.30 V with coulometry, since infrared spectroscopy showed that no bulk oxidation products are formed at that potential. Adsorption was carried out in solutions of 1 mM ethanol or 1,2-ethanediol for 10 minutes. After adsorption the total charge released during direct oxidation of the adsorbate Q_{ox} is determined in a cyclic voltammogram. The ratio of the adsorption charge and the total oxidation charge for 'direct' oxidation Q_{ads}/Q_{ox} was 1.3 for ethanol and 1.5 for 1,2-ethanediol.

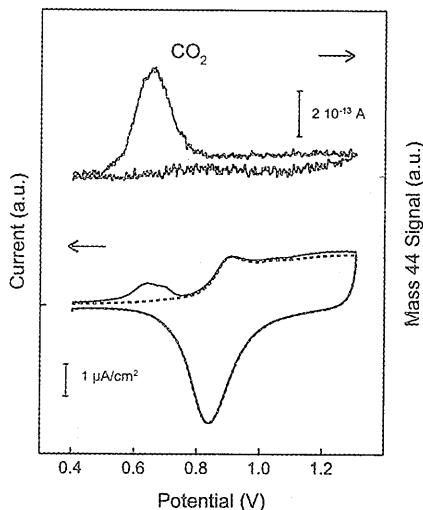


Fig. 8: DEMS measurement obtained after adsorption of dichloromethane in 0.5 M HClO₄. 'Direct' oxidation (—) and blank (---). Scan rate 2 mV/s, $m/e = 44$ (CO₂). Real area 79 cm².

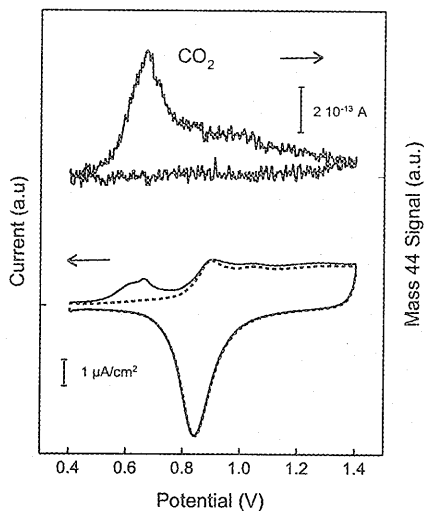
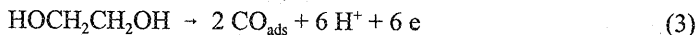


Fig. 9: DEMS measurement obtained after adsorption of ethane in 0.5 M HClO₄. 'Direct' oxidation (—) and blank (---). Scan rate 2 mV/s, $m/e = 44$ (CO₂). Real area 79 cm².

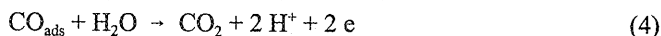
3.4 Discussion

3.4.1 1,2-Ethanediol

The observation of substantial amounts of adsorbed carbonmonoxide with IR spectroscopy for 1,2-ethanediol indicates that this molecule adsorbs C-C(OH) dissociatively on platinum. The ratio $Q_{\text{ads}}/Q_{\text{ox}}$ of 1.5 and the n_{ox} value of 2.1 electrons per CO₂ measured with DEMS clearly show that adsorbed CO is the only irreversible adsorbate that is formed according to:



The adsorbed carbonmonoxide is oxidized at higher potential according to:



This conclusion is in agreement with previous reports for 1,2-ethanediol that observed CO in the presence of 1,2-ethanediol in solution [6, 7, 18]. However, no investigations have been carried out so far concerning the irreversible adsorbate in acid electrolyte.

From the oxidation charge Q_{ox} in combination with $n_{\text{ox}} = 2.1$ a coverage of 0.52 CO

molecules per platinum atom can be calculated using the equation

$$\theta = \frac{Q_{ox}}{n_{ox} Q_H^0} \quad (5)$$

with Q_H^0 is the charge involved in the oxidation of adsorbed hydrogen in a voltammogram obtained in 0.5 M HClO₄. The integrated CO absorbances for 1,2-ethanediol and CO data in Table 1 are in agreement with the calculated CO coverage of 0.52 for 1,2-ethanediol given that the CO coverage for gaseous CO was found to be 0.7 in separate experiments. In our view the lower CO coverage for 1,2-ethanediol is connected to spatial requirements for the dissociation of C-C and C-H and O-H bonds during adsorption. Energetically the breaking of the C-C, C-H and O-H bonds forms apparently no obstacle on the route to CO formation. The formation of the platinum-carbon bond and the multiple C-O bond must be the driving force for this process.

We encounter a discrepancy between cyclic voltammetry and IR spectroscopy when the hydrogen blocking due to CO adsorbates from 1,2-ethanediol is analysed in simple terms of linear and bridge bonded CO. The hydrogen adsorption has decreased with 87% of its original value and on average every CO molecules blocks 1.67 (0.87/0.52) hydrogen sites. When it is assumed that linear adsorbed CO displaces one hydrogen atom and bridge bonded CO displaces two hydrogen atoms, the displacement ratio H/CO = 1.67 indicates that 67% of the adsorbed CO is bridge bonded and 33% is linearly bonded. However our IR experiments reveal only a small fraction of bridge bonded CO while the majority is linear bonded CO. These simple assumptions concerning the blocking of hydrogen adsites by CO molecules have often been made in the past by various researchers.

We must consider that it has recently been shown for compressed CO adlayers on Pt(111) electrodes that in IR spectroscopy considerable intensity transfer from the multiple bonded CO vibration to the linear bonded CO vibration can occur due to dynamic dipole-dipole coupling [29]. The ratio of the integrated absorbances for linear and bridge bonded CO was a factor 4 higher than expected on the basis of STM measurements. The phenomenon of intensity transfer has been found also in IR studies that were carried out in Ultra High Vacuum [24]. However, even when the different cross sections for linear and bridge bonded CO are included, our IR results are not in agreement with the cyclic voltammetry results that suggest that 67% is bridge bonded and 33% is linearly bonded CO. Such a discrepancy between the IR and voltammetry results has also been noted in the case of adsorbed CO formed after CO₂ reduction in phosphate buffer at pH = 6.8 [30] and the authors suggested the presence of IR insensitive species such as side-on adsorbed CO, a concept that has been introduced previously [31].

Also the assumption that linear CO displaces one hydrogen atom and bridge bonded CO two

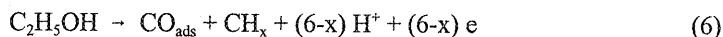
hydrogen atoms might be somewhat oversimplified. Connected to this is the assumption that hydrogen atoms are adsorbed atop, although this has never been demonstrated. The assumption that bridge bonded CO blocks on average two platinum atoms is based on the assumption that no densely packed islands are present where bridge bonded CO blocks on only one platinum atom.

STM work has shown that even on Pt(111) CO adlayers can have a complicated structure like $(\sqrt{19} \times \sqrt{19})R23.4^\circ$ -13CO with a CO coverage of 0.68 [29]. Part of the CO molecules are bonded asymmetrically inbetween atop and bridging geometries. The behaviour of asymmetrically bonded CO in IR spectroscopy is typically linear, but it might possibly prevent the adsorption of two hydrogen atoms.

On the basis of the arguments presented above we emphasize that one should be very careful in translating experimentally obtained charge data like Q_{ox} and ΔQ_H into a molecular picture of the adlayers in terms of linearly and bridge bonded CO. In this respect IR measurements are more conclusive.

3.4.2 Ethanol

In the case of ethanol all data point in the direction of C-C(OH) dissociative adsorption as the only pathway leading to irreversible adsorbates, as was also found for 1,2-ethanediol. The substantial amount of CO observed with IR spectroscopy demonstrates that dissociative adsorption occurs. The integrated CO absorbance is only 30 % lower than for 1,2-ethanediol, where C-C(OH) dissociative adsorption was demonstrated to be the only pathway, leading to $\theta_{CO} = 0.52$. The first step in C-C(OH) dissociative ethanol adsorption is probably the partial dehydrogenation of the molecule followed by dissociation of the C-C bond resulting in adsorbed CO and a CH_x according to:

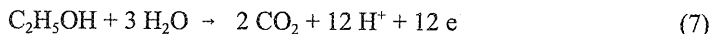


The formation of methane in the reduction of the adsorbate layer shows that CH_x species are present after adsorption and the absence of ethane formation strongly suggests that non-dissociated C_2 species are not present. In a previous report a small amount of ethane was observed in addition to methane [13]. The n_{ox} value of 2.5 obtained for ethanol confirms that CO is not the only adsorbate and supports the claim that CH_x groups are present. Our conclusion that C-C(OH) dissociative adsorption is the only adsorption pathway leading to irreversible adsorbates is in agreement with several others [7-11], as opposed to non-dissociative adsorption as the only pathway [1]. A combination of C-C(OH) dissociative and non-dissociative adsorption has also been suggested [2, 12, 13].

Only few data are present on the adsorption of ethanol on platinum in Ultra High Vacuum. Thermal Desorption Spectrometry demonstrated that C-C(OH) dissociation of adsorbed

ethanol molecules in CO and CH_x takes place at room temperature on Pt(111) [32], Pd(111) [33] and Pd(110) [34]. The CH_x group is dehydrogenated to surface carbon on platinum in contrast with palladium where the CH_x group desorbed as CH₄. These data show that the adsorption mechanism under Ultra High Vacuum conditions is very similar to adsorption in the liquid phase.

Before analysing the n_{ox} value of 2.5 found with DEMS we will show that the data found with Coulometry are in good agreement with the DEMS results. FTIRS and DEMS have shown that CO₂ is the only product formed in the oxidation of the irreversible adsorbate layer, whereas IR spectroscopy has shown that at the adsorption potential of 0.3 V used in the coulometry experiments no acetic acid is formed. This means that the obtained adsorption charge Q_{ads} can be completely ascribed to adsorption. Therefore, the Q_{ads}/Q_{ox} ratio of 1.3 found with Coulometry suggests that of the 12 electrons liberated in the total oxidation of an ethanol molecule to CO₂ according to

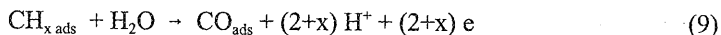


6.8 electrons are liberated during adsorption and 5.2 are liberated in the oxidation of the adsorbate. Since 2 CO₂ molecules are formed in the oxidation of a single ethanol adsorbate, 2.6 electrons per CO₂ molecule are released. This value is in good agreement with the value of 2.5 found with DEMS.

Quantitative analysis of the n_{ox} value of 2.5 found with DEMS shows that a follow-up oxidation from CH_x to CO can occur after dissociation. Formation of equal amounts of CO and CH_x during adsorption would result in n_{ox} values between 3 (x=0) and 4.5 (x=3), according to;

$$n_{ox} = \frac{n_{ox, CO} + n_{ox, CH_x}}{2} \quad (8)$$

taking n_{ox, CO} =2 and n_{ox, CH_x} = (4+x). Since no methane was observed during the adsorption, it must be concluded that the observed n_{ox} value of 2.5 does not originate from the removal of CH_x species during adsorption, but from a follow-up reaction of CH_x. This means that a fraction of the CH_x species is oxidized to CO_{ads}; such a reaction mechanism has been proposed recently [7]:



This conclusion is supported by recent FTIRS measurements of Shin et al. who detected ¹³CO after adsorption of ¹³CH₃CH₂OH at potentials equal to our adsorption potential [35]. The conclusion that CH_x species can be oxidized to CO is supported by the DEMS data that we obtained for dichloromethane and ethane. The low n_{ox} values of 3.2 for dichloromethane and

3.3 for ethane can only be caused by the presence of adsorbates with low n_{ox} values like CO. The CH_3 group of ethanol and the CH_2 group from dichloromethane seem to behave quite similarly upon adsorption as follows from a quantitative analysis of the n_{ox} number for ethanol. In the case of ethanol both the adsorbates formed from the $-CH_3$ and $-CH_2OH$ group contribute evenly to the n_{ox} value of 2.5, and both contributions can be calculated when it is assumed that the conversion of the CH_2OH group to CO_{ads} is complete using

$$\frac{n_{ox, -CH_3} + n_{ox, -CH_2OH}}{2} = 2.5 \quad (10)$$

$$n_{ox, -CH_2OH} = 2 \quad (11)$$

It follows from this relation that for the contribution of the adsorbate from the $-CH_3$ group $n_{ox, CH_2OH} = 3.0$ electrons per formed CO molecule. This number is close to the value of 3.2 found for the irreversible adsorbates from dichloromethane demonstrating that the oxidation behaviour of the CH_3 group of ethanol is similar to the CH_2 group from CH_2Cl_2 .

Combining the n_{ox} value found with DEMS with the voltammetry data gives the total adsorbate coverage as well as possible CO and CH_x coverages. We will show that these data are in agreement with our IR data. It can be calculated from the oxidation charge Q_{ox} in combination with the n_{ox} value of 2.5 that the adsorbate coverage is 0.44 per platinum atom, using the relation $\theta = Q_{ox} / (n_{ox} Q_H^0)$. This coverage is somewhat lower than for 1,2-ethanediol, where 0.52 CO molecules per platinum atom were found. The exact adsorbate composition can be calculated as well from the fractional contribution of the CO and CH_x groups to the n_{ox} value of 2.5, using the relations:

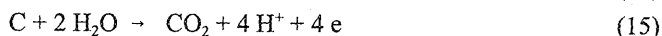
$$\frac{\theta_{CO}}{\theta_{CO} + \theta_{CH_x}} n_{ox, CO} + \frac{\theta_{CH_x}}{\theta_{CO} + \theta_{CH_x}} n_{ox, CH_x} = 2.5 \quad (12)$$

$$\theta_{CO} + \theta_{CH_x} = 0.44 \quad (13)$$

with $n_{ox, CO} = 2$ and $n_{ox, CH_x} = (4+x)$. From these equations it follows that in the case of C as the coadsorbate ($x=0$) the CO coverage is 0.33 and for CH_3 as the coadsorbate the CO coverage is 0.40. This result is in good agreement with the IR data presented in Table 1 which show a 33% lower integrated CO absorption for ethanol with respect to 1,2-ethanediol, for which θ_{CO} was established as 0.52.

Evaluation of the charges involved in the reduction and in the 'direct' and 'indirect' oxidation of ethanol in view of the C-C(OH) dissociative reaction mechanism gives information on the oxidation state of the CH_x species. As a result of the reduction of the adsorbate, the charge Q_{ox} involved in the 'indirect' oxidation is lower than the charge Q_{ox} for the 'direct' oxidation.

The ratio $Q_{\text{red}}/\Delta Q_{\text{ox}}$ of 1.2 suggests that the hydrogenated species is a carbon species with the average oxidation state zero, since in the reduction as well as the oxidation of elemental carbon four electrons are involved according to:



It is assumed that during the reductive potential cycle no currentless processes occur like the dissociation of C-H bonds giving adsorbed hydrogen.

It is unlikely that ethanol generates COH species that contribute to hydrogenation at low potentials since no evidence was found for such a species in the case of 1,2-ethanediol. Therefore it seems appropriate to conclude that elemental carbon is the only species that is hydrogenated to methane at low potentials. It must be noted that only a fraction of the carbon residue is hydrogenated. No firm conclusions can be drawn on the nature of the carbon residues that are insensitive to hydrogenation. The reason for the partial hydrogenation might be the occurrence of carbonaceous phase on the surface, that are insensitive towards hydrogenation. Elemental carbon can be formed through further dehydrogenation of CH_x species according to:



The conclusion that carbon atoms are formed is in accordance with the absence of C-H vibrations in the IR spectrum in Figure 3 within the detection limit of 0.01 %T. In contrast with our measurements, C-H vibrations were observed with FTIRS [13] at 2960, 2920 and 2850 cm^{-1} with intensities of approximately 0.1 %T that were ascribed to an adsorbed ethoxy species. EELS also observed C-H vibrations after transfer of the electrode to UHV [36].

IR and Thermal Desorption studies of CH_3 adspecies on Pt(111) in UHV support our conclusion that complete dehydrogenation of the CH_x species has occurred. IR studies have shown that adsorbed CH_3 moieties on Pt(111) at 150 K are characterized by a single C-H band at 2885 cm^{-1} of approximately 0.07 %T at saturation coverage [37-39]. Adsorbed CH_3 species are subject to dehydrogenation at temperatures above 230 K and the C-H stretch vibration at 2885 cm^{-1} in the IR spectrum has completely disappeared after increasing the temperature to 300 K [37-41], indicative of complete dehydrogenation to carbon species. In accordance with this, complete dehydrogenation of adsorbed CH_2 species formed from CH_2Cl_2 is observed on Pd(100) at room temperature [42]. It is characteristic for UHV experiments that adsorbed hydrogen formed in dehydrogenation of methyl fragments desorbs in the temperature region 280-350 K, indicating that at room temperature some adsorbed hydrogen can be present [37]. However, in our electrochemical adsorption experiments at 0.4 V dissociation of C-H bonds is accompanied by oxidation of the hydrogen atom to a proton.

The energy involved in the oxidation might generate an extra driving force for C-H dissociation, favouring complete dehydrogenation of CH_x species to carbon.

3.5 Conclusions

In the present study we have shown on the basis of FTIRS and DEMS measurements that both 1,2-ethanediol and ethanol adsorb C-C(OH) dissociatively. During adsorption 1,2-ethanediol is completely dehydrogenated to CO_{ads} . In the adsorption of ethanol the alcohol group is completely dehydrogenated to CO_{ads} and half of the methyl groups are oxidized to CO_{ads} . Of the other half, a large fraction is dehydrogenated to a hydrogenable C_{ads} species and a small fraction is formed that is insensitive towards hydrogenation. The nature of the latter is unknown. Infrared spectroscopy has revealed that for both ethanol and 1,2-ethanediol CO_{ads} is adsorbed linearly.

References:

- [1] J. Willsau, J. Heitbaum, *J. Electroanal. Chem.* 194, 27, 1985.
- [2] B. Bittins-Cattaneo, S. Wilhelm, E. Cattaneo, H.W. Buschmann, W. Vielstich, *Ber. Bunsenges. Phys. Chem.* 92, 1210, 1988.
- [3] L.-W.H. Leung, S.-C. Chang, M.J. Weaver, *J. Electroanal. Chem.* 266, 317, 1989.
- [4] T. Iwasita, B. Rasch, E. Cattaneo, W. Vielstich, *Electrochim. Acta* 34, 1073, 1989.
- [5] S.-C. Chang, L.-W.H. Leung, M.J. Weaver, *J. Phys. Chem.* 94, 6013, 1990.
- [6] L.-W.H. Leung, M.J. Weaver, *Langmuir* 6, 323, 1990.
- [7] U. Schmiemann, U. Müller, H. Baltruschat, *Electrochim. Acta* 40, 99, 1995.
- [8] F. Cases, M. López-Atalaya, J.L. Vázquez, A. Aldaz, *J. Electroanal. Chem.* 278, 433, 1990.
- [9] F. Cases, E. Morallon, J.L. Vázquez, J.M. Perez, A. Aldaz, *J. Electroanal. Chem.* 350, 267, 1993.
- [10] Cases, F.; Vázquez, J. L.; Perez, J. M.; Aldaz, A. *J. Electroanal. Chem.* 310, 403, 1991.
- [11] M.-C. Morin, C. Lamy, J.M. Leger, J.L. Vázquez, A. Aldaz, *J. Electroanal. Chem.* 283, 287, 1990.
- [12] R. Holze, *J. Electroanal. Chem.* 246, 449, 1988.
- [13] T. Iwasita, E. Pastor, *Electrochim. Acta* 39, 531, 1994.
- [14] H. Hitmi, E.M. Belgsir, J.-M. Leger, C. Lamy, R.O. Lezna, *Electrochim. Acta* 39, 407, 1994.
- [15] J.A. Caram, C. Gutiérrez, *J. Electroanal. Chem.* 323, 213, 1992.
- [16] B. Beden, M.-C. Morin, F. Hahn, C. Lamy, *J. Electroanal. Chem.* 229, 353, 1987.
- [17] Christensen, P.A; Hamnett, A. *J. Electroanal. Chem.* 1989, 260, 347.
- [18] F. Hahn, B. Beden, F. Kadirgan, C. Lamy, *J. Electroanal. Chem.* 216, 169, 1987.
- [19] O. Wolter, J. Heitbaum, *Ber. Bunsenges. Phys. Chem.* 88, 2, 1984.
- [20] R. Ianniello, V.M. Schmidt, U. Stimming, J. Stumper, A. Wallau, *Electrochim. Acta* 39, 1863, 1994.
- [21] D.S. Corrigan, M.J. Weaver, *J. Electroanal. Chem.* 239, 55, 1988.
- [22] B. Beden, A. Bewick, K. Kunimatsu, C. Lamy, *J. Electroanal. Chem.* 142, 345, 1982.
- [23] F.A. de Bruijn, B.F.M. Kuster, G.B. Marin, *submitted to J. Catal.*

- [24] B.N.J. Persson, R. Ryberg, *J. Phys. Rev. B* 24, 6954, 1981.
- [25] A. Crossley, D.A. King, *Surf. Sci.* 95, 131, 1980.
- [26] B.E. Hayden, A.M. Bradshaw, *Surf. Sci.* 125, 187, 1983.
- [27] D. Hoge, M. Tüshaus, E. Schweizer, A.M. Bradshaw, *Chem. Phys. Lett.* 151, 230, 1988.
- [28] B.E. Hayden, K. Kretzschmar, A.M. Bradshaw, R.G. Greenler, *Surf. Sci.* 149, 406, 1985.
- [29] I. Villegas, M.J. Weaver, *J. Chem. Phys.* 101, 1648, 1994.
- [30] S. Taguchi, T. Ohmori, A. Aramata, M. Enyo, *J. Electroanal. Chem.* 369, 199, 1994.
- [31] Y. Ikezawa, H. Fujisawa, F. Ishi, *Surf. Sci.* 218, 246, 1989.
- [32] F. Zaera, H. Hoffmann, *J. Phys. Chem.* 95, 6297, 1991.
- [33] F. Zaera, *Langmuir* 7, 1998, 1991.
- [34] H. Fairbrother, X.D. Peng, R. Viswanathan, P.C. Stair, M. Trenary, J. Fan, *Surf. Sci. Lett.* 285, L455, 1993.
- [35] J. Shin, W.J. Tornquist, C. Korzeniewski, C.S. Hoaglund, *Surf. Sci.* 364, 122, 1996.
- [36] P. Gao, C.-H. Lin, C. Shannon, G.N. Salaita, J.H. White, S.A. Chaffins, A.T. Hubbard, *Langmuir* 7, 1515, 1991.
- [37] B.A. Sexton, K.D. Rendulic, A.E. Hughes, *Surf. Sci.* 121, 181, 1982.
- [38] J.L. Davis, M.A. Barteau, *Surf. Sci.* 187, 387, 1987.
- [39] R. Shekhar, M.A. Barteau, *Catal. Lett.* 31, 221, 1995.
- [40] J. Fan, M. Trenary, *Langmuir* 10, 3649, 1994.
- [41] C. French, I. Harrison, *Surf. Sci.* 342, 85, 1995.
- [42] Y.-N. Wang, J.A. Marcor, G.W. Simmons, K. Klier, *J. Phys. Chem.* 94, 7597, 1990.

Chapter 4

The adsorption of C₃ alcohols, 1-butanol and ethene on platinized platinum as studied with FTIRS and DEMS

Abstract

The irreversible adsorption of several C₃ alcohols, 1-butanol and ethene on platinized platinum has been studied with Fourier Transform IR spectroscopy (FTIRS) and Differential Electrochemical Mass Spectrometry (DEMS) in perchloric acid electrolyte. Apart from 2-propanol all studied alcohols display C-C(O) dissociative adsorption as the only pathway active in the formation of irreversible adsorbates. 1,2,3-Propanetriol is the only compound that is fully converted to adsorbed CO, while all other primary alcohols generate hydrocarbon adspecies in addition to CO. No further C-C bond breaking is observed in these hydrocarbon adspecies, that were found to be highly dehydrogenated. The hydrocarbon species can be fractionally hydrogenated off the surface to form corresponding gaseous compounds. 2-Propanol and ethene do not undergo C-C dissociation to form CO, but are dehydrogenated considerably. For 2-propanol and ethene it was found that a small amount of oxygen incorporation occurs on the C₁ position, followed by decarbonylation to form CO.

4.1 Introduction

The study of the electro-oxidation of simple alcohols on platinum was initially urged by the possible application of these substances in the direct fuel cell [1]. Nowadays, methanol is regarded as the best candidate for application in fuel cells and is thus the most widely studied compound. 1,2-Ethanediol and ethanol have received less attention and studies concerning C₃ alcohols have been reported even less frequently. In spite of their unfitness for fuel cells, the number of studies concerning alcohol compounds has increased steadily over the past years, due to a growing fundamental interest in the adsorption and oxidation behaviour of these compounds. Electrochemical studies can generate relevant information for the selective oxidation of alcohol compounds with molecular oxygen on platinum catalysts in the liquid phase. Small alcohols can fulfill the role of model compounds in the study of larger alcohols like for example α -D-glucose or methyl- α -D-glucopyranoside.

The recent development of both infrared and mass spectroscopic techniques suitable for the solution phase has enabled a more systematical study of the adsorption and oxidation behaviour of alcohols, offering the possibility of gathering molecular information that had been impossible for electrocatalytic researchers so far. Several aspects of the adsorption behaviour of primary and secondary alcohols have been clarified with these spectroscopic techniques and will be summarized here.

It has been well established with FTIRS that adsorbed CO is formed during the adsorption of various primary alcohols and polyols; ethanol [2,3,4,5], 1,2-ethanediol [3,4,6], 1-propanol [3,7,8], 1,2- and 1,3-propanediol [3], 1,2,3-propanetriol [3], 1-butanol [3] and 2-propen-1-ol [9]. We will refer to this type of reaction as C-C(O) dissociative adsorption or decarbonylation. The IR data were used only in a single report to establish the CO coverage; ranging from 0.9 for methanol to 0.35 for 1-butanol [3]. The formation of adsorbed CO in the adsorption of primary alcohol and polyol compounds has been suggested also on the basis of cyclic voltammetry [10-13].

Non C-C(O) dissociative adsorption of primary alcohols has been reported in a number of cases to occur simultaneously with C-C dissociative adsorption. For ethanol [2], 1-propanol [8] and 2-propen-1-ol [9], C-H vibrations were observed that were ascribed to non-dissociated adspecies. Most primary alcohols form adsorbates that are susceptible to reduction at potentials in the hydrogen region and it has been found with DEMS that gaseous compounds are formed as a result. These products give information on the composition of the adsorbates. It is reported for ethanol that ethane is formed in addition to methane in the ratio 1:6 [2], in contrast with others who only found methane [4,14,15]. For 1-propanol, ethane and propane were found in the ratio of 3.5 : 1 [8]. These results show that in some cases non-dissociative adsorption occurs in addition to dissociative adsorption. It was further proposed

for ethanol [2] and 1-propanol [8] that the non-dissociated adspecies can undergo C-C(O) bond cleavage during reduction, leading to an increased CO coverage and methane and ethane formation, respectively. This means that the degree of non C-C dissociative adsorption is higher than indicated by the reduction products found with DEMS. Due to contrasting results, the issue is still open whether solely C-C dissociative adsorption occurs or that dissociative and non-dissociative adsorption occur simultaneously.

So far only few data have been reported that give information on the exact composition of the alkyl groups that are formed in the C-C(O) dissociative adsorption of primary alcohols. For ethanol we suggested previously that oxidation of the CH_x group to C and CO occurs [4]. In the case of 1-propanol C₂H_{6,ads} [7] and C₂H_{5,ads} [8] adspecies were proposed, whereas also dissolution of the adspecies has been proposed [10].

There is general agreement for secondary alcohols that no C-C dissociation occurs during adsorption [3,7,11,16,17]. This conclusion is supported by the observation that no CO is formed during adsorption and that reduction of the 2-propanol adsorbate results in formation of propane [16]. Several adsorbate structures were proposed for 2-propanol [16], but more data are necessary to clarify this point.

Ethane was found with DEMS to be the main product in the reduction of ethene adsorbates indicating that no C-C bond breaking has occurred. Isotope experiments have shown that the adsorption of ethene on Pt(110) is accompanied by partial oxygen uptake, while the adsorbates on Pt(111) do not undergo oxygen uptake [14].

In this chapter we investigate for several primary alcohols and polyols whether the adsorption on platinumized platinum is solely C-C(O) dissociative or that dissociative and non-dissociative adsorption occur simultaneously. In a previous paper [4] we concluded for 1,2-ethanediol and ethanol that the C-C dissociative adsorption on platinumized platinum is the only pathway that is active in the formation of irreversible adsorbates. We will also deal with the point of the proposed C-C(O) bond dissociation during adsorbate reduction since this is important in the issue of dissociative versus non-dissociative adsorption. Little is known about the composition of the coadsorbates that are formed in addition to CO and we will focus on this point. Therefore we aim to determine the degree to which these adspecies dehydrogenate.

The adsorbates formed from 2-propanol and ethene are studied to compare the extent of dehydrogenation in the case of non C-C dissociative adsorption with that occurring in dissociative adsorption. Fourier Transform IR Spectroscopy (FTIRS), Differential Electrochemical Mass Spectrometry (DEMS) and cyclic voltammetry are used to characterize the irreversible adsorbates.

4.2 Experimental

Infrared measurements were performed with a Biorad FTS 45A spectrometer, equipped with a liquid nitrogen cooled MCT detector. All IR spectra were recorded with 4 cm^{-1} resolution. The bottom of the electrochemical cell consists of an CaF_2 prism with 65° beveled edges. The platinum electrode has a diameter of 9 mm and is embedded in a PTFE holder. P-polarized light has been used in all IR measurements. DEMS measurements were performed with a Leybold Quadravac PGA 100 mass spectrometer. The details of the experimental setup are given in a previous report [18]. The products were examined for carbondioxide ($m/z = 44$, CO_2^+), methane ($m/z = 15$, CH_3^+), ethane ($m/z = 30$, C_2H_6^+), propene ($m/z = 42$, C_3H_6^+), propane ($m/z = 44$, C_3H_8^+), butene ($m/z = 56$, C_4H_8^+) and butane ($m/z = 58$, $\text{C}_4\text{H}_{10}^+$). Electrochemical measurements were performed with an Autolab PGSTAT 20 computer controlled potentiostat. A $\text{Hg}/\text{Hg}_2\text{SO}_4$ electrode was used as a reference-electrode. All potentials will be referred to RHE. All measurements were performed with platinized platinum, that was obtained by electrodeposition from a $0.05\text{ M H}_2\text{PtCl}_6 + 0.01\text{ M HCl}$ solution on smooth platinum. A deposition current of $10\text{ mA}/\text{cm}^2$ was used for the DEMS gauze-electrode, while $0.5\text{ mA}/\text{cm}^2$ was used for the IR electrode. The electrode areas, determined from the hydrogen desorption region in the cyclic voltammogram, were 53 cm^2 and 10 cm^2 respectively. Platinized platinum was chosen in order to minimize the influence of impurities on the adsorption process as well as to increase the mass signals in the DEMS technique. Potential cycling between 0 and 1.5 V was carried out until a stable voltammogram was obtained. Electrolytes were prepared using ultrapure water ($18.2\text{ M}\Omega$) obtained with an Elga water purification system. In the infrared experiments 0.1 M HClO_4 was used and for cyclic voltammetry and the DEMS measurements 0.5 M HClO_4 was used. Oxygen was removed from the electrolyte with Argon 4.6.

Adsorption experiments were performed at 0.4 V for 10 minutes with 1 mM or 5 mM concentrations of the various alcohol compounds. The potential of 0.4 V was chosen on one hand high enough to enable adsorption in the absence of adsorbed hydrogen, which might react with the adspecies and on the other hand low enough to suppress oxidation reactions of the adsorbate. The adsorption current has nearly decreased to zero after 10 minutes, indicating that the time was long enough for the adsorption to be complete. Ethylene (Hoek Loos, purity 2.7) and CO (Hoek Loos, purity 4.6) were bubbled through the solution for 10 minutes. All other chemicals, p.a. quality, were obtained from Merck. After adsorption the electrolyte was replaced by blank electrolyte while keeping the electrode at the adsorption potential.

4.3 Results

4.3.1 DEMS and Cyclic Voltammetry

After adsorption of the alcohol compound at 0.4 V for 10 minutes, followed by replacement of the alcohol containing solution by fresh electrolyte, a scan is started in the anodic direction and subsequently the mass signal for CO₂ is recorded. This procedure will be referred to as 'direct' oxidation. Combining the DEMS and cyclic voltammetry results gives the number of electrons, n_{ox} , liberated in the adsorbate oxidation per formed CO₂ molecule. This requires calibration of the mass spectrometer for CO₂, which is carried out by measuring the oxidation of adsorbed CO to CO₂ in a reference experiment. This yields the calibration factor K_{CO} according to:

$$K_{CO} = \left(\frac{Q_{ox}}{Q_{mass}} \right)_{CO} \quad (1)$$

where Q_{ox} is the coulometric charge involved in the oxidation of CO to CO₂ and Q_{mass} represents the integrated mass current $\int i_{mass} dt$. The n_{ox} value for 1,2,3-propanetriol can then be obtained from the value Q_{ox}/Q_{mass} measured for the alcohol oxidation according to:

$$n_{ox} = \left(\frac{Q_{ox}}{Q_{mass}} \right)_{1,2,3-propanetriol} \frac{1}{K_{CO}} n_{ox}^{CO} \quad (2)$$

where $n_{ox}^{CO} = 2$ electrons per CO₂ molecule. In contrast with the 'direct' oxidation, the scan can also be started in the cathodic direction after adsorption at 0.4 V followed by electrolyte exchange. This procedure will be referred to as 'indirect' oxidation. Concomitantly the mass response for possible reduction products can be followed during the reduction. In the subsequent anodic scan the CO₂ mass response is followed again.

Figure 1 shows the current and CO₂ ($m/z = 44$) mass response for the indirect oxidation of 1,2,3-propanetriol adspecies. No reduction of the adspecies is observed in the potential region below 0.4 V and as a result the oxidation profiles for 'direct' and 'indirect' oxidation are the same. An oxidation peak is observed in the double layer region at 0.65 V. This peak resembles that of the oxidation of 1,2-ethanediol adsorbates very well, which were shown to consist solely of adsorbed CO [4]. The dotted line represents the second cycle, which equals the cyclic voltammogram for platinumized platinum in fresh 0.5 M HClO₄. The charge involved in the oxidation was 114 $\mu\text{C}/\text{cm}^2$ and 82% of the hydrogen sites were blocked after adsorption. For the oxidation of these adspecies it was found that n_{ox} is 1.9 e/CO₂.

It is shown in the Figures 2 to 6 for the various compounds that different oxidation profiles are observed for the 'direct' and 'indirect' oxidation as a result of the preceding reduction during the latter. For all these compounds, the oxidation charge involved in the 'direct'

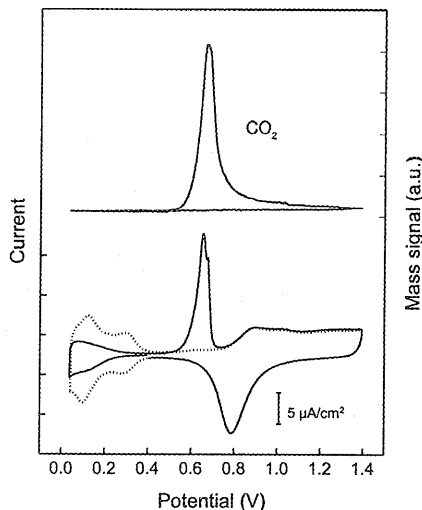


Fig. 1: C.V. and DEMS measurement of 1,2,3-propanetriol adsorbates; 'indirect' oxidation (—), blank (·····). $E_{ads} = 0.4$ V in 1 mM 1,2,3-propanetriol. Electrolyte 0.5 M $HClO_4$, scan rate 5 mV/s, $m/z = 44$ (CO_2^+).

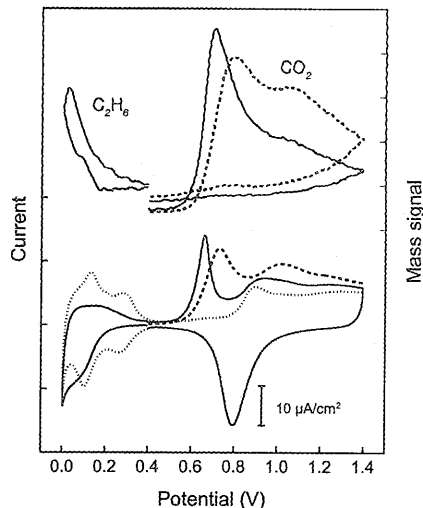


Fig. 2: C.V. and DEMS measurement of 1-propanol adsorbates; 'direct' (-----), 'indirect' oxidation (—) and blank (·····). $E_{ads} = 0.4$ V in 10 mM 1-propanol. Electrolyte 0.5 M $HClO_4$, $v = 10$ mV/s, $m/z = 44$ (CO_2^+), $m/z = 30$ ($C_2H_6^+$).

oxidation is higher than in the 'indirect' oxidation as shown in Table 1 and this observation implies that in the reduction adsorbates are removed from the surface. This is confirmed by the DEMS measurements that are discussed below.

In the 'direct' oxidation of 1-propanol, represented by the dashed line in Figure 2, an oxidation peak is found at 0.73 V in the double layer region, followed by a broad oxidation wave that extends throughout the oxide region with an maximum at 1.02 V. At the reverse potential the oxidation wave is not completed as shown by the dashed line in Figure 2. The oxidation is accompanied by formation of CO_2 ($m/z=44$). In the 'indirect' oxidation, represented by the solid line in Figure 2, a reduction is observed below 0.2 V that is accompanied by the formation of ethane ($m/z=30$). A small contribution at $m/z=15$ was

Table 1: Charge involved in the 'direct' and 'indirect' oxidation of various alcohol compounds and ethene after adsorption at 0.4 V.

Compound	Q_{ox} direct oxidation ($\mu C/cm^2$)	Q_{ox} indirect oxidation ($\mu C/cm^2$)	Q_{red} ($\mu C/cm^2$)
1-propanol	564	354	131
1,3-propanediol	371	248	83
1,2,3-propanetriol	114	-	-
2-propanol	389	116	98
1-butanol	649	304	115
ethene	793	149	192

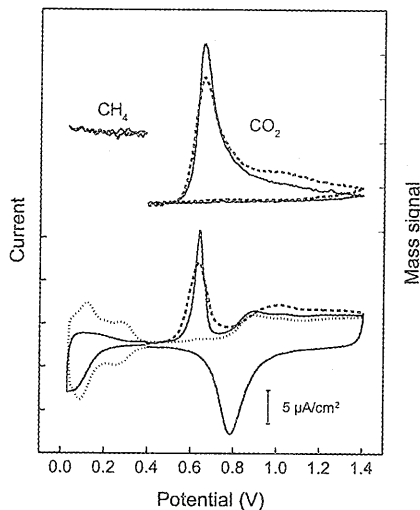


Fig. 3: C.V. and DEMS measurement of 1,3-propanediol adsorbates; 'direct' (-----), 'indirect' oxidation (—) and blank (.....). $E_{ads} = 0.4$ V in 5 mM 1,3-propanediol. Electrolyte 0.5 M HClO₄, scan rate 5 mV/s, $m/z = 44$ (CO₂⁺), $m/z = 15$ (CH₃⁺).

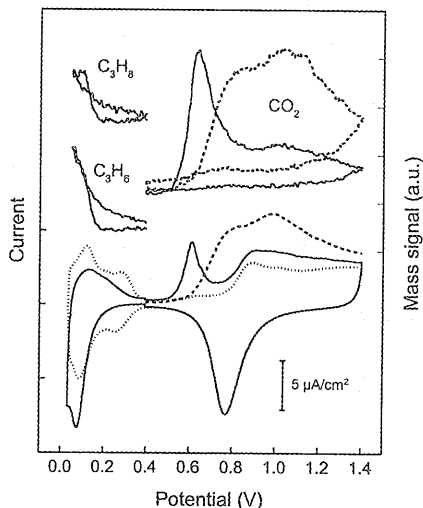


Fig. 4: C.V. and DEMS measurement of 1-butanol adsorbates; 'direct' (-----), 'indirect' oxidation (—) and blank (.....). $E_{ads} = 0.4$ V in 5 mM 1-butanol. Electrolyte 0.5 M HClO₄, scan rate 5 mV/s, $m/z = 44$ (CO₂⁺, C₃H₈⁺), $m/z = 42$ (C₃H₆⁺).

observed and this could be fully ascribed to the fragmentation of ethane. This indicates that no methane is formed during reduction of the adsorbate. Only a small signal was found for propane at $m/z=44$ in the hydrogen adsorption region, where reduction of the adsorbates occurs. After taking into account of the fragmentation patterns and relative ionization probabilities the ratio of ethane to propane was found to be roughly 50/1. Several scans had to be carried out to complete the reduction; 95 $\mu\text{C}/\text{cm}^2$ was involved in the first cycle and after five cycles the total charge was 131 $\mu\text{C}/\text{cm}^2$. The charge involved in the reduction, Q_{red} , given in Table 1, could be determined by subtracting the anodic part of the scan below 0.4 V, due to oxidation of adsorbed hydrogen, from the cathodic part of the scan below 0.4 V, due to hydrogenation and formation of adsorbed hydrogen. The oxidation peak in the double layer region, recorded after reduction of the adsorbate, has narrowed and shifted 0.07 V in negative direction with respect to the 'direct' oxidation to 0.66 V. The form of this peak now resembles the oxidation peak of adsorbed CO [19] and the concomitant CO₂ production has changed similarly, cf Figure 2 upper part. It follows further from the anodic branch of the hydrogen region that still 73% of the Pt-H sites are blocked after reduction of the adsorbate. The number of electrons, n_{ox} , liberated per CO₂ molecule was found to be 3.5 for the 'direct' oxidation and 3.1 for the 'indirect' oxidation.

Figure 3 shows the results for 1,3-propanediol. It is clear by comparison with Figure 2 that the doubled number of hydroxyl moieties on 1,3-propanediol is responsible for a lower oxidation

wave in the oxide region and the oxidation profile therefore resembles the CO oxidation more than 1-propanol. The oxidation profile can be regarded as intermediate between 1-propanol and 1,2,3-propanetriol. In the 'direct' and 'indirect' oxidation a peak is observed at 0.64 V. As shown in Table 1, the charge involved in the reduction is lower for 1,3-propanediol than for 1-propanol, demonstrating that a lower fraction of the adsorbate is sensitive towards hydrogenation. The only product observed in the reduction is methane. The n_{ox} values found were 2.5 e/CO₂ for the 'direct' oxidation and 2.2 e/CO₂ for the 'indirect' oxidation, the latter being close to the value of 2 e/CO₂ for adsorbed CO.

The effect of increasing the chain length by a single carbon atom can be seen when cyclic voltammograms for 1-butanol and 1-propanol are compared. For 1-butanol, a broad double peak with maxima at 0.8 and 1.04 V is observed in the 'direct' oxidation as shown in Figure 4. When compared to the 'direct' oxidation profile of 1-propanol, the oxidation peak in the double layer region is less pronounced and has become a shoulder that is shifted 0.07 V in anodic direction. The relative contribution of oxidation in the oxide region has increased with respect to 1-propanol while the charge involved in the reduction is relatively lower than for 1-propanol. In the 'indirect' oxidation a well defined CO like peak is present in the double layer region at 0.61 V. This peak is smaller than for the 'indirect' oxidation of 1-propanol. The n_{ox} values found were 3.7 e/CO₂ for the 'direct' oxidation and 3.6 e/CO₂ for the 'indirect' oxidation. The reduction of the adsorbate at 0.08 V is accompanied by propene ($m/z = 42$) and propane ($m/z = 44$) formation. Only a small contribution was found for butane at $m/z = 58$ in the hydrogen adsorption region, where reduction of the adsorbates occurs. After taking into account of the fragmentation patterns and relative ionization probabilities the (propene + propane)/butane ratio was found to be roughly 100/1. No methane or ethane was observed after correction for the fragmentation of propane.

The 'direct' and 'indirect' oxidation profiles obtained from 2-propanol in Figure 5 demonstrate that this secondary alcohol behaves quite different from primary alcohols. A broad wave is present in the 'direct' oxidation in the oxide region, with a maximum at 1.02 V, while only a small contribution is visible in the double layer region. It is shown in Table 1 that the charge involved in the 'direct' oxidation is much lower than for 1-propanol and a larger fraction of the adsorbate is susceptible towards hydrogenation, that leads to the formation of propene ($m/z = 42$) and propane ($m/z = 44$). In the 'indirect' oxidation a small oxidation peak is found at 0.65 V, indicating that a small amount of CO might have been formed. The n_{ox} values found were 3.8 e/CO₂ for the 'direct' oxidation and 5.2 e/CO₂ for the 'indirect' oxidation.

The 'direct' and 'indirect' oxidation profiles of ethene adsorbates formed at 0.4 V are given in Figure 6. In the 'direct' oxidation a broad wave starts at 0.5 V and extends throughout the oxide region and is clearly not completed at the reverse potential of 1.4 V. The wave contains a maximum at 0.85 V and a shoulder at 1.04 V. However, in the double layer, where CO-like

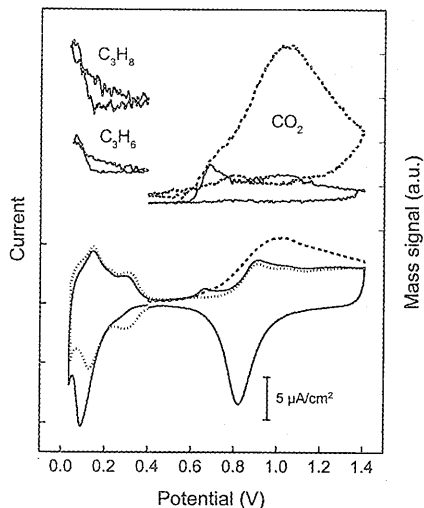


Fig. 5: C.V. and DEMS measurement of 2-propanol adsorbates; 'direct' (-----), 'indirect' oxidation (—) and blank (.....). Adsorption at 0.4 V in 5 mM 2-propanol. Electrolyte 0.5 M HClO₄, scan rate 5 mV/s, $m/z = 44$ (CO₂⁺, C₃H₈⁺), $m/z = 42$ (C₃H₆⁺).

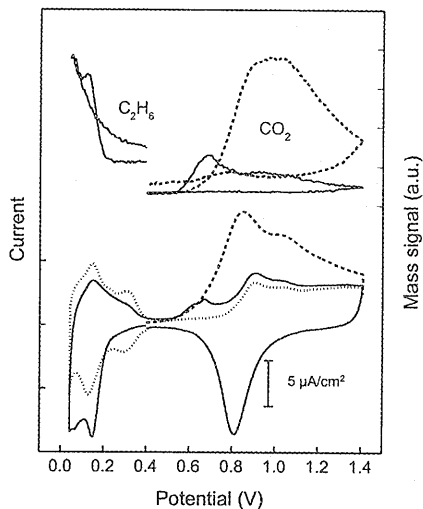


Fig. 6: C.V. and DEMS measurement of ethene adsorbates; 'direct' (-----), 'indirect' oxidation (—) and blank (.....). Adsorption at 0.4 V by bubbling ethene. Electrolyte 0.5 M HClO₄, scan rate 5 mV/s, $m/z = 44$ (CO₂⁺), $m/z = 30$ (C₂H₆⁺).

adsorbates are expected, a relatively low oxidation current is established. When 'indirect' oxidation is performed a large reduction peak is present at 0.15 V, that is accompanied by the formation of ethane ($m/z = 30$) and a small amount of butane ($m/z = 58$). It follows from the anodic scan that after reduction only 16% of the hydrogen adsites are covered with adsorbate. In the subsequent scan a small oxidation peak is present in the double layer region at -68 mV, combined with a broad wave extending from 0 to 700 mV in the oxide region. From this observation it follows that the majority of the ethene adsorbates is removed from the surface during the reduction reaction. The n_{ox} values found were 4.0 e/CO₂ for the 'direct' oxidation and 3.7 e/CO₂ for the 'indirect' oxidation.

Table 2: n_{ox} (e/CO₂) values for the 'direct' and 'indirect' oxidation of various alcohol adsorbates determined with DEMS after adsorption at 0.4 V.

Compound	n_{ox} direct oxidation (e/CO ₂)	n_{ox} indirect oxidation (e/CO ₂)
1-propanol	3.5	3.1
1,3-propanediol	2.5	2.2
1,2,3-propanetriol	1.9	-
2-propanol	3.8	5.2
1-butanol	3.7	3.6
ethene	4.0	3.7

4.3.2 Infrared Spectroscopy

Infrared spectra, given as $\Delta R/R_0$ ($\Delta R=R_1-R_0$), were obtained by subtracting the single beam spectra that were obtained at the adsorption potential before (R_0) and after (R_1) a potential excursion to 1.4 V. The spectrum obtained for 1,2,3-propanetriol is shown in Figure 7. At 1120 cm^{-1} a positive going band from ClO_4^- [20] is observed, due to an increase in concentration as a result of migration processes involved in the oxidation of the 1-propanol adsorbate. Apart from this band, the only IR bands observed were a negative going band at 2054 cm^{-1} , due to linearly adsorbed CO [21], a positive going band at 2344 cm^{-1} , that originates from the formation of CO_2 present in the thin layer and a broad band around 1650 cm^{-1} due to an uncompensated water bending mode. No C-H bands could be observed in the wavenumber region around 3000 cm^{-1} . The infrared spectra obtained for 1-propanol, 1,3-propanediol and 1-butanol are virtually the same as for 1,2,3-propanetriol. Figure 8 compares the spectra in the $1900\text{-}2100\text{ cm}^{-1}$ range obtained after adsorption of the various alcohols with the spectrum obtained after adsorption of pure CO. The alcohol derived CO vibrations are substantially lower and broader than the CO vibrations obtained from pure CO; additionally, they have shifted to lower wavenumbers, as is expected for lower CO coverages. In the case of 2-propanol and ethene only small CO vibrations were observed at 2010 cm^{-1} as shown in Figure 9, where the spectrum for 1-butanol is given for comparison.

The integrated CO absorbances give a good indication of the CO coverage formed after adsorption of the various compounds. It has been reported for FTIRS studies in Ultra High Vacuum on platinum single crystals that the integrated CO absorbance is not linearly related to the CO coverage [22-26]. It must also be considered that coadsorbates next to CO might

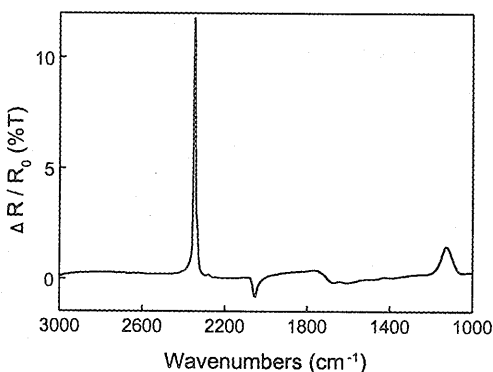


Fig. 7: Infrared spectrum of 1,2,3-propanetriol adsorbate, obtained after adsorption at 0.4 V in 1 mM 1,2,3-propanetriol. Electrolyte 0.1 M HClO_4 . $E_0 = 0.4\text{ V}$, $E_1 = 0.4\text{ V}$ after potential excursion to 1.4 V, resolution 4 cm^{-1} .

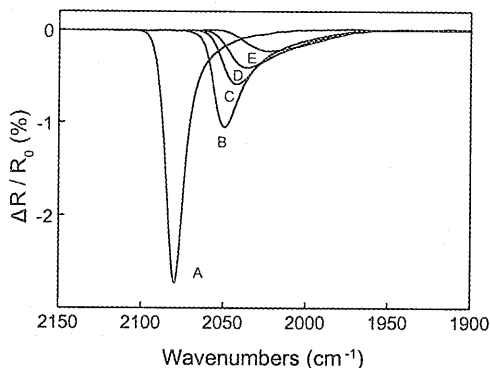


Fig. 8: Infrared spectrum in the wavenumber region of linear adsorbed CO after adsorption of CO (A), 5 mM 1,2,3-propanetriol (B), 1,3-propanediol (C), 1-propanol (D), 1-butanol (E). Electrolyte 0.1 M HClO₄, E₀ = 0.4 V, E₁ = 0.4 V after potential excursion to 1.4 V, resolution

alter the vibrational properties of CO to some extent with respect to pure CO adlayers. The data are shown in Table 3, taking the absorbance of gaseous CO as unity. It can be concluded that 1,2,3-propanetriol generates the highest amount of CO, followed by 1,3-propanediol, 1-propanol and 1-butanol. Ethene and 2-propanol yield very small CO coverages. The amount of CO formed after adsorption of ethanol described in a previous study [4] is intermediate between 1-propanol and 1,3-propanediol. The amount of CO formed in the adsorption of 1,2-ethanediol is equal to that from 1,2,3-propanetriol [4]. Leung and Weaver [3] have determined CO coverages in the presence of the reactant alcohol with FTIRS and they reported higher

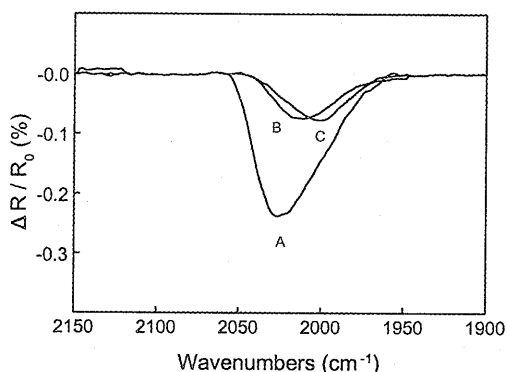


Fig. 9: Infrared spectrum in the wavenumber region of linear adsorbed CO after adsorption of 1-butanol (A), 2-propanol (B) and ethene (C). Electrolyte 0.1 M HClO₄, E₀ = 0.4 V, E₁ = 0.4 V after potential excursion to 1.4 V, resolution 4 cm⁻¹.

Table 3: Integrated absorbance of the CO vibration observed after adsorption of various compounds. Adsorption potential 0.4 V.

Compound	Vibration frequency (cm ⁻¹)	Integrated absorbance (a.u.)
CO	2080	1
1-propanol	2040	0.38
1,3-propanediol	2048	0.53
1,2,3-propanetriol	2054	0.69
1-butanol	2025	0.30
2-propanol	2010	0.07
ethene	2000	0.06

coverages than in our measurements; between 0.9 for methanol and 0.35 for 1-butanol. However the trend in the CO coverage for various alcohol compounds is the same as in our case.

It is remarkable that for all substances reported here no C-H vibrations were observed in the wavenumber region between 2800 and 3000 cm⁻¹ within the detection limit of 0.01 %T. This is in contrast with previous reports for ethanol [2], 1-propanol [8] and 2-propanol [16], where C-H bands of 0.04, 0.15 and 0.04 %T were found, respectively. The noise level in our measurements is low enough to detect vibrations with the typical intensities between 0.05 and 0.15 %T, observed for methyl and ethyl species on platinum in Ultra High Vacuum [27,28]. We studied the hydrogenation of the alcohol adsorbates with IR to see if the products that are formed during reduction can be observed while they are trapped in the thin layer. We found for 2-propanol a small C-H band at 2920 cm⁻¹ of 0.03 %T after stepping the potential from -0.3 V to -0.65 V.

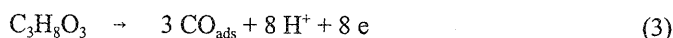
It was reported previously that hydrogenation of ethanol and 1-propanol adsorbates results in CO formation during reduction together with methane and ethane [2,8]. This reaction is important for the interpretation of the product distribution in DEMS during reduction. We found also that cycling through the hydrogen region resulted in an increase of the integrated CO absorbance when the electrode was in the thin layer configuration during reduction. However, FTIRS shows that the increase of the CO vibration is accompanied by a disappearance of CO₂ in the thin layer as shown by a negative band at 2343 cm⁻¹. To examine whether the CO increase was only due to reduction of CO₂ that has accumulated in the thin layer we performed an experiment in which the reduction was carried out while the electrode was positioned in the bulk of the solution. After the reduction the electrode was brought in the thin layer configuration to record the IR subtract spectrum. This spectrum was compared with one obtained without previous hydrogenation of the adsorbate and only a small 3 cm⁻¹ shift of the CO vibration to lower wavenumbers was observed upon reduction, while the integrated absorbance was equal. The small shift is probably due to the removal of coadsorbates during

the reduction. This experiment clearly demonstrates that the increase of the CO vibration that is found when the electrode is in the thin layer configuration during reduction is indeed due to reduction of CO₂ that has accumulated in the thin layer.

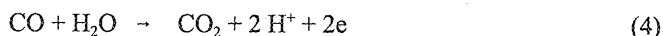
4.4 Discussion

4.4.1 1,2,3-Propanetriol

The adsorption of 1,2,3-propanetriol yields a considerable amount of CO as detected with FTIRS. This indicates that 1,2,3-propanetriol undergoes decarbonylation during adsorption. The n_{ox} value of 1.9 electrons per CO₂, found with DEMS, implies that this decarbonylation reaction is complete and thus CO is the only adsorbate formed according to;



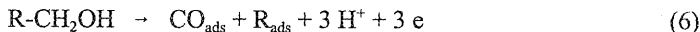
Afterwards the adsorbate is oxidized in the cyclic voltammogram according to:



The conclusion that 1,2,3-propanetriol decarbonylates completely is supported by the absence of an adsorbate reduction in the cyclic voltammogram at potentials in the hydrogen region. Complete decarbonylation was also found for 1,2-ethanediol [4] and we conclude that this adsorption behaviour is general for all small alcohols that contain an OH moiety on every carbon atom. Adsorbed CO was also observed with EMIRS for 1,2,3-propanetriol in 0.1 M NaOH electrolyte on the basal planes of platinum [12]. No investigations have been carried out so far for 1,2,3-propanetriol adspecies formed at low pH. From the charge Q_{ox} involved in the direct oxidation in combination with the n_{ox} value of 2 e/CO₂ a coverage of 0.53 CO molecules per platinum atom can be calculated, using the relation $\theta = Q_{\text{ox}} / (Q_{\text{H}}^0 n_{\text{ox}})$, where Q_{H}^0 is the charge involved in the hydrogen desorption in blank sulfuric acid electrolyte. This CO coverage is nearly equal to that found for 1,2-ethanediol [4], but lower than after adsorption of pure CO at 0.4 V, which is established from cyclic voltammetry to be 0.7. The lower coverage with respect to adsorption of CO can be ascribed to the ensemble effect; above a certain coverage the ensembles of uncovered platinum atoms will become too small for dissociative adsorption. The integrated CO absorption measured with FTIRS, as shown in Table 3, is in agreement with the CO coverage calculated from the oxidation charge in the cyclic voltammogram. Whereas oxidation charges give CO coverages of 0.53 and 0.7 for 1,2,3-propanetriol and pure CO, FTIRS gives integrated CO absorbances of 0.69 and 1.

4.4.2 1-Propanol, 1,3-propanediol and 1-butanol - Qualitative consideration

Our data indicate for these alcohol compounds that decarbonylation is the dominant pathway in the formation of irreversible adsorbates. As shown in Table 3, FTIRS demonstrates that considerable amounts of CO_{ads} are formed and this indicates that C-C dissociation occurs according to;



It is clear that CO cannot be the only product since not enough OH groups are present on these alcohol compounds to enable full conversion to CO_{ads} as was observed for 1,2,3-propanetriol and 1,2-ethanediol [4]. The n_{ox} values in Table 2 for 1-propanol, 1,3-propanediol and 1-butanol show indeed that CO is not the only adsorbate, since n_{ox} values higher than two are indicative of adsorbates other than CO. For instance, a $-\text{CH}_x$ group is characterized by a n_{ox} value of $(4+x) \text{ e}/\text{CO}_2$. Note that the R_{ads} species can undergo further oxidation reactions and we will discuss the composition of these adspecies below. The mechanism is likely to proceed via initial adsorption via the lone pair of the oxygen atom, followed by oxidation of the hydroxylproton and C-H protons and subsequently C-C dissociation to give CO.

Our DEMS measurements show that, in contrast with some earlier reports [2,8,9], the decarbonylation mechanism is the only pathway active in the formation of irreversible adsorbates. The products formed in the adsorbate reduction give important information on the composition of the coadsorbates that are formed next to CO. In the case of 1-propanol, ethane was observed as by far the major reduction product, while hardly any propane was found. This demonstrates that C-C(O) dissociative adsorption must be the dominant adsorption pathway, since non-dissociative adsorption would lead to a considerable amount of propane in the reduction. The absence of methane shows that these C_2 adspecies do not dissociate further into C_1 species. The same conclusion also holds for the other compounds; 1,3-propanediol and 1-butanol. In the case of 1,3-propanediol, methane was observed as the only reduction product, indicating that CO and CH_x adspecies have been formed during adsorption. For 1-butanol, the major products found in the reduction are propene and propane, demonstrating that 1-butanol is transformed into CO_{ads} and a C_3 species.

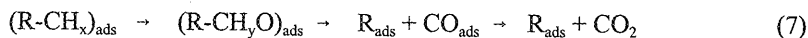
Our finding for 1-propanol contrasts with results of Pastor et al. who found ethane and propane in the ratio of 3.5:1 [8], whereas we find 50:1. This difference might be connected with the type of electrode used; whereas we used platinumized platinum grids, Pastor et al. used electrodes that were obtained by deposition of a DODUCO Pt lacquer suspension on teflon. It is possible that the distribution of crystal faces is different from our electrodes. They further concluded on the basis of FTIRS that dissociation of the C-C(O) bond can occur not only at the adsorption potential but also during reduction of the adsorbate, resulting in the formation of CO and ethane. However, we established that the increase of the integrated CO absorption,

that was observed after reduction of the adsorbate, originated from the reduction of CO₂ to CO_{ads} that was present in the thin electrolyte layer. A control experiment in which the reduction of the adsorbate was carried out while the electrode was pulled back from the CaF₂ window proved that the CO coverage does not increase during reduction of the 1-propanol adsorbates. These experiments clearly show that the mechanism in which the C-C(O) bond is broken during reduction of the adsorbate is not active in our situation. Therefore we can safely conclude that the products formed during adsorbate reduction for the various compounds can be assigned to dissociated species that were already present after adsorption.

It is important to note that there is always a fraction of the adsorbate, apart from CO, that is not subject to hydrogenation. It is difficult to obtain information on the composition of these species. We can establish though that it concerns C_xH_y species, as indicated by the broad oxidation wave in the oxide region, which is atypical for adsorbed CO. In addition, the n_{ox} values exceeding 2 e/CO₂ for the 'indirect' oxidation, shown in Table 2, confirm that hydrocarbon adspecies remain present after reduction, since they are characterized by n_{ox} values higher than 4e/CO₂. Probably graphite formation causes the insensitivity towards hydrogenation of these adspecies.

The few data that have been reported on the adsorption of primary and secondary alcohols on platinum in Ultra High Vacuum show that the adsorption mechanisms in Ultra High Vacuum and in the liquid phase are quite similar. Thermal Desorption Spectrometry (TDS) demonstrated for ethanol, 1-propanol and 1-butanol that decarbonylation occurs at temperatures below room temperature on Pt(111) [30], Pd(111) [31] and Pd(110) [32]. No evidence was found for non-dissociative adsorption or splitting of the C-O bond. In the case of ethanol, CH_x species are formed in addition to CO [30-32]. No clear conclusions could be drawn on the composition of the carbon residue that was formed from 1-propanol and 1-butanol. On Pd(111) ethylene was formed during TDS of 1-propanol adsorbates, indicating that C₂ species are formed in the decarbonylation [31]. The decarbonylation mechanism was also found to be active at room temperature for 2-propan-1-ol [33], 2-propan-1-al [33] and even for a cyclic compound as furan on Pd(111) [34].

In general, our results show that C-C bond breaking only occurs when an oxygen atom is present at the C₁ position, so that CO formation can occur. The C₂ and C₃ species that are formed from 1-propanol and 1-butanol, respectively, do not display C-C bond breaking, due to the absence of an oxygen atom at the C₁ position. We conclude from this that the high adsorption energy of CO is the driving force for the dissociative adsorption. In our opinion, these observations can be generalized; the oxidation of hydrocarbons to carbondioxide on platinum at room temperature proceeds via oxygen incorporation on the C₁ position of the hydrocarbon, followed by decarbonylation and further oxidation to CO₂ according to:



4.4.3 1-Propanol, 1,3-propanediol and 1-butanol - Quantitative analysis

Quantitative analysis of the data obtained with DEMS and cyclic voltammetry gives valuable information on the (i) adsorbate coverages and (ii) composition of the coadsorbed C_xH_y species. Analysis of the charge Q_{ox} involved in the oxidation of the adsorption products, given in Table 1, in combination with the n_{ox} value obtained with DEMS, given in Table 2, gives the coverage of C atoms, present in the form of CO or C_xH_y adsorbates according to $\theta = Q_{ox}/(n_{ox} Q_H^0)$, where Q_H^0 is the charge involved in hydrogen desorption in blank electrolyte. For 1-propanol, 1,3-propanediol, 1-butanol and ethene respectively, θ values of 0.75, 0.67, 0.82 and 0.92 were found. These coverages are considerably higher than the coverages obtained for ethanol [4], 1,2-ethanediol [4] and 1,2,3-propanetriol; 0.44, 0.52 and 0.53 respectively.

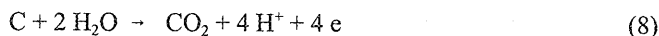
Analysis of the DEMS data can give the n_{ox} values of the C_xH_y species formed for the various alcohol compounds, providing information on their composition. We can infer from the experimental n_{ox} value for 1,3-propanediol that the CH_x group initially formed in the adsorption is fractionally oxidized to CO, as was also found for ethanol [4]. The n_{ox} value of the C_1 fragment can be derived from the n_{ox} value of 2.7 found with DEMS, assuming that the transformation of the two OH moieties to CO_{ads} is complete. A value of 3.5 e/ CO_2 is found using the relation $\frac{2}{3}n_{ox}^{CO} + \frac{1}{3}n_{ox}^{C1} = n_{ox}^{DEMS}$, with $n_{ox}^{CO} = 2$ and $n_{ox}^{DEMS} = 2.7$. An n_{ox} value lower than 4 can only be caused by COH or CO adspecies of which the former is highly unlikely since it was absent for adsorbates from 1,2-ethanediol [4] and 1,2,3-propanetriol. Thus it can be concluded that the C_1 species is partially oxidized to CO, a reaction that was also observed for ethanol, although to a somewhat higher extent [4]. Recent FTIRS experiments [35] using $^{13}CH_3CH_2OH$ demonstrated that the formation of $^{13}CO_{ads}$ started at 0 V vs SCE, confirming our conclusions. Ultra High Vacuum experiments have shown that the reaction between CH and CH_2 species with adsorbed oxygen atoms on Pt(111) occurs at temperatures above 200 K [36].

The n_{ox} value of 3.5 found for 1-propanol can be divided into the separate contributions of the CO and C_2 species, that are formed out of a single 1-propanol molecule. Since 1 and 2 CO_2 molecules are formed in the oxidation of the CO and C_2 group, respectively, the contribution of the C_2 group to the n_{ox} value of 1-propanol can be obtained using the relation $\frac{1}{3}n_{ox}^{CO} + \frac{2}{3}n_{ox}^{C2} = n_{ox}^{DEMS}$, with $n_{ox}^{CO} = 2$ and $n_{ox}^{DEMS} = 3.5$. In this way $n_{ox} = 4.3$ e/ CO_2 is calculated for the C_2 group.

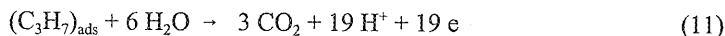
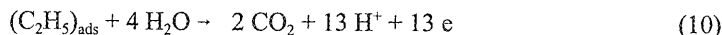
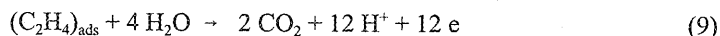
The n_{ox} value for the C_3 adsorbate formed from 1-butanol can be calculated in the same way. Using the relation $\frac{1}{4}n_{ox}^{CO} + \frac{3}{4}n_{ox}^{C3} = n_{ox}^{DEMS}$, with $n_{ox}^{CO} = 2$ and $n_{ox}^{DEMS} = 3.7$ e/ CO_2 , gives 4.3 e/ CO_2 for the C_3 group.

The n_{ox} values for the C_2 and C_3 adspecies from 1-propanol and 1-butanol, respectively, are very close to the n_{ox} value of 4.0 e/ CO_2 found for ethene. This shows that the non-CO adspecies formed from both propanol and butanol have a similar composition as the ethene adsorbates. The n_{ox} values, being close to 4e/ CO_2 , are characteristic for completely

dehydrogenated carbon according to;



In the case that these adspecies would have retained all hydrogen atoms, it would have been found that $n_{\text{ox}} = 6$ for ethene, $n_{\text{ox}} = 6.5$ for ethyl and $n_{\text{ox}} = 6.3$ for propyl adspecies according to:



Sun et al.[7] and Pastor et al.[8] suggested on the basis of the observation of C-H stretch vibrations just below 3000 cm⁻¹ with FTIRS that C₂H_{6,ads} and C₂H_{5,ads} respectively, were formed in the adsorption of 1-propanol. In our experiments we did not observe any C-H vibrations with FTIRS. However, note that in some occasions three uncompensated C-H bands below 3000 cm⁻¹ appeared in the spectra, that originate from adsorbed hydrocarbons on the mirrors inside the FTIR spectrometer. These vibrations are clearly visible in a single beam spectrum recorded in the absence of alcohol adsorbates, which indicates that they are of considerable intensity. These bands appear in the spectrum when the baseline has changed as a result of the transport of solvated ions through the thin layer, which accompanies any electrochemical reaction. The mechanical instability of the thin layer also readily causes changes in the base line, resulting in the appearance of the C-H bands. This phenomenon makes the assignment of observed C-H bands in the literature tentative. In agreement with the absence of C-H bands in the IR spectra, our DEMS and voltammetry results show that the hydrocarbon species are highly dehydrogenated and C₂H_{6,ads} and C₂H_{5,ads} species are therefore unlikely in our case. That 1-propanol is dehydrogenated to a large extent can also be inferred from the ratio $Q_{\text{ads}}/Q_{\text{ox}}$ of the charges involved in the adsorption and oxidation given in previous reports [10,13], although the authors come to a somewhat different conclusion on the products of the adsorption reaction.

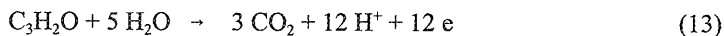
We must consider the possibility that C₂ and C₃ groups initially formed in the adsorption of 1-propanol, 1-butanol and ethene incorporate some oxygen. It has been shown with isotope experiments that 25% of the C atoms reacted with oxygen after adsorption of ethene at 0.5 V vs RHE on Pt(110) [14]. However, we performed the ethene adsorption at 0.4 V and we therefore expect a much lower degree of oxygen incorporation. In general, the uptake of oxygen atoms is strongly potential dependent as for instance with the oxidation of adsorbed CO, that occurs above a certain threshold potential. It is likely that the adsorption potential of 0.5 V used by Schmiemann et al. [14] is at the threshold potential for oxygen incorporation. In the case that oxygen uptake occurs in our experiments, dissociation of the molecule can occur

to form CO and CH_x, just as we found for ethanol [4]. Our experiments reported here show that such a dissociation reaction can occur even at high coverages and therefore we do not expect C-C(O) species as proposed by Schmiemann et al. to be stable. Indeed, we found a small amount of CO with FTIRS and a small CO-like peak in the 'indirect' oxidation of ethene in Figure 6. From the cyclic voltammogram, the CO coverage can be estimated to be 0.08, which means that $n_{ox} = 4.0$ is actually an average value for a mixed adlayer of C₂ species and CO. The contribution of the C₂ can then be calculated to be 4.2 e/CO₂ which means that the adsorbate consist mainly of highly dehydrogenated species like C₂ and C₂H, in addition to a small amount of CO.

4.4.4 2-Propanol

The formation of propane and propene as the only products in the electroreduction of 2-propanol adsorbate demonstrates that no substantial C-C bond cleavage occurs. However, a small amount of CO was observed with FTIRS. From the charge that is involved in the small oxidation peak at 0.65 V in the cyclic voltammogram the CO coverage is approximately 0.04. This CO coverage is similar to the CO coverage obtained with ethene. Probably this small amount of CO is formed as a result of oxygen incorporation at the C₁ position of the adsorbate, followed by C-C bond dissociation. From the oxidation charge and the n_{ox} value of 3.8 it follows that the coverage of C atoms is 0.48. The low CO coverage shows that additional oxygen incorporation into the 2-propanol residue is only minor, since the C atom coverage of 0.48 is low enough to enable decarbonylation. In this context, it should be reminded that the CO coverage for 1,2,3-propanetriol is 0.53. Since the incorporation of oxygen in 2-propanol is small, it is reasonable to assume that this will also hold for ethene.

It follows from the n_{ox} value of 3.8 for 2-propanol that the adsorbed residue is highly dehydrogenated. Since oxygen incorporation is believed to be small the n_{ox} value originates from species like C₃HO with 3.7 e/CO₂ or C₃H₂O with 4 e/CO₂ according to:



This result is in contrast with a previous report [16] that suggests on the basis of FTIRS that 2-propanol adsorbates consists of (CH₃-C-CH₃)_{ads}, (CH₃-CH-CH₃)_{ads}, (CH₃-COH-CH₃)_{ads} and (CH₃-CO-CH₃)_{ads}. However, these adsorbates are not present in our situation since they are characterised by much higher n_{ox} values of 6.0, 6.3, 5.7 and 5.3 e/CO₂ respectively than the experimentally found value of 3.8. A possible reason for this difference might be the type of electrode used; whereas we used platinized platinum, Pastor et al. used smooth platinum [16] These electrodes might expose different crystal planes, thus causing a different reactivity.

In addition, it also follows from the reduction and oxidation charges given in Table 1 that the

adsorbates of 2-propanol are highly dehydrogenated. The reduction of the adsorbate, that requires 98 $\mu\text{C}/\text{cm}^2$, results in a decrease of the oxidation charge from 389 to 116 $\mu\text{C}/\text{cm}^2$. We can conclude from this that for the reduction 98 $\mu\text{C}/\text{cm}^2$ is necessary while for the oxidation of the same adspecies to CO₂ 273 $\mu\text{C}/\text{cm}^2$ (=389-116) is required. Note that for the proposed adsorbates [16] given above the ratio of the reduction and oxidation charge varies for the four species from 1: 19 to 1: 4, when complete conversion to propane and carbon dioxide is assumed in the reduction and oxidation respectively. These ratios deviate considerably from the ratio of 1 : 2.8 found in our experiments.

Summarizing, we find for all compounds that the hydrocarbon species formed are highly dehydrogenated. UHV studies have shown that considerable dehydrogenation of hydrocarbon species can occur at room temperature. Adsorbed CH₃ species on Pt(111) are subject to dehydrogenation at temperatures above 230 K and the C-H stretch vibration at 2885 cm^{-1} in the IR spectrum has completely disappeared after increasing the temperature to 300 K [27-37], indicative of considerable dehydrogenation. In accordance with this, complete dehydrogenation of adsorbed CH₂ species, formed from CH₂Cl₂, is observed on Pd(100) at 300 K [38]. In UHV adsorbed hydrogen formed during dehydrogenation desorbs in the temperature region between 280 and 350 K. This means that a significant amount of adsorbed hydrogen remains on the surface, enabling an equilibrium to establish itself. In the electrochemical experiments, dehydrogenation is accompanied by oxidation of hydrogen to protons. The energy involved in the oxidation might generate an extra driving force for dehydrogenation. Given these facts, it is not surprising that we find considerable dehydrogenation of adsorbed hydrocarbon species. This result might explain the absence of C-H vibrations in the IR spectra.

Finally, we should like to comment on the relevance of adsorbate studies to the electrooxidation of alcohols. Leung and Weaver [3] have discussed the poisoning of alcohol electro-oxidation in relation to irreversible adspecies that are formed from the reactant alcohol itself. Since it was found with FTIRS that the electro-oxidation of the alcohol commences at the potential where adsorbed CO is oxidized, the authors concluded that CO was completely responsible for the poisoning of the reaction. They also noted that the inhibition is generally effective even though the initial CO coverage varies substantially with the alcohol compound. The poisoning effect of CO is well known in literature.

Our experiments have demonstrated that in the dissociative adsorption of primary alcohols and polyols hydrocarbon species are formed in addition to CO. The redox behaviour of these hydrocarbon fragments differs considerably from adsorbed CO, which is oxidized at relatively low potential in the double layer region, while the hydrocarbon fragments are oxidized at potentials in the oxide region. The hydrocarbon fragments cause a decrease of the active platinum surface in the same way that CO does and contribute therefore considerably to poisoning. In fact for large primary alcohols, like propanol and butanol, the site coverage due

to hydrocarbon fragments is probably larger than for CO. In addition, the lower affinity of these fragments towards oxidation implies that higher potentials are necessary to remove these species. In fact, the necessary potentials are beyond the region where alcohol oxidation proceeds with maximal rate. The presence of these poisoning hydrocarbon fragments nicely explains the observation that even at low CO coverages effective poisoning occurs [3].

It is well known that the oxidation of secondary alcohols proceeds with higher rate than most primary alcohols, and this has been ascribed to the absence of adsorbed CO on the surface during reaction [3]. However, our experiments show that irreversible adsorbates are formed from 2-propanol that are oxidized to CO₂ at potentials in the oxide region. These adspecies definitely cause poisoning of the electro-oxidation reaction. That the reaction rate is nevertheless higher than for primary alcohols and polyols is in our view probably due to a higher fraction of accessible platinum sites in the case of 2-propanol.

4.5 Conclusions

In this study on C₃ alcohols we have shown on the basis FTIRS, DEMS and cyclic voltammetry measurements that decarbonylation is by far the dominant pathway active in the formation of irreversible adsorbates from primary alcohols and polyols. In the case of 1,2,3-propanetriol the parent alcohol is completely dehydrogenated to adsorbed CO. The other primary alcohols studied here form in addition to CO a hydrocarbon adspecies, that can be partially hydrogenated off the surface to form gaseous compounds. No further C-C bond breaking occurs in these hydrocarbon adspecies after adsorption. It was found for both 2-propanol and ethene that the carbon backbone remains intact upon adsorption. As for the primary alcohols we found that these adspecies are highly dehydrogenated. It was found for 2-propanol and ethene that a small amount of oxygen incorporation occurs on the C₁ position, followed by decarbonylation to form CO.

References:

- [1] R. Parsons; T. VanderNoot, *J. Electroanal. Chem.*, 257, 9, 1988.
- [2] T. Iwasita, E. Pastor, *Electrochim. Acta*, 39, 531, 1994.
- [3] L.-W. H. Leung, M.J. Weaver, *Langmuir* 6, 323, 1990.
- [4] J.F.E. Gootzen, W. Visscher, J.A.R. van Veen, *Langmuir* 12, 5076, 1996.
- [5] R. Holze, *J. Electroanal. Chem.* 246, 449, 1988.
- [6] P.A. Christensen, A. Hamnett, *J. Electroanal. Chem.* 260, 347, 1989.
- [7] S. Sun, D. Yang, Z. Tian, *J. Electroanal. Chem.* 289, 177, 1990.
- [8] E. Pastor, S. Wasmus, T. Iwasita, M.C. Arevalo, S. Gonzalez, A.J. Arvia, *J. Electroanal. Chem.* 350, 97,

- 1993.
- [9] E. Pastor, S. Wasmus, T. Iwasita, M.C. Arevalo, S. Gonzalez, A.J. Arvia, *J. Electroanal. Chem.* 353, 81, 1993.
- [10] R.S. Goncalves, J.M. Legér, C. Lamy, *Electrochim. Acta* 33, 1581, 1988.
- [11] P.T.A. Sumodjo, E.J. da Silva, T. Rabockai, *J. Electroanal. Chem.* 271, 305, 1989.
- [12] M. Avramov-Ivic, J.-M. Leger, B. Beden, F. Hahn, C. Lamy, *J. Electroanal. Chem.* 351, 285, 1993.
- [13] E. Pastor, M.C. Arevalo, S. Gonzalez, A.J. Arvia, *Electrochim. Acta* 36, 2003, 1991.
- [14] U. Schmiemann, U. Muller, H. Baltruschat, *Electrochim. Acta* 40, 99, 1995.
- [15] B. Bittins-Cattaneo, S. Wilhelm, E. Cattaneo, H.W. Buschmann, W. Vielstich, *Ber. Bunsenges. Phys. Chem.* 92, 1210, 1988.
- [16] E. Pastor, S. Gonzalez, A.J. Arvia, *J. Electroanal. Chem.* 395, 233, 1995.
- [17] S.-G. Sun, Y. Lin, *J. Electroanal. Chem.* 375, 401, 1994.
- [18] O. Wolter, J. Heitbaum, *Ber. Bunsenges. Phys. Chem.* 88, 2, 1994.
- [19] R. Ianniello, V.M. Schmidt, U. Stimming, J. Stumper, A. Wallau, *Electrochim. Acta* 39, 1863, 1994.
- [20] D.S. Corrigan, M.J. Weaver, *J. Electroanal. Chem.* 239, 55, 1988.
- [21] B. Beden, A. Bewick, K. Kunimatsu, C. Lamy, *J. Electroanal. Chem.* 142, 345, 1982.
- [22] B.N.J. Persson, R. Ryberg, *J. Phys. Rev. B* 24, 6954, 1981.
- [23] A. Crossley, D.A. King, *Surf. Sci.* 95, 131, 1980.
- [24] B.E. Hayden, A.M. Bradshaw, *Surf. Sci.* 125, 187, 1983.
- [25] D. Hoge, M. Tüshaus, E. Schweizer, A.M. Bradshaw, *Chem. Phys. Lett.* 151, 230, 1988.
- [26] B.E. Hayden, K. Kretzschmar, A.M. Bradshaw, R.G. Greenler, *Surf. Sci.* 149, 406, 1985.
- [27] J. Fan, M. Trenary, *Langmuir* 10, 3649, 1994.
- [28] D. Howard Fairbrother, X.D. Peng, R. Viswanathan, P.C. Stair, M. Trenary, J. Fan, *Surf. Sci. Lett.* 285, L455, 1993.
- [30] B.A. Sexton, K.D. Rendulic, A.E. Hughes, *Surf. Sci.* 121, 181, 1982.
- [31] R. Shekhar, M.A. Barteau, *Cat. Lett.* 31, 221, 1995.
- [32] J.L. Davis, M.A. Barteau, *Surf. Sci.* 235, 235, 1990.
- [33] R. Shekhar, M.A. Barteau, *Surf. Sci.* 319, 298, 1994.
- [34] R. Ormerod, C.J. Baddeley, C. Hardacre, R.M. Lambert, *Surf. Sci.* 360, 1, 1996.
- [35] J. Shin, W.J. Tornquist, C. Korzeniewski, C.S. Hoaglund, *Surf. Sci.* 364, 122, 1996.
- [36] F. Solymosi, I. Kovacs, K. Révész, *Surf. Sci.* 356, 121, 1996.
- [37] C. French, I. Harrison, *Surf. Sci.* 342, 85, 1995.
- [38] Y.-N. Wang, J.A. Marcor, G.W. Simmons, K. Klier, *J. Phys. Chem.* 94, 7597, 1990.

On the adsorbates formed during the platinum catalyzed (electro)oxidation of ethanol, 1,2-ethanediol and methyl- α -D-glucopyranoside at high pH.

Abstract

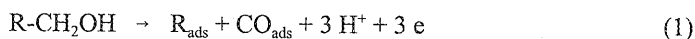
The irreversible adsorbates of ethanol, 1,2-ethanediol and methyl- α -D-glucopyranoside (MGP) have been studied with FTIRS and cyclic voltammetry. Both ethanol and 1,2-ethanediol display full C-C(OH) dissociative adsorption and dehydrogenation. In the case of ethanol adsorbed CO and C are formed of which the latter partially oxidizes further to adsorbed CO. In the case of 1,2-ethanediol CO is formed as the only adsorbate. The adsorption of MGP occurs similarly to the small alcohols; it decarbonylates to form adsorbed CO and a small fraction of C adatoms. It is shown that the catalytic alcohol oxidation can be regarded as an electrochemical process that consists of two independently acting half-reactions that determine the open circuit potential (o.c.p.). The roughness of the surface greatly affects the o.c.p. measured during catalytic alcohol oxidation; smooth platinum leads to high o.c.p. values and platinized platinum leads to low o.c.p. values. These low and high open circuit potentials correspond respectively to a diffusion limited regime where diffusion of oxygen is rate limiting and a kinetic regime. The reaction rate is considerably lower in the kinetic regime than in the diffusion limited regime. The surface is highly covered with adsorbed oxygen or hydroxyl during oxidation of ethanol and MGP in the kinetic regime, whereas the surface is devoid of adsorbed oxygen in the diffusion limited regime and is instead covered with a high steady state amount of CO and C species. The deactivation of the catalyst is found to occur both in the diffusion limited and in the kinetic regime of the MGP oxidation. Whereas in the diffusion limited regime the deactivation is caused by a slow accumulation of carbonaceous residue, in the kinetic regime changes in the properties of adsorbed oxygen cause deactivation.

5.1 Introduction

The platinum catalyzed oxidation of alcohols, especially polyols, in aqueous phase is attractive because of the mild reaction conditions and the high selectivities that can be obtained. In this way, various valuable intermediates for the food and pharmaceutical industry can be prepared. Catalytic oxidation also offers environmental advantages with respect to classical oxidation methods, since oxygen itself is reduced to water and thus waste production is low. A major problem in the catalytic oxidation of alcohols is the deactivation of the catalyst, that has been found for various catalytic oxidation reactions [1-9]. Four possible causes have been proposed to explain the deactivation phenomena; (i) chemical poisoning, (ii) overoxidation of the catalyst surface, (iii) corrosion and (iv) particle growth. Overoxidation is widely accepted as the probable cause of the loss of activity in catalytic literature, although some have found the adsorption of byproducts to be responsible for deactivation [2].

Electrochemical studies can provide valuable information on the catalytic oxidation of alcohols with oxygen in the liquid phase on supported platinum catalysts, since catalytic oxidation can be regarded as an electrochemical process. The electrocatalytic oxidation of small alcohols has received considerable interest in the context of possible applications in fuel cells [10]. As a result, most electrochemical studies have been carried out at low pH, so that carbon dioxide produced at the fuel cell anode is removed easily from the electrolyte, whereas at high pH carbonate is formed which accumulates in the electrolyte. This difference in reaction conditions complicates the translation of knowledge obtained with electrochemical studies to the catalytic alcohol oxidation.

These electrochemical studies have been combined with IR and mass spectrometry techniques that have been developed during the last two decades; reflection Fourier Transform IR spectroscopy (FTIRS) and Differential Electrochemical Mass Spectrometry (DEMS). These techniques have shown for primary alcohols at low pH that in addition to the formation of the acid and aldehyde, dehydrogenation and dissociation of the C-C(OH) bond occurs, leading to formation of adsorbed CO [11-18], according to:



It is important to note that CO has not only been observed after removal of the alcohol containing solution but also in the presence of high concentrations of the parent alcohol as in Figure 5 in Chapter 3. The concentrations of the alcohols were typically between 0.05 and 0.1 M [13, 17, 18]. This clearly demonstrates that CO formation is not blocked by the presence of adsorbed reactant or product molecules.

Little is known of the composition of the coadsorbates R_{ads} in equation 1 which are formed along

with CO and in previous papers we have paid attention to this subject [14,16]. The coadsorbates R display no further C-C bond breaking and are largely dehydrogenated. Part of the hydrocarbon adlayer can be hydrogenated at low potentials to the corresponding gaseous hydrocarbon whereas the other part is insensitive toward hydrogenation, probably due to graphite formation. The oxidation of C₁ can occur in the same potential region as for CO and at potentials where platinum is covered with oxides. Hydrocarbon adspecies containing two or more carbon atoms can only be oxidized to CO₂ in the oxide region.

It has been argued that, in addition to CO and R, irreversible adspecies are formed at low pH with the carbon backbone intact and several adsorbate structures have been proposed [12,17,18]. The few FTIRS experiments that have been carried out in basic electrolyte for ethanol and 1,2-ethanediol have established the formation of CO [11,19,20], but no claims have been made up to now that adspecies are formed with the carbon backbone intact. For secondary alcohols it is generally found that no CO is formed during adsorption [13,21,22]. The energy required to break two C-C bonds is apparently too high to enable CO formation. In the electrochemical literature CO has been generally indicated as the species that is responsible for poisoning of the alcohol electro-oxidation [10,13]. Therefore, the electrooxidation of alcohols only starts at potentials where CO is being oxidized to CO₂, generating free platinum sites. In Chapter 4 we suggested that not only CO is responsible for poisoning, but that the coadsorbates R_{ads} that are formed along with CO in the dissociative adsorption will also contribute to poisoning [16].

As yet it is unclear how to translate the observations made in electrochemical systems to the catalytic oxidation. Whereas CO formation is usually observed in electrochemical studies, the possibility of CO poisoning is not considered in papers concerning catalytic oxidations. For several reasons a comparison between electrochemical and catalytic oxidation is tentative. Electrocatalytic studies have generally involved simple alcohols and smooth platinum electrodes, whereas catalytic studies have been performed with complex cyclic polyols and carbon supported platinum catalysts. In addition, electrochemical studies use cyclic voltammetry, implying non-stationary conditions, whereas catalytic studies use stationary conditions. Up till now, open circuit potential measurements of catalytic reactions have provided the important insight that deactivation of the catalyst is accompanied by an increase of the catalyst potential [1,2,4,7-9]. There is no consensus, however, on the interpretation of this result. It has been attributed as an increase of the oxygen coverage as well as a result of site coverage by reactants, intermediates, or products.

The main theme of this chapter concerns the state of the catalytic surface during selective oxidation of alcohol compounds at high pH. The reaction conditions were varied such that the reaction rate was either limited by diffusion of oxygen or kinetically limited. We have chosen to study the oxidation of ethanol, which has been used as model compound in electrochemical and catalytic studies, and methyl- α -D-glucopyranoside (MGP), a cyclic polyol that can be selectively oxidized to methyl- α -D-glucosiduronate, an intermediate in the synthesis of vitamin

C. The irreversible adsorbates present during reaction were isolated and studied thereafter with cyclic voltammetry and FTIRS. The catalyst is known to deactivate during oxidation of MGP and special interest will be given to this reaction to establish the causes of deactivation. In order to obtain insight in the fundamental adsorption behaviour of alcohols, the composition of the adsorbates formed from ethanol, 1,2-ethanediol and MGP were studied with cyclic voltammetry and FTIRS. The results will be compared to those for acid electrolytes.

5.2 Experimental

Fourier Transform Infrared measurements were performed with a Biorad FTS 45A spectrometer, equipped with a liquid nitrogen cooled MCT detector. All IR spectra were recorded with 4 cm^{-1} resolution. The bottom of the electrochemical cell consists of an CaF_2 prism with 65° beveled edges. The platinum electrode has a diameter of 9 mm and is embedded in a PTFE holder. P-polarized light has been used in all IR measurements. Electrochemical measurements were performed with an Autolab PGSTAT 20 computer controlled potentiostat and a EG&G Parc model 175 universal programmer connected to a Wenking POS 73 potentiostat. A Hg/HgO electrode was used as a reference-electrode. All potentials will be referred to RHE. All measurements were performed with platinized platinum, that was obtained via electrodeposition from a $0.05\text{ M H}_2\text{PtCl}_6 + 0.01\text{ M HCl}$ solution on smooth platinum. Potential cycling between 0 and 1.5 V was carried out until a stable voltammogram was obtained. Electrolytes were prepared using ultrapure water ($18.2\text{ M}\Omega$) obtained with an Elga water purification system. In the infrared experiments and cyclic voltammetry experiments 0.1 M KOH was used. Oxygen was removed from the electrolyte with Argon 4.6.

Adsorption experiments were performed at 0.35 V for 10 minutes with 1 mM or 5 mM concentrations of the various alcohol compounds in 0.1 M KOH . CO (Hoek Loos, purity 4.6) was adsorbed at 0.15 V by leading CO through the solution for 10 minutes. All other chemicals, p.a. quality, were obtained from Merck. After adsorption the electrolyte was replaced by fresh 0.1 M KOH solution, while keeping the electrode at the adsorption potential.

5.3 Results

5.3.1 Adsorbate study

Ethanol was adsorbed from a 1 mM containing electrolyte solution at 0.35 V for 10 minutes. An anodic current was observed during adsorption, that amounts to a total charge of $323\text{ }\mu\text{C}/\text{cm}^2$. The ethanol solution is replaced by fresh electrolyte after adsorption and a cyclic voltammogram

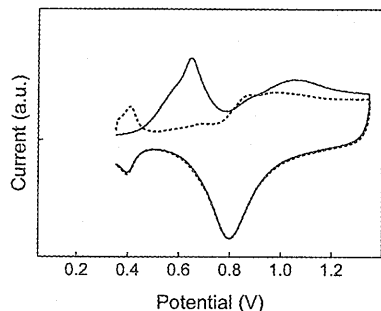


Fig. 1: C.V. of the oxidation of irreversible ethanol adsorbate on platinumized platinum: 'direct' oxidation (—) and blank (---). $E_{ads} = 0.35$ V in 1 mM ethanol in 0.1 M KOH, followed by electrolyte exchange. Scan rate 5 mV/s

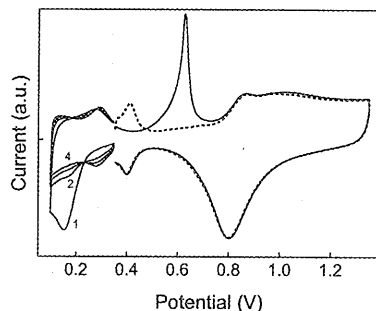


Fig. 2: C.V. of the oxidation of irreversible ethanol adsorbate on platinumized platinum: 'indirect' oxidation (—) and blank (---). $E_{ads} = 0.35$ V in 1 mM ethanol in 0.1 M KOH, followed by electrolyte exchange. Scan rate 5 mV/s.

is subsequently recorded. If the scan is started at the adsorption potential in the positive direction, referred to as 'direct' oxidation, a broad peak is present at 0.65 V, as shown by the full line in Figure 1. The dashed curve represents the voltammogram recorded in blank electrolyte. A broad oxidation wave is present in the oxide region, that is not completely terminated at the reversal potential of 1.35V. However, the amount of charge associated with oxidation of adsorbate in a second cycle is only very small. If the oxidation is preceded by cycling 4 times through the hydrogen region, referred to as 'indirect oxidation', then a reduction wave is observed at potentials below 0.25 V as shown in Figure 2. The subsequent oxidation at 0.65 V has narrowed and shifted to 0.60 V. The broad oxidation wave at higher potential has nearly completely vanished. The total oxidation charge, including the peak at low potential as well as the broad wave at higher potential, has decreased from 263 $\mu\text{C}/\text{cm}^2$ for the 'direct' oxidation to 130 $\mu\text{C}/\text{cm}^2$ for 'indirect' oxidation. The charge involved in the reduction, Q_{red} , can be determined by subtracting the charge involved in the anodic part of each cycle below 0.35 V from the charge involved in the cathodic part of the scan below 0.35 V, adding up the charges of the 4 reduction cycles. The cathodic part of the scan consists of both reduction of adsorbate and formation of adsorbed hydrogen from solution protons on uncovered platinum sites. The anodic part of the scan only consists of oxidation of adsorbed hydrogen. Subtracting both values gives the charge involved in reduction; $Q_{red} = 122 \mu\text{C}/\text{cm}^2$. Note that hydrogen that is liberated during adsorption by C-H bond breaking is immediately oxidized to H^+ during the adsorption and is thus not involved in the reactions described here.

The cyclic voltammogram of 1,2-ethanediol adsorbates formed at 0.35 V from 1 mM 1,2-ethanediol shows no significant reduction in the potential region below 0.35 V, in contrast with ethanol. This means that the 1,2-ethanediol adsorbates are insensitive toward hydrogenation. Only an oxidation wave is present at 0.60 V with a shoulder at 0.57 V, as shown in Figure 3. No oxidation wave is observed at potentials in the oxide region. The total oxidation charge in the

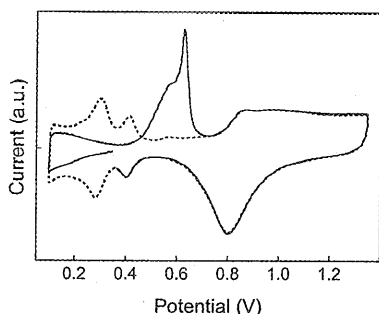


Fig. 3: C.V. of the oxidation of irreversible 1,2-ethanediol adsorbates: 'indirect' oxidation (—) and blank (---). $E_{ads} = 0.35$ V in 1 mM 1,2-ethanediol in 0.1 M KOH, followed by electrolyte exchange. Scan rate 5 mV/s.

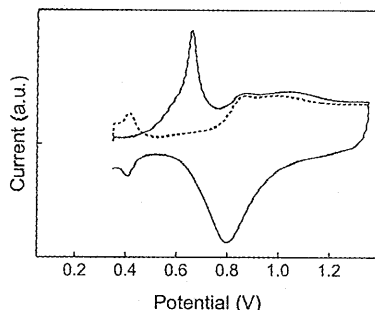


Fig. 4: C.V. of the oxidation of MGP adsorbates: 'direct' oxidation (—) and blank (---). $E_{ads} = 0.35$ V in 1 mM MGP in 0.1 M KOH, followed by electrolyte exchange. Scan rate 5 mV/s.

cyclic voltammogram is $198 \mu\text{C}/\text{cm}^2$ and the charge transferred during adsorption was $269 \mu\text{C}/\text{cm}^2$, which leads to a Q_{ads}/Q_{ox} ratio of 1.36.

The cyclic voltammogram recorded after adsorption of 5 mM methyl- α -D-glucopyranoside at 0.35 V is depicted in Figure 4. In the direct oxidation, represented by the solid line, a peak is present at 0.65 V in the double layer region and a small broad oxidation wave is present in the potential region between 1.05 and 1.35 V in the oxide region. The amount of charge involved at high potential is considerably lower than for ethanol, making the voltammogram similar to that of 1,2-ethanediol. The total oxidation charge, including the peak at low potential as well as the broad wave at higher potential is $250 \mu\text{C}/\text{cm}^2$ for the 'direct' oxidation.

For comparison, we measured the cyclic voltammogram of CO, that was adsorbed at 0.15 V for 10 minutes, followed by electrolyte exchange. As shown in Figure 5, the oxidation of adsorbed CO starts at 0.25 V and displays three peaks at 0.38, 0.57 and 0.63 V. The oxidation peaks at 0.63 and 0.57 V are in agreement with a previous study of adsorbed CO on polycrystalline platinum in KOH electrolyte [23]. This study further showed the peak positions to depend

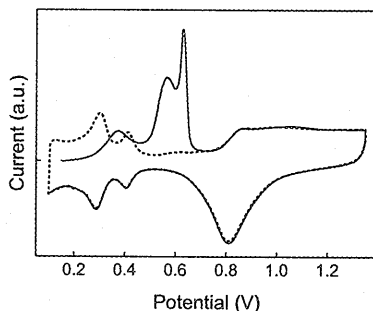


Fig. 5: C.V. of the oxidation of adsorbed CO on platinumized platinum in 0.1 M KOH. $E_{ads} = 0.15$ V. Scan rate 5 mV/s.

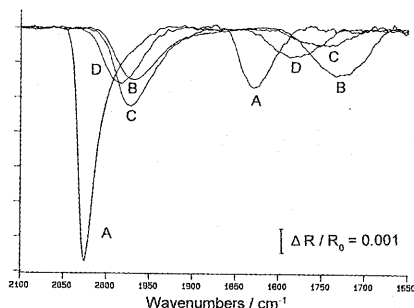


Fig. 6: FTIRS spectrum, given as $R_0 - R_1/R_0$, in the wavenumber region for CO_{lin} and $\text{CO}_{\text{bridge}}$, after adsorption of (A) CO, (B) 1,2-ethanediol, (C) ethanol and (D) MGP at 0.15 V for CO and 0.35 V for the alcohols. Resolution 4 cm^{-1} , $E_0 = E_1 = 0.35 \text{ V}$.

strongly on the scan rate used and a third oxidation peak at 0.44 V was observed only at a sufficient low scan rate of 4 mV/s. In our experiments this peak is observed even at much lower potential, probably as a result of a lower adsorption potential. It is remarkable that adsorbed CO can be susceptible toward oxidation at such a low potential, where platinum is usually covered with hydrogen, thus expecting reducing conditions instead of oxidizing conditions. It is for the first time that adsorbed CO is found to oxidize at such a low potential. Comparison of the cyclic voltammogram obtained for CO with those of 1,2-ethanediol, ethanol and MGP shows that it is very similar to that of 1,2-ethanediol, but differs somewhat from that of ethanol and MGP.

We have also performed adsorption experiments of CO, ethanol and 1,2-ethanediol at 0.45 V, which will not be extensively discussed here. We confine ourselves to the remark that all charges involved in the oxidation of adsorbates formed at 0.45 V are approximately 30% lower than after adsorption at 0.35 V, due to considerable further oxidation of the initially formed adsorbate. This was confirmed by the observation that the current did not converge to zero during adsorption. IR spectra were obtained by subtracting single-beam spectra before (R_0) and after (R_1) oxidation of the adsorbate. The first single beam was obtained at the adsorption potential of 0.35 V whereas the second was obtained at 0.35 after a potential excursion to 1.35 V. Figure 6 compares the spectra, given as $\Delta R/R_0$ ($\Delta R = R_0 - R_1$), in the wavenumber region between 2100 and 1600 cm^{-1} as obtained for ethanol, 1,2-ethanediol, MGP and CO. This wavenumber region is typical for linear and bridge bonded CO. It is clear from the vibrations around 2050 and 1800 cm^{-1} that both linear and bridge bonded CO are present on the surface. The relative amount of bridge bonded CO is larger than was observed in acid electrolyte [14]. The CO vibrations for the various alcohol compounds are smaller than after adsorption of CO and they have shifted to lower wavenumbers as expected for decreasing CO coverage. Although the CO coverage is not exactly proportional to the integrated absorbance, it can nevertheless give a fair indication. Whereas the CO peaks of the alcohols in Figure 6 appear much smaller than for pure CO, the integrated CO absorbances, and thus the CO coverages, are nevertheless considerable due to the broadness of the IR peaks.

5.3.2 Measurement of open circuit potentials: implications of surface roughness

We have determined the effect of surface roughness on the open circuit potentials measured during catalytic ethanol oxidation. Before measurement of the o.c.p., the solution was saturated with oxygen for 15 minutes, while keeping the electrode in a reduced state at 0.1 V. During the actual o.c.p. measurement oxygen was led over the solution. Figure 7 shows the o.c.p. for smooth and platinized platinum in a solution of 0.1 M ethanol in 0.1 M KOH. For smooth platinum the o.c.p. quickly rises to 1 V whereas for platinized platinum the o.c.p. stabilizes at 0.35 V. When oxygen was passed through instead of over the solution, the o.c.p. increased for platinized platinum, the value depending on the flow rate. It is well known that the rate of the electrochemical reduction of oxygen at 0.35 V under the conditions used is diffusion limited, whereas the electrochemical oxidation of ethanol is kinetically limited. Therefore, introducing convection in the cell does not influence the rate of ethanol oxidation whereas the rate of oxygen reduction increases. It follows then that the increase of the o.c.p. when oxygen was passed through instead of over the cell is a result of the improved oxygen transport to the electrode. The open circuit potential of 0.35 V during ethanol oxidation indicates that no adsorbed oxygen is present on the surface during reaction. For smooth platinum the o.c.p. did not change when oxygen was led through the solution, indicating that the reaction rate is kinetically limited. The o.c.p. of 1 V indicates that a high coverage of adsorbed oxygen- or hydroxylspecies is present. The large difference between the open circuit potential for smooth and platinized platinum originates from the difference in roughness, which will be discussed in the next section. According to the additivity principle of Wagner and Traud [24] the open circuit potential can be envisaged as the potential where the two half reactions each proceed with the same current, although of opposite sign. However, this only holds when the redox couples act independently. We performed some simple experiments on platinized platinum to check whether this was the case for the catalytic ethanol oxidation by measuring separately the oxygen reduction current and the oxidation current in 0.1 M ethanol at 0.35 V, which corresponds to the o.c.p. measured for

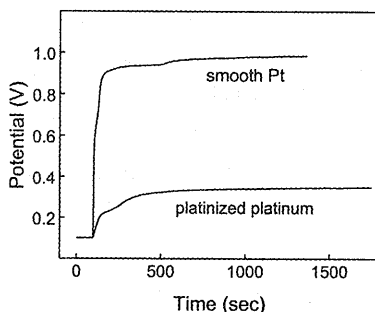


Fig. 7: Open circuit potential during catalytic oxidation of 0.1 M ethanol in 0.1 M KOH with O_2 on smooth and platinized platinum. The catalyst was reduced at 0.1 V before the measurement.

the catalytic ethanol oxidation on platinized platinum, as shown in Figure 7. In accordance with the Wagner and Traud principle, we found the current values for oxygen reduction and ethanol oxidation to be exactly the same but of opposite sign, which confirms that the catalytic oxidation of ethanol with oxygen can be envisaged as an electrochemical process consisting of two independently acting half reactions. In agreement with this conclusion we found that the presence of 0.1 M ethanol had absolutely no effect on the size of reduction current of oxygen at 0.1 V, where ethanol oxidation does not yet occur.

5.3.3 Isolation of adsorbates present during diffusion limited oxidation

We devised an experiment to isolate the adsorbates that are present on the surface during the diffusion limited oxidation of the alcohol on platinized platinum. This consists of interruption of the oxidation by applying a potential of 0.15 V, where the oxidation reaction stops and intermediates can be hydrogenated off the surface. Among the irreversible C-C(OH) dissociative adsorbates that are possibly present during reaction, CO will remain on the surface at 0.15 V, whereas CH_x species can be hydrogenated off the surface. The catalytic oxidation was carried out in a quiescent solution of 1.7 mM ethanol in 0.1 M KOH, saturated with oxygen. The o.c.p. stabilized at 0.41 V and was only weakly dependent on the ethanol concentration; for 17 mM ethanol the open circuit potential shifted to 0.38 V. After 5 minutes of reaction at this potential, the reaction was interrupted by the potential step to 0.15 V and the oxygen supply was stopped and replaced by argon. Subsequently, the reactant solution was replaced by fresh 0.1 M KOH electrolyte, followed by cyclic voltammetric analysis of the adsorbate layer. The resulting voltammogram is shown as the full line in Figure 8. The dashed line represents the second cycle, being equal to a cyclic voltammogram recorded in blank KOH. The ethanol oxidation was also carried out electrochemically at 0.41 V, in the absence of oxygen. The cyclic voltammogram recorded afterward, represented by the dashed-dotted line in Figure 8, coincides almost completely with the solid line, indicating that the same adsorbates are present during catalytic and electrochemical oxidation. The charge involved in the oxidation of the adsorbates is $113 \mu\text{C}/\text{cm}^2$ and it follows from this that the surface is considerably covered with adsorbates. Note that during the potential step to 0.15 V loss of C adspecies occurs, implying that the actual coverage is even higher.

The irreversible adsorbates formed during ethanol oxidation on platinized platinum were also studied with FTIRS, although under slightly different conditions; the electrode had a smaller roughness and the ethanol concentration was increased to 10 mM. The open circuit voltage established at 0.46 V under these conditions. After 5 minutes the potential was stepped to 0.15 V and the electrolyte was exchanged for fresh base electrolyte, followed by the IR measurement. The IR spectra obtained after electrochemical and catalytic oxidation are shown in Figure 9 in the wavenumber region between 2200 and 1100 cm^{-1} . The negative bands at 1980 and 1725 cm^{-1} originate from linear and bridge bonded CO, respectively. The positive band at 1400 cm^{-1}

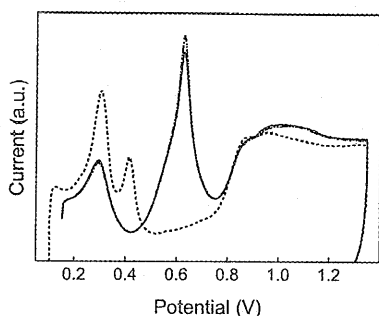


Fig. 8: C.V.'s after catalytic (—) and electrochemical (---) ethanol oxidation at 0.41 V on platinumized platinum, followed by a potential step to 0.15 V and electrolyte replacement. Scan rate 5 mV/s.

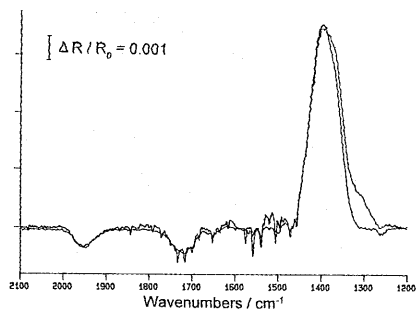


Fig. 9: FTIR spectra, given as $R_0 - R_1 / R_0$ after catalytic and electrochemical oxidation at 0.46 V on platinumized platinum, followed by a potential step to -0.8 V and electrolyte replacement. Resolution 4 cm^{-1} , $E_0 = E_1 = 0.46$ V.

originates from carbonate species that are formed in the oxidation of the adsorbate. The IR experiments confirm the voltammetry experiment, showing that electrochemical and catalytic oxidation result in the same adsorbates during reaction. When the electrochemical oxidation of 1.7 mM ethanol on platinumized platinum was performed at 0.55 V instead of 0.41 V as described above, the voltammogram shown in Figure 10 is obtained after a potential step to 0.15 V, followed by electrolyte exchange. The coverage of irreversible adsorbates is now very low, in contrast with the results for 0.41 V. However, when the experiment was repeated at 0.55 V with a tenfold higher ethanol concentration, the adsorbate coverage increases considerably. These observations show that for 1.7 mM ethanol the reaction rate was determined by diffusion of ethanol to the surface, whereas for 17 mM the rate was kinetically limited. FTIR experiments give further information on the products formed during the diffusion limited and kinetically rate limited ethanol oxidation. An experiment was performed in which a potential scan was made from 0.25 V, where a reference IR spectrum was recorded, to 0.55 V in the presence of 17 mM ethanol. The first spectrum recorded at 0.55 V contained two clear peaks at 1405 cm^{-1} and 1550 cm^{-1} of approximately equal size. These vibrations can be assigned to the presence of acetate in the thin layer. However, the ratio of the peak heights for the two vibrations differs from the ratio expected for acetate. This indicates that also carbonate is formed, which displays a single vibration at 1402 cm^{-1} . A second IR spectrum that was recorded at 0.55 V immediately after the first, displays a growth of the band at 1402 cm^{-1} , whereas the band at 1550 cm^{-1} remains equal. This indicates that now the acetate formation has stopped and carbonate is formed as the only product. When the electrode is pulled up from the CaF_2 window into the bulk of the solution, the current increases suddenly, indicating that the reaction had become diffusion limited during the FTIR measurement. This demonstrates that carbonate is formed as the only product when the rate of electrochemical ethanol oxidation becomes limited by diffusion of ethanol to the surface. A control experiment was carried out with an ethanol concentration of 0.1 M, which is high

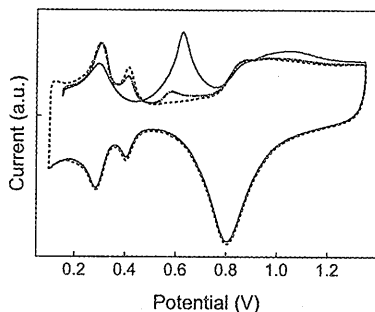


Fig. 10: C.V.'s obtained after ethanol oxidation at 0.55 V for 1.7 mM (---) and 17 mM (—), followed by potential step to 0.15 V and electrolyte replacement.

enough to prevent the diffusion of ethanol to be rate limiting. Indeed, only bands at 1405 and 1550 cm^{-1} were observed, indicating that acetate was the major product in this situation.

The same trends were obtained when the experiments were performed with MGP, apart from the fact that the open circuit potential does not reach a constant value, as described in the next section.

5.3.4 Catalyst deactivation during MGP oxidation

Some experiments were performed to study the deactivation of the catalytic oxidation of methyl- α -D-glucopyranoside. Figure 11 shows the o.c.p. as a function of time for the catalytic oxidation of 50 mM MGP on a platinized platinum catalyst in 0.1 M KOH saturated with oxygen. Before the start of the measurement the potential was held at 0.1 V in order to reduce the surface. Figure 11 shows that in contrast with ethanol the o.c.p. steadily increases in time, until it reaches a value of 0.8 V whereafter it increases to 0.99 V, where it remains stable as long as 16 hours. This steady increase is in agreement with previous experiments for MGP oxidation on platinized platinum [1]. When oxygen is passed through the solution during the experiment the o.c.p. increased in the low potential region, whereas no effect was observed when the o.c.p. was 0.99 V. This shows that the reaction is diffusion limited in oxygen for low potentials and is kinetically limited at 0.99 V. The o.c.p. also increases faster when oxygen is led through the solution.

We used the same experimental procedure as described for ethanol to study the irreversible adsorbates that are present on the surface during reaction. In this way we can obtain information concerning the steady increase of the open circuit potential in Figure 11. After a certain reaction time a potential of 0.35 V is applied, followed by exchange of the solution for fresh 0.1 M KOH. The potential of 0.35 V was chosen to prevent eventually present carbon species to be reduced off the surface, in contrast with the value of 0.15 V used for ethanol. Note however, that at 0.35 V further C-C(OH) dissociative adsorption of MGP can occur. After electrolyte exchange, a cyclic voltammogram is recorded to analyze the adsorbates that are formed during reaction,

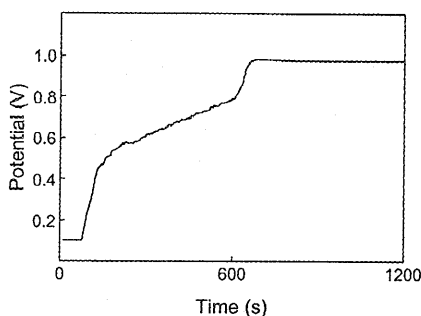


Fig. 11: Open circuit potential during the catalytic oxidation of 50 mM MGP in 0.1 M KOH on platinumized platinum.

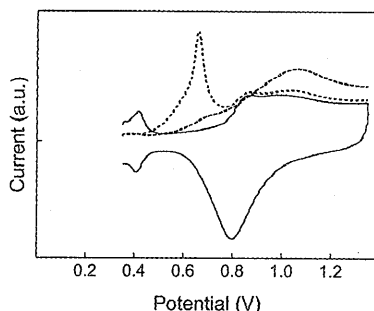


Fig. 12: C. V.'s recorded after catalytic MGP oxidation for 1 minute (—) and 10 minutes (---), followed by potential step to 0.35 V. Blank (· · ·). Scan rate 5 mV/s.

shown in Figure 12. We found profound changes in the cyclic voltammogram that were recorded after various reaction times, corresponding to catalytic oxidation at different open circuit potentials. After 1 minute reaction time the oxidation peak in the double layer region is large, whereas the broad oxidation wave in the oxide region was small. For increasing reaction time and increasing open circuit potential, the CO-like peak at low potential decreased whereas the broad wave at high potentials increased. We plotted in Figure 13 the charge involved in the peaks at low and high potentials as a function of reaction time. It is clearly shown that the increase of the reaction potential is correlated with changes in the adsorbates that are present on the surface during reaction.

We performed some further experiments to see whether reduction treatments during reaction can reactivate the catalyst. The experiment was started with clean platinumized platinum, that is exposed to a solution of 10 mM MGP saturated with oxygen. The increase of the open circuit potential with time is shown in Figure 14. After 10 minutes, a potential of 0.45 V is applied, at which platinum oxides are reduced immediately off the surface to water, whereas reducible hydrocarbon fragments remain on the surface. Figure 14 shows that indeed some reactivation occurs as indicated by the lowered open circuit potential. However, the potential increases fast and seems to continue the initial curve. When the potential is stepped to 0.1 V, the open circuit potential decreases more and equals the curve measured for clean platinum.

It is remarkable that once the potential has reached 0.99 V it remains constant for long times at 0.99 V, whereas it has been reported that the catalyst deactivates during operation in the kinetic regime [1,4,25]. Therefore, we performed some experiments to study the characteristics of the MGP oxidation at high potentials. We performed some experiments in which the MGP oxidation was carried out electrochemically at 0.99 V. Before the start of the reaction the potential was held at 0.1 V to reduce the surface. Figure 15 shows that the current decreases in

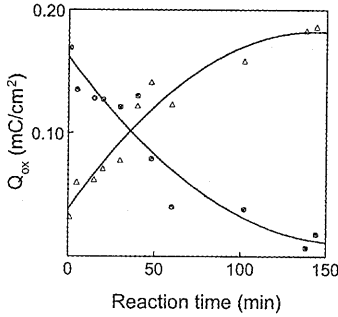


Fig. 13: Charge Q_{ox} involved in the oxidation waves at low (-) and high (+) potentials after catalytic MGP oxidation for various times, followed by a potential step to 0.35 V and electrolyte replacement.

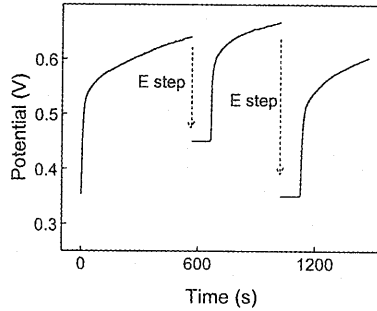


Fig. 14: Open circuit potential during catalytic MGP oxidation and the effect of potential during reductive treatment.

time. After 30 minutes the imposed potential was removed, whereafter the equilibrium potential established. As shown in Figure 15 this results in a quick decrease of the potential to 0.25 V. After 2 minutes the imposed potential of 0.99 V was restored again and the current recovered its original value, indicating that the catalyst was reactivated. These results are similar to those obtained for the catalytic MGP oxidation on carbon supported platinum catalysts in a slurryphase reactor [1]. This experiment was repeated except that the reaction was now interrupted by a potential step to either 0.45 or 0.1 V. At 0.45 V oxides are reduced and carbon species remain unaffected whereas both oxides and carbon species are reduced at 0.1 V. We found that after a

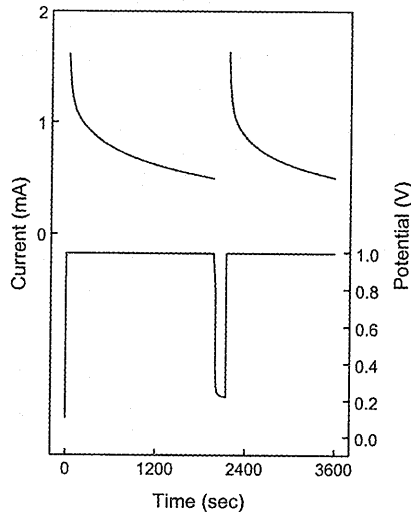


Fig. 15: Deactivation of MGP oxidation in time at 1.0 V and reactivation at open circuit potential. MGP concentration = 50 mM.

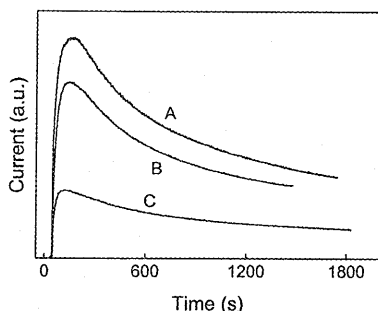


Fig. 16: The oxidation of 50 mM MGP in time at 0.99 V on electrodes preoxidized at 0.99 V for (A) 0, (B) 15 and (C) 60 minutes.

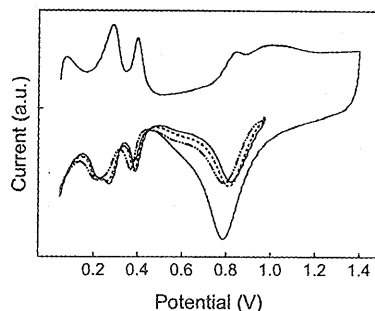


Fig. 17: The reduction of platinum oxide after polarization of the platinized platinum electrode for 0 (—), 15 (---) and 60 minutes (-.-.) at 0.99 V.

potential step to both 0.45 V and 0.1 V the activity is restored to the same value when the potential was stepped subsequently to 0.99 V.

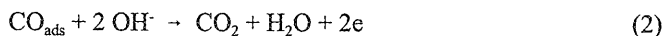
These results suggest that the state of adsorbed oxygen plays a role in the deactivation of the MGP oxidation. We further investigated the role of adsorbed oxygen by preoxidizing the electrode surface at 0.99 V for a fixed time in base electrolyte before admitting an MGP containing solution to the cell. With this experiment we can establish whether deactivation is strictly related to MGP oxidation or relates solely to the properties of the adsorbed oxygen species. Three current-time curves after 0, 15 and 60 minutes preoxidation are given in Figure 16, which show that the MGP oxidation current has decreased considerably after preoxidation of the platinum electrocatalyst. However, it is remarkable that the initial rate after 15 minutes of preoxidation, curve B, does not correspond to the oxidation after 15 minutes MGP oxidation in curve A in Figure 16. Apparently the rate of deactivation is higher in the presence of MGP. Nevertheless, it has been demonstrated that time dependent changes in the oxide covered platinum surface are involved in the deactivation of MGP oxidation. We also recorded cyclic voltammograms to study the electrochemical reduction of the formed oxygen adsorbates during preoxidation. The results are given in Figure 17 and it is shown that the oxide reduction peak slightly shifts to negative potentials for increasing preoxidation times. It is not possible from these voltammograms to determine whether the oxygen coverage might have increased a little because the broad oxygen reduction peak is difficult to integrate.

The current for MGP oxidation in Figure 15 can be translated to turnover frequencies per Pt atom, when it is assumed that the oxidation of MGP to MGP-ox is 100% selective and thus $4e$ are consumed; this yields 0.0016 MGP/(Pt sec) for $t=1200$ seconds. This value is in good agreement with the reaction rates found for carbon supported platinum catalysts in a slurry phase reactor at $\text{pH} = 8$ operated in the kinetic regime [1,4].

5.4 Discussion

5.4.1 Adsorbate study

The observation of considerable amounts of both linear and bridge bonded CO on platinized platinum with FTIRS for 1,2-ethanediol and ethanol demonstrates that these molecules decarbonylate during adsorption, at least to a certain extent. The formation of adsorbed CO at high pH has also been observed with EMIRS in the presence of 1,2-ethanediol [26], whereas no CO vibrations were observed with FTIRS [11]. A FTIRS study of ethanol adsorbates on platinum single crystals in NaOH electrolyte has shown that only linearly bound CO is formed on Pt(110), solely bridge bonded CO is formed on Pt(100) and no CO vibration was observed on Pt(111) [19]. On the basis of these results we can ascribe the linear and bridge bonded CO vibrations in our spectra to CO species adsorbed on Pt(110) and Pt(100) related sites on the electrode surface. These two surface geometries each correspond to a pair of hydrogen adsorption/desorption peaks in the cyclic voltammogram in Figure 1. This assignment of the hydrogen peaks in the cyclic voltammogram can also be made for platinum in acid electrolyte and is in accordance with an extensive electrochemical study of hydrogen desorption on single crystals [27]. The strongly bonded hydrogen peak at 0.41 V can be assigned to a stepped (100) surface, e.g. (210), (310) and (410), whereas the weakly bonded hydrogen peak originates from a Pt(110) surface geometry. The $Q_{\text{ads}}/Q_{\text{ox}}$ values of 1.23 and 1.36 for ethanol and 1,2-ethanediol, respectively, give additional quantitative information on the composition of the irreversible adsorbates. In the case of 1,2-ethanediol the value of 1.36 suggests that in the total oxidation of this molecule to CO_2 , 5.8 electrons are transferred during adsorption and 4.2 electrons are transferred during oxidation of the adsorbate. Since 2 CO_2 molecules are formed in the oxidation of a single 1,2-ethanediol molecule, it follows that $4.2/2 = 2.1$ electrons are transferred per CO_2 molecule in the oxidation of the adsorbate. This value is within the margin of error equal to the value of 2 for CO according to:

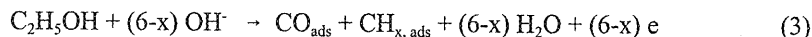


In addition, the absence of a reduction at potentials below 0.35 V and the absence of an oxidation at high potentials in the oxide region confirm that CO is the only adsorbate formed in the adsorption of 1,2-ethanediol. We found in a previous study [14] in acid electrolyte likewise that the adsorption of 1,2-ethanediol is completely dissociative. This implies that the adsorption of 1,2-ethanediol is independent of the pH and the type of electrolyte used. In accordance with this conclusion, the oxidation profile of the 1,2-ethanediol adsorbate shows a close resemblance with the oxidation profile of CO, apart from the lower coverage for 1,2-ethanediol with respect to CO. However, the adsorption of CO was performed at 0.15 V, whereas 1,2-ethanediol was adsorbed

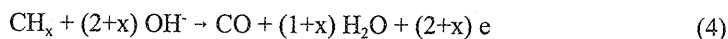
at 0.35 V. When the curve in Figure 3 is compared with a voltammogram of CO that is also adsorbed at 0.35 V, only a small difference remains. The lower coverage for 1,2-ethanediol is probably due to spatial requirements of the C-C dissociative reaction.

The three peak structure for CO oxidation has been observed earlier for polycrystalline platinum [23], in contrast with single crystal studies, that generally report a single oxidation peak for the various crystal planes. Only at high coverages a prewave is observed for Pt(100) in carbonate electrolyte [28]. We can assign the main oxidation peaks at 0.63 and 0.57 V in the cyclic voltammogram to the different crystal planes that are predominant at the electrode surface. Comparing the voltammograms in Figure 2 and 3 for ethanol and 1,2-ethanediol provides further evidence for the assignment of the CO oxidation peaks. The shoulder at 0.57 V is much more pronounced in Figure 3 for 1,2-ethanediol than for ethanol in Figure 2. Moreover more weakly bonded hydrogen is present after adsorption of ethanol with respect to 1,2-ethanediol. This shows that there is a close correlation between the weakly bonded hydrogen sites and the CO oxidation wave at 0.57 V. In combination with the FTIRS results we can assign the oxidation peak at 0.57 V to linear adsorbed CO on Pt(110) related sites whereas the oxidation peak at 0.63 V can be assigned to bridge bonded CO on Pt(100) related sites. The third CO oxidation at 0.38 V originates from adsorbed CO molecules that are very weakly bonded and therefore we can correlate this oxidation wave with the presence of a densely packed CO adlayer, on one or both crystal planes.

In the case of ethanol, the $Q_{\text{ads}}/Q_{\text{ox}}$ value of 1.23 indicates that of the 12 electrons transferred in the total oxidation of an ethanol molecule to CO_2 , 6.6 electrons are involved in the adsorption and 5.4 electrons are transferred in the oxidation. Since two CO_2 molecules are formed in the total oxidation of a single ethanol molecule, this implies that 2.7 electrons per CO_2 molecule are involved. This value is close to the characteristic value for CO, indicating that the molecule is largely dehydrogenated. The integrated CO absorbances for 1,2-ethanediol and ethanol are approximately of the same size and since full decarbonylation was concluded for 1,2-ethanediol this leads to the conclusion that ethanol adsorbs also fully dissociative, according to:



Quantitative analysis of the n_{ox} value then shows that a follow-up oxidation of CH_x to CO occurs after the initial C-C(OH) dissociative reaction. Formation of equal amounts of CO and CH_x would result in n_{ox} values between 3 ($x=0$) and 4.5 ($x=3$). An n_{ox} value lower than 3 can only be obtained when one of the adsorbates has oxidized further than C and therefore we conclude that the value of 2.7 originates from a follow-up oxidation of CH_x to CO according to:



We have concluded in a previous study [14] that the same follow up reaction of CH_x also occurs in acid electrolyte, where $n_{\text{ox}} = 2.5$ was found. A recent FTIRS study [29] using labeled ethanol provided direct spectroscopic proof for this reaction, as shown by the formation of $^{13}\text{CO}_{\text{ads}}$ from $^{13}\text{CH}_3\text{CH}_2\text{OH}$ at potentials equal to the adsorption potential used by us in acid electrolyte.

An important difference between ethanol and 1,2-ethanediol is the presence of a reduction below 0.35 V for ethanol. This reduction was also reported for Pt(110) [19] and polycrystalline Pt [10] in contrast with Pt(100) and Pt(111) [19]. No interpretation of this reduction peak has been given up to now, but we assign this peak to the reduction of CH_x to CH_4 according to:



Due to the removal of CH_x species in the reduction, the amount of charge involved in the subsequent oxidation in Figure 2 is lower than in the 'direct' oxidation in Figure 1. The ratio of the reduction charge and the decrease in the oxidation charge $Q_{\text{red}}/\Delta Q_{\text{ox}}$ gives information on the oxidation state of the CH_x species that have been reduced to CH_4 . The ratio $Q_{\text{red}}/\Delta Q_{\text{ox}} = 0.9$ found here in KOH electrolyte demonstrates that the CH_x species are fully dehydrogenated to C, since both in the reduction of C to CH_4 and the oxidation of C to CO_2 , 4 electrons are involved, giving $Q_{\text{red}}/\Delta Q_{\text{ox}} = 1$. In the case of CH or CH_2 , $Q_{\text{red}}/\Delta Q_{\text{ox}}$ values of 0.6 and 0.33 would have been expected.

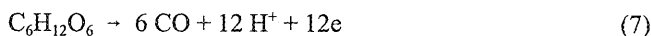
Combining the n_{ox} values found for ethanol and 1,2-ethanediol with the oxidation charges determined with cyclic voltammetry gives the adsorbate coverage according to:

$$\theta = \frac{Q_{\text{ox}}}{(n_{\text{ox}} Q_{\text{H}}^0)} \quad (6)$$

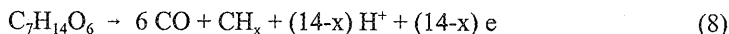
where Q_{H}^0 is the charge involved in the desorption of a monolayer of hydrogen, determined in blank electrolyte. This procedure results in adsorbate coverages of 0.45 for ethanol and 0.46 for 1,2-ethanediol. In the case of 1,2-ethanediol the adlayer consists completely of CO, whereas for ethanol the adlayer consists of CO and C. It can be calculated from the n_{ox} value of 2.7 that the adlayer consist of 65% CO and 35% C, corresponding to coverages of 0.29 for CO and 0.16 for C. The CO coverage is in quite good agreement with the CO coverage calculated from the charge involved in the 'indirect' oxidation: 0.30, assuming that C_{ads} has been completely reduced to methane. Comparing the charges involved in the 'direct' and 'indirect' oxidation of ethanol adsorbates shows that the C species are oxidized in the double layer region as well as in the oxide region. The charge involved in the oxide region in Figure 1, corresponds to $\theta_{\text{C}} = 0.09$ monolayers when we assume that 4 electrons are involved in the oxidation of C to CO_2 , whereas the oxidation charge for C_{ads} in the double layer region corresponds to $\theta_{\text{C}} = 0.07$. We want to stress that the FTIRS results are in agreement with the conclusions given above, that were obtained only from the charges involved in cyclic voltammetry. The normalized integrated CO

absorbances of 0.45 ± 0.05 for both ethanol and 1,2-ethanediol, are in accordance with the respective ratios of the CO coverages that were calculated from cyclic voltammetry.

The results for MGP show that the C-C(OH) dissociative adsorption does not only occur for simple alcohol compounds but also occurs for more complex cyclic polyols. However, we cannot conclude from our measurements that the C-C dissociative adsorption of MGP is complete. Some experiments with glucose have shown that a small reduction is visible at low potentials and a small contribution is present in the oxide region. This implies that the decarbonylative adsorption is not complete, although it is the major adsorption pathway according to:



In the case of MGP then it seems reasonable to conclude that decarbonylative adsorption is not the sole adsorption route, although it is the dominant one, according to:

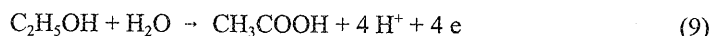


Adsorbate studies have shown that dissociation of the reactant alcohol into CO and C can occur at potentials where the oxidation to acetaldehyde and acetic acid does not occur. This demonstrates that the decarbonylative reaction is thermodynamically favored over the oxidation of ethanol to ethanal and acetic acid. However, if the surface is completely covered with dissociative adsorbates, oxidation is the only possible reaction pathway.

We believe that the formation of CO and CH_x adsorbates in the case of ethanol, 1,2-ethanediol and MGP occurs during exposure of the electrode to the alcohol solution and not after exchange of the alcohol solution for base electrolyte. This is based on the observation by us (Chapter 3, Figure 5) and by others [13, 17, 18] with FTIRS that at low pH that CO is readily formed even in the presence of high concentrations of the parent alcohol. This was found for numerous primary alcohols but also for polyols. The concentrations of the alcohols were typically between 0.05 and 0.1 M. There are no indications that the situation would be different for the adsorption of alcohols at high pH.

5.4.2 Open circuit potential measurements: implications of surface roughness

In this section we will discuss the difference in open circuit potential (o.c.p.) values for the catalytic ethanol oxidation on smooth and platinumized platinum. We have demonstrated with simple experiments that the catalytic alcohol oxidation can be regarded as an electrochemical process and the different o.c.p. values for smooth and platinumized platinum originate from a difference in kinetics of the two half reactions involved;



Such a local cell mechanism has already been proposed by others [24,30-33]. The oxygen reduction is diffusion limited below 0.8 V, and as a result it does not increase after roughening of the electrode surface. However, the ethanol oxidation is kinetically limited over the complete potential region and thus increases proportionally with the electrode area upon roughening of the electrode surface. As schematically shown in Figure 18 there is for smooth platinum no potential below 0.8 V where the current of the half reactions are equal, leading to a further increase of the o.c.p. to 1 V, where the surface is highly covered with adsorbed oxygen or hydroxyl and where the oxygen reduction has almost, but not completely, ceased. The reaction rate of the catalytic ethanol oxidation is not limited by diffusion of oxygen to the surface but is kinetically limited. In a previous report it has been concluded that the rate of the catalytic ethanol oxidation in the kinetic regime corresponds to a surface of which only 9% of the surface atoms are available for the oxidation reaction and 91% is covered. This conclusion was reached by comparing the oxidation rate on carbon supported platinum catalysts in a slurry phase reactor with kinetic data of electrochemical adsorption studies on platinum foil [25].

For platinized platinum the o.c.p. stabilizes at 0.35 V after reductive startup of the reaction as a result of the increased ethanol oxidation with respect to smooth platinum, as schematically shown in Figure 18. In contrast with smooth platinum the reaction rate is now O_2 diffusion limited and can be further increased by improving the mass transport of oxygen to the surface. Such a low

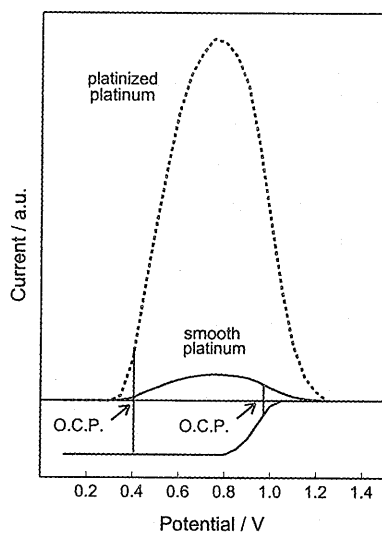


Fig. 18: Current-potential curves for ethanol oxidation and oxygen reduction on smooth and platinized platinum.

open circuit potential has also been found for the catalytic oxidation of 2-propanol [30] and ethanol [1] on platinized platinum. On the basis of our experiments we conclude that it is not allowed to compare the results of o.c.p. measurements on platinized platinum, which proceed in the O_2 diffusion limited regime, with measurement on carbon supported platinum in the kinetic regime as was done by Vleeming et al. [1] and Schuurman et al. [4].

The rate of alcohol oxidation is quite different in the O_2 diffusion limited regime and the kinetic regime. The reduction rate of oxygen at 1 V is shown in Figure 18 to be much lower than in the diffusion limited regime below 0.8 V, which indicates that the catalytic oxidation of alcohols in the kinetic regime proceeds at much lower rate than in the diffusion limited situation. Note that the occurrence of the local cell mechanism implies that adsorbed oxygen is not involved in a direct reaction with the alcohol as has been proposed in several reaction mechanisms.[1,4-6,34-36]. Adsorbed oxygen or hydroxyl causes both the electrochemical oxygen reduction and the electrochemical ethanol oxidation to be inhibited. When adsorbed oxygen or hydroxyl were involved in the oxidation of alcohols a positive correlation would be expected between the oxygen coverage and the activity for low coverages. However, this correlation has never been demonstrated with electrochemical techniques.

Summarizing, the catalytic alcohol oxidation performed in the kinetic regime corresponds to a high open circuit potential and thus a surface highly covered with oxygen or hydroxyl. In our view the situation for the alcohol oxidation in the kinetic regime can readily be referred to as overoxidation, since the high oxygen coverage causes the reaction rate to be much lower than in the diffusion limited regime. On the contrary, studies in the diffusion limited regime correspond to a low open circuit potential and thus a surface that is completely free of adsorbed oxygen or hydroxyl.

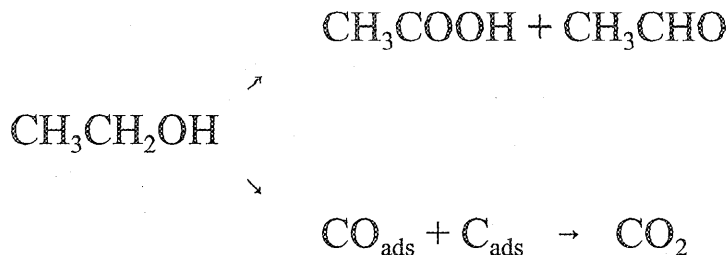
The experiments on platinized platinum nicely illustrate that catalytic oxidation reactions proceed through a local cell mechanism. This has important consequences for the transport of reactants and products on porous electrodes. Since its reduction is diffusion limited, oxygen will not diffuse deeply into the pores of the electrode but react in the surface region. Ethanol, however, reacts at the entire surface including deeply in the pores. The electrons that are transferred from ethanol to the metal during oxidation are transported through the metal to the surface of the electrode where they are used to reduce oxygen. The question is what the implications of these results are for carbon supported catalysts in a slurryphase reactor. The transport of oxygen to the surface of the catalyst particles is much better in a slurryphase reactor than in our experiments, which suppresses the likeliness of diffusion limitation. However, our experiments have shown that the roughness factor of the electrode is a very important parameter. For a carbon catalyst particle the roughness factor can be defined as the ratio of the true platinum surface in a particle and the outer surface of the carbon particle. This ratio depends on several factors as the platinum content of the catalyst and the size of the carbon particles. This roughness factor can be quite high for carbon supported platinum catalysts and in this respect it can resemble platinized

platinum. Depending on the type of alcohol, the catalyst properties and reaction conditions the oxidation in a slurry reactor can proceed in the kinetic regime or in the diffusion limited regime. In the case that the reaction rate is limited by diffusion of oxygen, the high conductivity of the carbon support enables the local cell mechanism to occur by conduction of electrons through the carbon support, which leads to a situation where the outer shell of the catalyst particle reduces oxygen and both the outer and inner part of the particle oxidizes the alcohol. The electrons migrate through the carbon support from the inner part to the outer shell of the particle where they reduce oxygen. This phenomenon has also consequences for the pH inside the catalyst pores; in the oxidation of the alcohol OH^- ions are consumed and as a result an OH^- gradient can arise inside these pores.

5.4.3 Adsorbates present during O_2 diffusion limited oxidation

Catalytic studies on alcohol oxidations are often carried out in the O_2 diffusion limited regime [2] and in some cases this has been confirmed with potential measurements [2,9,35,37]. We found that the electrode surface is highly covered with CO and C adsorbates during the O_2 diffusion limited ethanol oxidation on platinized platinum. We cannot establish the exact coverage during the reduction since after the potential step to 0.15 V reduction of C species occurs. The adsorbate coverage during reaction depends on the o.c.p., which itself depends on several factors like the electrode roughness, ethanol concentration and the mass transport of oxygen. We suggest that in all cases where alcohol oxidation has been carried out in the diffusion limited regime [2,9,35,37], the surface is also highly covered with irreversible adsorbates which are formed from the reactant alcohol. The reported open circuit potentials can be so low that they correspond to values in the so called hydrogen region and on that basis it was concluded by some [2] that the catalyst surface is actually covered with hydrogen during reaction. However, it should be kept in mind that in such a situation the surface is highly covered with irreversible adsorbates and not many platinum sites are left for hydrogen to adsorb. As a result only a low hydrogen coverage is necessary to reach fairly negative potentials, which means that the hydrogen coverage is much lower than suggested by some as they refer to a reduced surface [2]. In fact, the open circuit potential of 0.41 V found in our ethanol oxidation experiments does not correspond to a situation that the surface contains any adsorbed hydrogen.

Our experiments have demonstrated that the electrochemical and catalytic oxidation of ethanol result in the same coverage of irreversible adsorbates on the catalyst surface as long as the electrochemical potentials are equal. This supports the view that the catalytic oxidation can be regarded as an electrochemical process and therefore information obtained with electrochemical tools can be directly transferred to the catalytic oxidation. The key parameter is the potential. We have clarified that the CO + C coverage is a steady state coverage and that CO and C adsorbates are not only present during the initial phase of the reaction. No adspecies remained on the surface when the rate of electrochemical ethanol oxidation was made limited by diffusion



Scheme 1: Possible oxidation routes for ethanol.

of ethanol, which proves that the rate of C-C(OH) dissociative adsorption and subsequent oxidation to CO_2 is then higher than the diffusion rate of ethanol and thus the CO_2 selectivity is 100%. A subsequent increase of the ethanol concentration at this potential made the reaction rate kinetically limited again, leading to a high coverage of CO and C adspecies, which demonstrates that continuously new CO and C adspecies are being formed by C-C(OH) dissociative adsorption during oxidation of ethanol to acetaldehyde and acetic acid. This demonstrates that CO is not only initially present during startup of the reaction, but is continuously being formed. The possible reactions are given in Scheme 1.

Our results also indicate that in the O_2 diffusion limited regime some CO_2 is continuously formed as a product next to acetic acid and acetaldehyde. The actual CO_2 selectivity is unknown in our experiments. The CO_2 selectivity depends strongly on both the reactant concentration and on the catalyst potential, which depends on factors like the reactant concentration, the oxygen mass transport and the metal surface area. In general, the CO_2 selectivity is expected to decrease for increasing reactant concentration.

Our experiments on the O_2 diffusion limited oxidation of MGP have shown clearly that the increase of the open circuit potential with time is correlated with an increase of adsorbates that are oxidized at high potentials in the oxide region, whereas the amount of adsorbates that oxidize at low potentials diminish. The oxidation at high potential in the oxide region is typical for adsorbed hydrocarbon species C_xH_y , whereby CO_2 is formed. The increase of the o.c.p. can easily be understood in terms of the two electrochemical half reactions. As the surface becomes covered with these site blockers, less platinum is available for the oxidation of MGP. Because the electrochemical oxidation rate of MGP is kinetically limited, a build-up of carbonaceous residue will result in an inhibition of the MGP oxidation as less Pt surface is available for reaction. However, the electrochemical reduction of oxygen is diffusion limited and this reaction is not affected by an increasing coverage of irreversible adspecies. We infer this from the experiments with ethanol and oxygen, where the presence of 0.1 M ethanol had no effect on the oxygen reduction rate at 0.1 V. As a result the open circuit potential increases in order to maintain a net zero current. Our conclusion contrasts with those in the literature, where the slow

increase of the open circuit potential was referred to as overoxidation [1].

5.4.4 Adsorbates present in the kinetic regime

We found that when the o.c.p. reaches 0.8 V, which corresponds to the peak potential for MGP oxidation, it quickly rises to 0.98 V, and thus the reaction transfers from diffusion limited regime to the kinetic regime. As in the case of ethanol, the platinum surface is highly covered with adsorbed oxygen or hydroxyl at 0.98 V and the majority of the carbon species formed during deactivation probably oxidizes to CO_2 at this potential. The o.c.p. remained constant within 20 mV for 16 hours, which implies that the coverage of adsorbed oxygen or hydroxyl remains equal. Nevertheless, we found the catalyst both to deactivate when electrochemical MGP oxidation was carried out at 0.98 V and to reactivate after reduction of the adsorbed oxygen species at o.c.p., which is in perfect agreement with a study on carbon supported platinum in a slurry phase in the kinetic regime [1]. This means that the deactivation does not originate from a slow increase of the oxygen coverage, since this would require an increase of the open circuit potential.

Our experiments have demonstrated that the adsorbed oxygen species slowly change in time when the electrode is preoxidized in the absence of alcohol. The shift of the oxygen reduction peak in the cyclic voltammogram after different preoxidation times implies an increase of the adsorption energy of the oxygen species. In this way we can understand that while the open circuit potential during catalytic MGP oxidation in the kinetic regime remains constant the catalyst nevertheless deactivates due to changes in the oxygen adspecies. However, it should be reminded that the adsorbed oxygen atoms themselves are not involved in the catalytic oxidation but act only as site blockers. Apparently the slow change in the properties of adsorbed oxygen results in a decreased ability of the catalyst to reduce molecular oxygen and to oxidize MGP, probably by a decreased accessibility of the platinum surface for either molecular oxygen and MGP.

5.5 Conclusions

The irreversible adspecies formed after adsorption of ethanol and 1,2-ethanediol have completely undergone C-C(OH) dissociation accompanied by full dehydrogenation to form CO and C species in the case of ethanol and only CO in the case of 1,2-ethanediol. The C species are partially oxidized further to CO. These results show that the adsorption behaviour of these compounds at high pH is completely analogous with that at low pH [14,16]. The adsorption behaviour of the cyclic polyol MGP is similar to that of the small alcohols as the molecule completely decarbonylates to form adsorbed CO and a small fraction of C.

All our experiments show that the catalytic alcohol oxidation can be regarded as an

electrochemical process, consisting of two independently acting halfreactions that determine the open circuit potential. The roughness of the electrode surface greatly affects the o.c.p. during catalytic alcohol oxidation; smooth platinum leads to high o.c.p. values and platinumized platinum leads to low o.c.p. values. These low and high open circuit potentials correspond a diffusion limited regime where diffusion of oxygen is rate limiting and a kinetic regime, respectively. The reaction rate in the kinetic regime is considerably lower than in the diffusion limited regime. During oxidation of ethanol and MGP in the kinetic regime, the surface is highly covered with adsorbed oxygen or hydroxyl. In contrast with this the surface is devoid of adsorbed oxygen in the diffusion limited regime and is instead covered with a high steady state amount of CO and C species, which are continuously being formed by C-C(OH) dissociative adsorption. The catalyst is found to deactivate both in the diffusion limited as in the kinetic regime for MGP oxidation. Whereas in the diffusion limited regime the deactivation is caused by accumulation of carbonaceous residue, in the kinetic regime changes in the properties of O/OH_{ads} cause deactivation and not a plain increase of the coverage of O/OH_{ads}.

References:

- [1] J.H. Vleeming, F.A. de Bruijn, B.F.M. Kuster and G.B. Marin, in *Catalyst Deactivation, Studies in Surface Science and Catalysis*, ed. B. Delmon and G.F. Froment, Amsterdam 88, 467, 1994.
- [2] T. Mallat and A. Baiker, *Catalysis Today* 19, 247, 1994.
- [3] T. Mallat, A. Baiker and L. Botz, *Appl. Catal. A* 86, 147, 1992.
- [4] Y. Schuurman, B.F.M. Kuster, K. van der Wiele and G.B. Marin, *Appl. Catal. A* 89, 47, 1992.
- [5] P.J.M. Dijkgraaf, M.J.M. Rijk, J.Meuldijk and K. Van der Wiele, *J. Catal.* 112, 329, 1988.
- [6] P.J.M. Dijkgraaf, H.A.M. Duisters, B.F.M. Kuster and K. Van der Wiele, *J. Catal.* 112, 337, 1988.
- [7] T. Mallat, Z. Bodnar, P. Hug and A. Baiker, *J. Catal.* 153, 131, 1995.
- [8] C. Brönniman, Z. Bodnar, P. Hug, T. Mallat and A. Baiker, *J. Catal.* 150, 199, 1994.
- [9] T. Mallat, Z. Bodnar and A. Baiker, in *ACS Symp. Series, Catalytic selective oxidations* ed. S.T. Oyoma and J.W. Hightower, Washington 523, 308, 1993.
- [10] R. Parsons and T. VanderNoot, *J. Electroanal. Chem.* 257, 9, 1988.
- [11] P.A. Christensen and A. Hamnett, *J. Electroanal. Chem.* 260, 347, 1989.
- [12] T. Iwasita and E. Pastor, *Electrochim. Acta*, 39, 531, 1994.
- [13] L.-W. H. Leung and M. J. Weaver, *Langmuir* 6, 323, 1990.
- [14] J. F. E. Gootzen, W. Visscher and J. A. R. van Veen, *Langmuir* 12, 5076, 1996.
- [15] R. Holze; *J. Electroanal. Chem.*, 246, 449, 1988.
- [16] J.F.E. Gootzen, A.H. Wonders, W. Visscher and J.A.R. van Veen, *in print Langmuir*.
- [17] E. Pastor, S. Wasmus, T. Iwasita, M. C. Arevalo, S. Gonzalez and A. J. Arvia, *J. Electroanal. Chem.* 350, 97, 1993.
- [18] E. Pastor, S. Wasmus, T. Iwasita, M. C. Arevalo, S. Gonzalez and A. J. Arvia, *J. Electroanal. Chem.* 353, 81, 1993.
- [19] M. Lopéz-Atalaya, E. Morallón, F. Cases, J.L. Vázquez and J.M. Pérez, *J. Power Sources* 52, 109, 1994.
- [20] J.M. Pérez, E. Muñoz, E. Morallón, F. Cases, J.L. Vázquez and A. Aldaz, *J. Electroanal. Chem.* 368, 285,

1994.

- [21] S. Sun, D. Yang and Z. Tian, *J. Electroanal. Chem.* 289, 177, 1990.
- [22] P. T. A. Sumodjo, E. J. da Silva and T. Rabockai, *J. Electroanal. Chem.* 271, 305, 1989.
- [23] E. Santos and M.C. Giordano, *J. Electroanal. Chem.* 172, 201, 1984.
- [24] C. Wagner and W. Traud, *Z. Elektrochem.* 44, 391, 1938.
- [25] F.A. de Bruijn, PhD Thesis Eindhoven University of Technology, 1996.
- [26] F. Hahn, B. Beden, F. Kadirgan and C. Lamy, *J. Electroanal. Chem.* 216, 169, 1987.
- [27] N. Furuya and S. Koide, *Surf. Sci.* 220, 18, 1989.
- [28] E. Morallón, J.L. Vázquez, J.M. Pérez, B. Beden, F. Hahn, J.M. Léger and C. Lamy, *J. Electroanal. Chem.* 344, 289, 1993.
- [29] J. Shin, W. J. Tornquist, C. Korzeniewski and C. S. Hoaglund, *Surf. Sci.* 364, 122, 1996.
- [30] R. DiCosimo and G.M. Whitesides, *J. Phys. Chem.* 93, 768, 1989.
- [31] G. Horanyi, G. Vertes and P. König, *Acta Chim. Hung.* 72, 179, 1972.
- [32] A. Hoffmann and A.T. Kuhn, *Electrochim. Acta* 9, 835, 1964.
- [33] T. Mallat and A. Bäiker, *Catalysis Today* 24, 143, 1995.
- [34] J.A.A. van den Tillaart, B.F.M. Kuster and G.B. Marin, *Appl. Catal. A* 120, 127, 1994.
- [35] J.M. Nicoletti and G.M. Whitesides, *J. Phys. Chem.* 93, 759, 1989.
- [36] L. Jelemensky, B.G.M. Kuster and G.B. Marin, *Catal. Lett.* 30, 269, 1995.
- [37] T. Mallat, Z. Bodnar and A. Bäiker, in *Heterogeneous Catalysis and Fine Chemicals III, Studies in Surface Science and Catalysis*, ed. M. Guisnet et al., Amsterdam 78, 377, 1993.

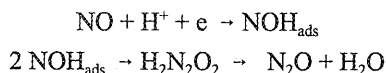
The study of NO adsorbate layers on platinized platinum in the liquid phase with cyclic voltammetry, DEMS and FTIRS

Abstract

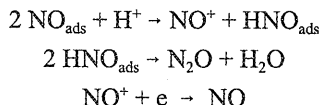
The irreversible adsorbates formed after exposure of platinum to an NO-containing solution were studied with Differential Electrochemical Mass Spectrometry (DEMS), Fourier-Transform Infrared Spectroscopy (FTIRS) and cyclic voltammetry. DEMS and FTIRS show that only a very small amount of N_2O is formed in the reduction of the adsorbate, indicating that mainly non-volatile products are formed. FTIRS shows, in addition, vibrations of NO at wavenumbers characteristic of adsorbed NO on Pt(100) and Pt(110) sites. These two different adsorption sites are characterized by separate reduction peaks in the cyclic voltammogram. Further, it was established with FTIRS that the adsorbate is transformed to N_2O and NH_4^+ in the reduction, and to NO_3^- in the oxidation. Analysis of the charges involved in the reduction and oxidation of the irreversible adsorbates demonstrates that coadsorbates are present next to NO. The coadsorbates consist of adsorbed nitrogen atoms, formed by the dissociation of NO. This view is supported by previously reported studies in Ultra High Vacuum (UHV). A new mechanism for the reduction of NO to N_2O in the liquid phase is proposed on the basis of NO dissociation.

6.1 Introduction

The reduction of nitric oxide in acid medium on platinum electrodes has been extensively studied using electrochemical techniques [1-12]. The selectivity of the reaction was found to depend largely on the reduction potential. At potentials above 0.35 V, N₂O is found as the only product [1-4]. Several mechanisms have been proposed to account for N₂O formation. The most frequently reported mechanism [1,3-6,8-10] consists of a single electron reduction of the NO molecule, followed by dimerization and N₂O formation according to;

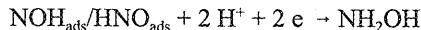


Some authors have proposed HNO_{ads} instead of NOH_{ads} as an intermediate in the formation of N₂O [1,3,4,10]. So far, no direct evidence has been presented for the existence of NOH or HNO as an intermediate in the NO reduction. A second mechanism, based on a study in concentrated perchloric acid [7], consists of the disproportionation of NO followed by N₂O formation and electron transfer according to:

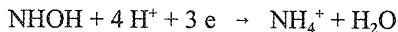


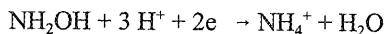
Rotating disk experiments on smooth platinum electrodes demonstrated that the NO reduction to N₂O is diffusion limited [9-11].

At potentials lower than 0.35 V, NH₂OH and NH₄⁺ are observed in addition to N₂O [1-4,12]. The product distribution depends on the reduction potential and the supporting electrolyte. Maximum selectivities for hydroxylamine of 70% [1] and 78% [2] were found in concentrated sulfuric acid. Strongly adsorbing species like chloride, carbon monoxide [3], and sulfur [12] have a promoting effect on the hydroxylamine selectivity. It is generally proposed that the NOH_{ads}/HNO_{ads} species is the intermediate in the formation of hydroxylamine according to:



Ammonium can be formed by a hydrogenolysis of NH₂OH [1,3,5,7] or NHOH [3] according to:





It has recently been demonstrated that a close correlation exists between the properties of adsorbed NO molecules in the liquid phase and in Ultra High Vacuum. IR studies on platinum single crystal electrodes show that solvent coadsorption has a limited effect (35-70 cm^{-1}) on the vibration frequencies with respect to Ultra High Vacuum data [14-17]. The adsorption of NO is structure sensitive in Ultra High Vacuum as well as in the liquid phase and the N-O stretch vibration was found to vary by 125 cm^{-1} for the three basal planes of platinum. This implies that Ultra High Vacuum studies are highly relevant to adsorption processes in the liquid phase. Particularly interesting is the observation in Ultra High Vacuum that partial dissociation of NO occurs at room temperature on Pt(100) [18], Pt(310) [18] and Pt(410) [18-20] in contrast with Pt(111) [21], Pt(110) [22,23], Pt(210) [24] and polycrystalline platinum [25] for which only molecular adsorption was found. Palladium behaves qualitatively in the same way as platinum; of the three basal planes, Pd(100) displays partial dissociation at room temperature, while molecular adsorption was observed on Pd(110) [26] and Pd(111) [26,27]. This chapter describes the application of cyclic voltammetry, Differential Electrochemical Mass Spectrometry (DEMS) and Fourier-Transform IR spectroscopy (FTIRS) to the characterization of the adsorbates formed after contact between platinized platinum and NO-containing solutions. These results will be interpreted in the context of single-crystal data obtained in UHV studies. A new mechanism for N_2O formation in the liquid phase will be proposed that is based on NO dissociation, in contrast with the generally held view that NOH/HNO adspecies are the key intermediates in N_2O formation.

6.2 Experimental

Infrared measurements were performed with a Biorad FTS 45A spectrometer, equipped with a liquid-nitrogen cooled MCT detector. All spectra were recorded with 4 cm^{-1} resolution.

The electrochemical cell, made of glass, equipped with a CaF_2 prism with 65° beveled edges to obtain a high reflection angle was placed on top of the sample room. The electrode consisted of a platinum disk of 9 mm diameter embedded in teflon (PTFE). The infrared beam was focused on the electrode by one flat and one ellipsoidal mirror, with which the optimal spot size could be obtained. A polarizer was placed in the sample room of the spectrometer to obtain p-polarized light.

DEMS measurements were performed with a Leybold Quadruvac PGA 100 mass spectrometer. The experimental setup is similar to the one described previously [13]. The products were examined for N_2O ($m/z = 44$), N_2 ($m/z = 28$) and NH_3 ($m/z = 17$).

Electrochemical measurements were performed with an Autolab PGSTAT 20 computer-controlled potentiostat. The rotating-ring-disk measurements were performed with a Tacussel BI-PAD bipotentiostat. A Hg/Hg₂SO₄ electrode was used as a reference electrode. All potentials will be referred to the reversible hydrogen electrode (RHE). All measurements were performed with platinized platinum, prepared by electrodeposition from a H₂PtCl₆ solution. The electrodes used in the DEMS and IR measurements are characterized by a real area of 124 cm² and 10 cm², respectively, as derived from the charge involved in the hydrogen desorption in the voltammogram in 0.5 M H₂SO₄. Potential cycling between 0 and 1.5 V was carried out until a stable voltammogram was obtained. Electrolytes were prepared using ultrapure water (18.2 MΩ) obtained with an Elga water purification system. In the infrared experiments 0.1 M H₂SO₄ (Merck p.a.) was used and, for cyclic voltammetry and the DEMS measurements, 0.5 M H₂SO₄ was used. Oxygen was removed from the electrolyte with Argon (Hoek Loos, purity 4.6). Before use, NO (Hoek Loos, purity 2.0) was bubbled through a concentrated KOH solution to remove impurities.

6.3 Results

A platinum electrode was exposed to NO-saturated 0.5 M H₂SO₄ electrolyte for 10 minutes. During this adsorption process the open circuit potential rose to 0.93 V and then declined to 0.90 V. With DEMS, no gaseous products such as N₂ or N₂O were found within the detection limit of the apparatus during adsorption at open circuit potential. After replacement of the electrolyte with fresh 0.5 M H₂SO₄, a scan was started at 0.90 V in the cathodic direction, depicted as the solid line in Figure 1. The cyclic voltammogram shows that the electroreduction of the adsorbate starts at 0.43 V, prior to the formation of adsorbed hydrogen which begins at 0.38 V in NO-free electrolyte. The main part of the reduction takes place in the hydrogen region, consisting of two equally sized peaks at 0.28 V and 0.22 V. The total charge involved in the reduction is 398 μC/cm². The electrode area was determined from the anodic charge in the hydrogen region in blank electrolyte. DEMS demonstrates that N₂O is formed in the potential region between 0.68 and 0.28 V with a maximum at 0.40 V. No N₂ was observed in this potential region. Furthermore, the cyclic voltammogram contains a small reduction peak at 0.78 V and Figure 1 shows that this reduction is not correlated with N₂O formation, but is probably due to the reduction of platinum oxides. The amount of N₂O was determined by comparison with the amount of CO₂ detected after oxidation of a monolayer of CO. When the different relative ionization probabilities of both molecules and the fragmentation patterns are taken into account, it follows that the amount of N₂O that is formed in the double layer region equals less than 1% of a monolayer. A small reduction current was

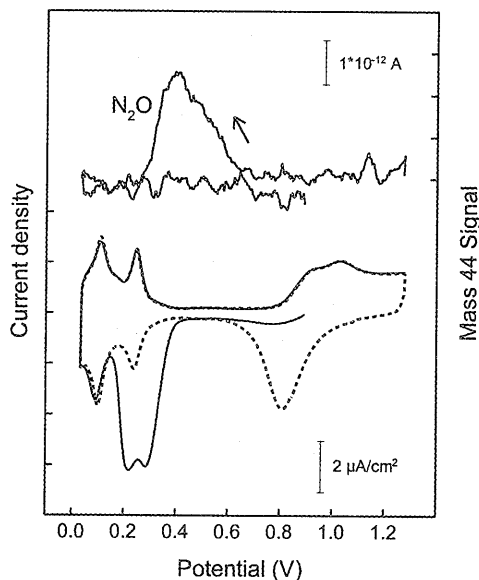


Figure 1: DEMS measurement obtained after adsorption of an NO-containing electrolyte at open-circuit potential. First (—) and second (---) cycle. Scan rate 2 mV/s, $m/z = 44$ (N_2O^+). Electrolyte 0.5 M H_2SO_4 , real area 124 cm^2 .

observed in the double layer region when an experiment was carried out with increased sensitivity. This reduction current is too small to observe in Figure 1. Thus, it follows that the formation of N_2O is accompanied by charge transfer. Note that such a small amount of N_2O could only be observed due to the roughness of the electrode. It is remarkable that the formation of N_2O decreases at a potential, where reduction of the adsorbate starts in earnest in the cyclic voltammogram. Since the cell design causes a tailing of the product mass peak, it is difficult to establish exactly at which potential the formation of N_2O stops. However, it is clear from Figure 1 that no N_2O is formed at potentials below 0.28 V. Since only small amounts of N_2O are observed it can be concluded that the majority of the electroreduction products are non-volatile. Indeed, the possible products hydroxylamine and ammonium [1-4,12] are protonated under these reaction conditions. Our observations are in agreement with literature data which show that, in the continuous reduction of NO on platinum, N_2O is observed as the only product at potentials above 0.35 V while at lower potentials NH_2OH and NH_4^+ are also observed [1-4].

Single-crystal studies have shown that the electroreduction of adsorbed NO is structure-sensitive [14-17]. For Pt(100) and Pt(110) a peak potential was reported at 0.19 V and 0.27 V, respectively. These potentials are close to the values found in our measurements which seems to suggest that NO is present on (100) and (110) related sites on our electrode. For Pt(111)

two peaks are reported at 0.12 V and 0.3 V, the latter coinciding with the peak observed on Pt(110). No significant contribution is observed in our measurements in the potential region characteristic for NO reduction on Pt(111) sites. We will return to this point later.

In a second experiment NO was adsorbed at 0.68 V. A steady state reduction current is now observed together with a constant N_2O mass signal ($m/z = 44$). Both the reduction current and the N_2O mass signal increase upon convection of the solution, indicating that the reaction is diffusion limited. It is obvious that the reduction current and the N_2O formation are correlated. However, no quantitative correlation can be established because the fraction of product molecules that reaches the vacuum chamber is lowered upon convection of the solution. The amount of N_2O and the reduction charge observed after electrolyte replacement in the cathodic scan are equal to those observed after adsorption at open-circuit potential.

The IR spectrum in Figure 2 was obtained after 10 minutes adsorption at 0.68 V in NO saturated electrolyte. The infrared spectrum, given as $\Delta R/R_0$ ($\Delta R = R_0 - R_1$), was obtained by changing the electrode potential from 0.78 (R_0) to 0.48 V (R_1), recording a single beam spectrum at every potential. The single-beam spectrum obtained at 0.78 V was taken as the reference. The spectrum in Figure 2 contains a positive band at 2231 cm^{-1} , that can be assigned to the N-N stretch vibration of dissolved N_2O in the thin layer [28]. The small band at 1285 cm^{-1} belongs to the N-O stretch vibration of N_2O [28]. The formation of N_2O was only observed in the first cathodic scan between 0.78 and 0.48 V. A repeated potential excursion from 0.78 to 0.48 V did not result in the additional formation of N_2O . The integrated N_2O absorbance is roughly 50 times lower than the integrated CO_2 absorbance found after oxidation of a monolayer of CO, confirming the above observation with DEMS that the amount of N_2O formed is very small. Given this fact, it is difficult to establish from the IR spectrum whether or not NO has disappeared in the formation of N_2O . The formation of N_2O has also been observed with IR spectroscopy on single crystal electrodes. Surprisingly, N_2O was only observed for Pt(100), and not for the Pt(110) and Pt(111) crystal planes [14].

In addition to the vibrations of N_2O , bipolar peaks are observed at $1790/1730\text{ cm}^{-1}$ and $1650/1590\text{ cm}^{-1}$. The bipolar character of these peaks arises from a shift to lower wavenumbers as the electrode potential is decreased. This phenomenon, the so-called Stark effect, is well known for adsorbed CO on platinum and it was also recently observed for adsorbed NO [14-17]. Moreover, the Stark effect proves that the IR features are connected to adsorbed species. An infrared study of NO adsorbed on single crystal electrodes produced a bipolar peak centred at 1640 cm^{-1} for Pt(100) after a potential shift from 0.65 to 0.95 V. The same frequency was also found on this crystal plane for a c(4x2) adsorbate layer with an NO coverage of 0.5 in UHV [29]. A bipolar peak centred at 1700 cm^{-1} was found for Pt(111), but for Pt(110) no bipolar band was found after shifting the potential from 0.65 to 0.95 [14]. However, a band at 1760 cm^{-1} was observed after stripping the adsorbate in a potential step from 0.8 to 0.1 V [14]. In UHV experiments, a vibration at 1760 cm^{-1} was found on Pt(110)

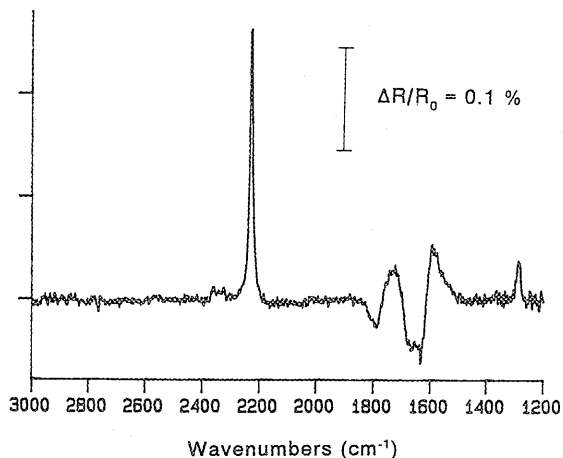


Fig. 2: Infrared spectra ($\Delta R/R_0$, $\Delta R = R_0 - R_1$) obtained after adsorption for 10 min. at 0.68 V. First spectrum recorded at 0.78 V (R_0), second spectrum at 0.48 V (R_1). Electrolyte 0.1 M H_2SO_4 . Resolution 4 cm^{-1} .

[22], that was assigned to linearly bonded NO. On the basis of these single crystal data, the bipolar vibration at 1790/1730 cm^{-1} can be ascribed to NO adsorbed on (110) sites and the bipolar band at 1650/1590 cm^{-1} can be ascribed to NO adsorbed on (100) sites. Furthermore, it was found in UHV studies that different IR vibrations exist for adsorbed NO at low and high coverages. The NO vibrations found in our experiments demonstrate that we are dealing with high NO coverages.

At low adsorbate coverages, the bipolar peak at 1650/1590 cm^{-1} remains present in the spectrum, but the bipolar band at 1790/1730 cm^{-1} was no longer observed. The lowest adsorbate coverage studied with IR was 130 $\mu C/cm^2$, roughly 30% of the maximum charge found in reduction.

Lowering the potential from 0.48 to 0.08 V does not yield peaks related to the additional formation of N_2O , but a broad positive band occurs at 1460 cm^{-1} , as shown in Figure 3a. A negative band is present at 1210 cm^{-1} , that can be assigned to a decrease of HSO_4^- concentration due to migration. After performing reference experiments with $(NH_4)_2SO_4$, the band at 1460 cm^{-1} could be ascribed to NH_4^+ ions in the thin layer, in accordance with a previous report [30]. No vibrations were observed that could be assigned to NH_2OH formation. Figure 3 shows that increasing the potential from 0.68 to 1.38 V after adsorption generates a double peak in the IR spectrum at 1356 and 1393 cm^{-1} . Exactly the same vibrations were found in reference experiments where nitrate ions were allowed to diffuse into the thin layer. Reference experiments with nitrite produced a vibration at 1239 cm^{-1} . No vibration was observed at this wavenumber in our experiments, indicating that complete oxidation of the adsorbate to nitrate has occurred. The positive band at 1210 cm^{-1} stems from

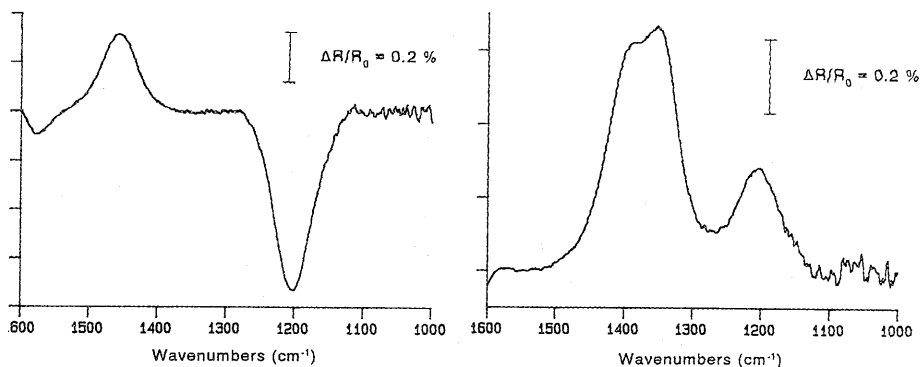


Figure 3: Infrared spectra ($\Delta R/R_0$, $\Delta R = R_0 - R_1$) for the reduction (left spectrum) and the oxidation (right spectrum) obtained after 10 minutes adsorption at 0.68 V. For the reduction and oxidation $E_1 = 0.68$ V and $E_2 = 0.68$ V, after potential excursions to 0.03 V and 1.38 V, respectively. Electrolyte 0.1 M H_2SO_4 . Resolution 4 cm^{-1} .

an increase in HSO_4^- concentration due to migration.

A rotating ring-disk experiment was performed to obtain additional information on the products formed during the reduction of the adsorbate. The adsorption was carried out at 0.48 V in NO-saturated electrolyte for 10 minutes followed by electrolyte replacement; a constant adsorption current was observed. It is possible with this experiment to discriminate between the formation of ammonium and hydroxylamine, since only the latter is sensitive to oxidation on the platinum ring. The chemisorbed species are reduced after adsorption in a cathodic scan, while the ring was kept at a constant potential of 1.18 V at a rotation speed of four revolutions per second. No oxidation current was observed on the ring electrode during reduction of the adsorbate, demonstrating that ammonium ion is the only product formed.

Information on the composition of the adsorbate can be obtained by analysing the charges involved in reduction and oxidation of the adsorbate layer. First, the reduction charge Q_{red} is determined by performing two cycles in the hydrogen region. The second cycle equals the voltammogram of the blank electrolyte and the charge Q_{red} is determined by subtracting the second from the first cycle. Then, the adsorption procedure is repeated, but now the adsorbate is oxidized. Five cycles in the oxide region are necessary for complete removal of the adsorbate layer. The concurrent charge Q_{ox} is determined by using the fifth cycle as the reference. The ratio Q_{red}/Q_{ox} gives information on the adsorbate composition.

The NO concentration in the solution was found to have an effect on the adsorbate coverage as well as the adsorbate composition. It has been shown that the NO reduction to N_2O is diffusion-limited in this potential region [9-11], so that the adsorption current can be taken as a measure for NO concentration. The charge that is necessary for reduction of the adsorbate can be taken as an estimate for the coverage. Table 1 shows the relation of the charge Q_{red} involved in the adsorbate reduction with the NO concentration as indicated by the adsorption current i_{ads} . The ratio Q_{ox}/Q_{red} gives information on the adsorbate composition and again Q_{red}

Table 1: The charge involved in reduction Q_{red} of the adsorbate layer as a function of cathodic adsorption current density i_{ads} . Adsorption was carried out at 0.48 V for 10 minutes.

i_{ads} ($\mu\text{A}/\text{cm}^2$)	Q_{red} ($\mu\text{C}/\text{cm}^2$)
0.44	206
0.76	210
6.6	353
13.2	409

Table 2: The ratio Q_{ox}/Q_{red} as a function of the reduction charge Q_{red} . Adsorption was carried out at 0.48 V for 10 minutes.

Q_{red} ($\mu\text{C}/\text{cm}^2$)	Q_{ox}/Q_{red}
206	1.06
210	0.90
353	0.73
409	0.75

can be taken as an estimate of the adsorbate coverage. Table 2 presents the ratio Q_{red}/Q_{ox} as a function of Q_{red} . It follows from the data that adsorbate composition changes with coverage. These results will be discussed in the next section.

6.4 Discussion

The IR measurements clearly demonstrate that adsorbed NO is present after the platinum electrode has been in contact with an NO-containing solution. To our knowledge, it is the first time that adsorbed NO has been observed on polycrystalline platinum in the liquid phase with IR spectroscopy. The assignment of the various NO vibrations is based on single-crystal studies. Our results confirm once more that the vibrational characteristics of NO adsorbed on platinum in the liquid phase are very similar to those for UHV conditions.

From our cyclic voltammetry and IR spectroscopy data, we conclude that NO is present on (100) and (110) related sites, while no features characteristic for adsorption on (111) sites were found. Close comparison of the hydrogen peaks in the voltammogram in 0.5 M H_2SO_4 with single crystal data [31] suggests that the hydrogen peak at 0.10 V can be assigned to (110) sites, while the peak at 0.24 V coincides with the peak potential for Pt(310) sites. The latter consists of (100) terraces divided by steps in a (110) geometry. No voltammetric

features are present that can be assigned to Pt(111) and this is consistent with the absence of the NO vibration for Pt(111) sites in IR spectroscopy.

The reduction of NO adsorbates to NH_4^+ may be considered as a hydrogenation reaction of NO involving adsorbed hydrogen, although some opposing facts arise from the experimental work. Cyclic voltammetry has shown that the reduction of NO proceeds more easily on Pt(110) than on Pt(100) [16], as indicated by the higher reduction potential. This is opposite to the trend observed for adsorbed hydrogen, which is formed at a higher potential on Pt(100) with respect to Pt(110) [31]. On Pt(110) NO is reduced at a potential at which no adsorbed hydrogen is present and this seems to suggest that adsorbed hydrogen is not in a simple manner involved as a reactant in the reduction of NO. This situation is similar to the oxidation of CO to CO_2 on platinum which occurs at potentials prior to oxide formation. The data suggest that the structure sensitivity of the reaction is not connected to the Pt-H interaction but to the Pt-NO interaction. The different NO stretch vibrations observed on Pt(110) and Pt(100) indicate that the metal-adsorbate interaction is clearly structure sensitive.

The formation of NH_4^+ as the only product in the reduction of the NO adlayer differs from the product distribution during reduction of dissolved NO on platinum catalysts, which is carried out commercially by BASF. Whereas our experiments result in full reduction to NH_4^+ , the BASF process results also in partial reduction of NO to NH_2OH . This situation is equal to that for the oxidation of alcohols as discussed in the Chapters 3 to 5 where oxidation of adsorbed layers results in full oxidation to CO_2 and oxidation of dissolved alcohol results also in partial oxidation products. We believe this trend is connected to the adsorbate coverage during reaction; a highly covered surface is unable to break neither C-C bonds in order to form CO_2 nor NO bonds in order to form NH_4^+ .

Our conclusion that high NO coverages are present in the potential region between 0.68 and 0.38 V is in contradiction with electrochemical literature that supports the theory that NO is reduced to NOH_{ads} or HNO_{ads} at these potentials, leading to the formation of N_2O [1-12]. However, our IR data do not prove unambiguously that NO_{ads} is the only adsorbate present on the surface. It is possible that the vibrations of NOH_{ads} or HNO_{ads} are too weak to observe in our experiments.

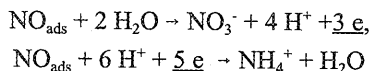
Additional information on the adsorbate composition can be obtained from analysing the $Q_{\text{ox}}/Q_{\text{red}}$ ratios given in Table 2. The quantities Q_{ox} and Q_{red} can be written as:

$$Q_{\text{ox}} = Q_{\text{H}}^0 \theta_{\text{tot}} n_{\text{ox}}$$

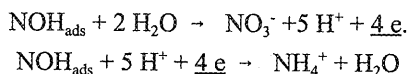
$$Q_{\text{red}} = Q_{\text{H}}^0 \theta_{\text{tot}} n_{\text{red}}$$

with Q_{H}^0 the anodic charge of the hydrogen region, θ_{tot} the total adsorbate coverage and n_{ox} and n_{red} are the average number of electrons involved in the oxidation or reduction of a single adsorbate species, respectively. From these equations it follows that the ratio $Q_{\text{ox}}/Q_{\text{red}}$ is equal

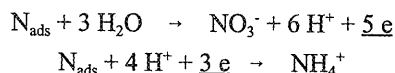
to $n_{\text{ox}}/n_{\text{red}}$. In combination with the rotating ring-disk experiment, our IR experiments have shown that NH_4^+ is the only product in the adsorbate reduction, and NO_3^- is the only product in the oxidation. When NO is the only adsorbate present on the surface, the ratio $Q_{\text{ox}}/Q_{\text{red}}$ is $3/5$, as follows from the corresponding reduction and oxidation reactions of NO:



However, Table 2 clearly shows that significantly higher $Q_{\text{ox}}/Q_{\text{red}}$ ratios are found, indicating that coadsorbates exist with a higher $n_{\text{ox}}/n_{\text{red}}$ ratio. These coadsorbates are apparently reduced and oxidized in the same potential region as adsorbed NO, since no separate peaks were observed with cyclic voltammetry. NOH_{ads} and HNO_{ads} are characterized by an $n_{\text{ox}}/n_{\text{red}}$ ratio of 1, according to the following reduction and oxidation reactions:



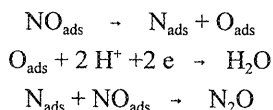
In UHV partial dissociation of adsorbed NO on the Pt(410), Pt(310) and the Pt(100) plane have been observed at room temperature. The presence of Pt(100) sites on our electrode surface has been demonstrated by the characteristic NO vibration and by the peak potentials for NO reduction in the cyclic voltammogram of Figure 1. In addition, the peak potential of 0.24 V for the strongly bonded hydrogen adspecies corresponds with the peak potential for stepped (100) surfaces [31] and therefore supports the view that 100 related sites are present on the electrode surface. On the basis of these facts we feel that the possibility of NO dissociation must be considered, resulting in the formation of adsorbed nitrogen and oxygen atoms. The oxygen atoms can either be reduced to water or reside on the surface, depending on the adsorption conditions. Adsorbed nitrogen atoms are characterized by an $n_{\text{ox}}/n_{\text{red}}$ ratio of $5/3$ as shown in the following equations:



A distinction can be made between N_{ads} or $\text{NOH}_{\text{ads}}/\text{HNO}_{\text{ads}}$ as a coadsorbate of NO by combining the data in Table 2 with the results of FTIRS spectroscopy. The $Q_{\text{ox}}/Q_{\text{red}}$ ratios of 0.9 and 1.06 for low coverages can be interpreted in two ways; (i) an adsorbate layer consisting almost completely of NOH/HNO adspecies which are characterized by $Q_{\text{ox}}/Q_{\text{red}}=1$ or (ii) an adlayer consisting of a mixture of NO_{ads} and N_{ads} giving on average a $Q_{\text{ox}}/Q_{\text{red}}$ value of 1. Our IR measurements have shown that adsorbed NO could even be detected at low

adsorbate coverages, and this strongly suggests that the Q_{ox}/Q_{red} ratios of nearly unity originate from a mixture of adsorbed N and NO. Moreover, the small reduction observed at 0.78 V in the cathodic scan after adsorption at open circuit potential from platinumoxide, supports the idea of NO dissociation into N and O. The possibility of NO dissociation being a cause of the high open circuit potential during adsorption has been mentioned by Langer and Pate [4].

It is remarkable that, of the three basal planes of platinum, only the Pt(100) electrode is active in the formation of N_2O [14] in the liquid phase. Since this is the only plane active in the dissociation of NO at room temperature [18], we conclude that N_2O formation proceeds through NO dissociation according to:



In UHV studies approximately 10 to 20% of the NO adsorbates on (100) sites dissociates at room temperature [18]. The experimentally obtained Q_{ox}/Q_{red} ratio can be used to calculate the fraction of the adsorbate that consists of NO and of N species, using:

$$\begin{aligned} \left(\frac{Q_{ox}}{Q_{red}}\right)_{exp} &= f_{NO} \left(\frac{Q_{ox}}{Q_{red}}\right)_{NO} + f_N \left(\frac{Q_{ox}}{Q_{red}}\right)_N \\ f_{NO} + f_N &= 1 \end{aligned}$$

where f_{NO} and f_N are the fractions of the adsorbate that consists of NO and N species, respectively. It follows from the previously given reduction and oxidation reactions of NO and N that $(Q_{ox}/Q_{red})_{NO} = 3/5$ and $(Q_{ox}/Q_{red})_N = 5/3$. The experiment with the highest adsorbate coverage was characterized by an Q_{ox}/Q_{red} ratio of 0.75. From this experimentally derived ratio it can be calculated, using the equations given above, that 85% of the adsorbate consists of NO_{ads} and 15% consists of N_{ads} . The same value for Q_{ox}/Q_{red} was also found for irreversible adsorbates formed from nitrate on polycrystalline platinum at a similar adsorption potential³². For the experiments with lower coverages the Q_{ox}/Q_{red} ratio of approximately one indicate that the dissociated fraction increases. This means that, for low coverages, a higher dissociated fraction is found than the 10 to 20% reported in the UHV study on Pt(100). This might be due to the presence of sites with higher reactivity towards dissociation than Pt(100), such as stepped surfaces like Pt(310) and (410) [18]. Further, in our case, the adsorbed oxygen atoms formed in the dissociation of NO are immediately reduced to water, enabling higher N_{ads} coverages to be formed.

It is possible to calculate the total adsorbate coverage from the experimental ratio Q_{ox}/Q_{red} ,

independent of the nature of the coadsorbate, N or NOH. The average number of electrons involved in the reduction or oxidation of a single adsorbate species, n_{red} and n_{ox} , can be derived using the experimentally found $Q_{\text{ox}}/Q_{\text{red}}$ ($=n_{\text{ox}}/n_{\text{red}}$) ratio in combination with $n_{\text{ox}} + n_{\text{red}} = 8$. The latter follows from the fact that the oxidation state of the adsorbate lies between -III, the value for NH_4^+ , and +V for NO_3^- . Since in the reduction and oxidation of the adsorbate the only products are NH_4^+ and NO_3^- , respectively it follows automatically that $n_{\text{ox}} + n_{\text{red}} = 8$. Having calculated the n_{red} and n_{ox} values from the experimental $Q_{\text{ox}}/Q_{\text{red}}$ ratio, the total adsorbate coverage θ_{tot} can be calculated using the relation $Q_{\text{red}} = Q_{\text{ox}}^H \theta_{\text{tot}} n_{\text{red}}$. Using this procedure the saturation coverage is found to be 0.41, corresponding with a reduction charge of $398 \mu\text{C}/\text{cm}^2$. This value is somewhat lower than the saturation coverages of 0.46 and 0.51 reported for the Pt(110) and Pt(100) electrodes, respectively [16].

It is remarkable that such a small amount of N_2O is formed in the double-layer region in the cathodic scan after adsorption. This potential-dependent behaviour may be caused by several factors. First, the IR experiments demonstrated a shift of the NO stretch vibration frequency upon changing the electrode potential. This shift, known as the Stark effect, is well known for CO; the shift of the CO stretch vibration to lower wavenumbers upon lowering the potential is explained by extra donation of charge from the $d\pi_{\text{Pt}}$ orbital to the $2\pi^*$ orbital of the CO molecule, resulting in a weakening of the C-O bond [33]. At the same time, the M-C bond is strengthened, as indicated by a shift of the M-C stretch frequency to higher wavenumbers observed with Surface Enhanced Raman Spectroscopy (SERS) [34]. The same potential-dependent metal-adsorbate bonding is at hand for adsorbed NO and the extra charge in the antibonding orbitals might trigger the dissociation of a fraction of the NO molecules. The dissociation may be followed by recombination of an N species with an NO molecule to give N_2O . The corresponding current that was observed can be ascribed to the immediate reduction of the O atom formed in the dissociation. A second factor that may explain the N_2O formation in the cathodic scan after adsorption is the effect of the electrode potential on the bonding strength of both coadsorbed water and sulfate anions. It is known from radiotracer experiments [36] and IR spectroscopy [37] that the coverage of sulfate anions increases at higher electrode potentials. Electrochemical Quartz Crystal Microbalance (EQCM) measurements show that simultaneous adsorption of sulfate anions and water molecules occurs [38,39]. This means that the cathodic scan, recorded in fresh electrolyte after adsorption, is accompanied by a decreased ability for coadsorption of water and sulfate anions with decreasing potential and this may as well be responsible for the dissociation of some NO, leading to N_2O formation.

6.5 Conclusions

Infrared experiments have shown that adsorbed NO is present on the platinum electrode after exposure to NO-containing solutions. Vibrations characteristic of NO adspecies on (100) and (110) sites of platinum were observed. The presence of two separate reduction peaks in the cyclic voltammogram supports this conclusion. Evaluation of the charges involved in both the oxidation and reduction of the adsorbate layer leads to the conclusion that coadsorbates are present in addition to adsorbed NO. On the basis of our measurements, we conclude that the coadsorbates consist of nitrogen adatoms, formed by the dissociation of NO at room temperature. We therefore propose that the electrochemical reduction of NO to N_2O [1-12] proceeds through dissociation of NO, followed by recombination of NO with N. This contrasts with the general view that N_2O formation proceeds through dimerization of adsorbed NOH or HNO species to $H_2N_2O_2$ followed by N_2O formation.

References:

- [1] L.J.J. Janssen, M.M.J. Pieterse and E. Barendrecht, *Electrochim. Acta* 22, 27, 1977.
- [2] N.N. Savodnik, V.A. Shepelin and Ts.I. Zalkind, *Elektrokhimiya* 1, 408, 1971.
- [3] S.H. Langer and K.T. Pate, *Ind. Eng. Chem. Process Des. Dev.* 22, 254, 1983.
- [4] S.H. Langer and K.T. Pate, *Nature* 284, 434, 1980.
- [5] J. A. Colucci, M.J. Foral and S.H. Langer, *Electrochim. Acta* 30, 521, 1985.
- [6] N.N. Savodnik, V.A. Shepelin and Ts.I. Zalkind, *Elektrokhimiya* 1, 564, 1971.
- [7] B.G. Snider and D.C. Johnson, *Anal. Chim. Acta* 105, 9, 1979.
- [8] I. Paseka and J. Voňková, *Electrochim. Acta* 25, 1251, 1980.
- [9] I. Paseka and A. Hodinár, *Electrochim. Acta* 27, 1461, 1982.
- [10] P. Dutta, D. Landolt, *J. Electrochem. Soc.* 119, 1320, 1972.
- [11] R.R. Gadde, PhD Thesis University of Minnesota 1973
- [12] M.J. Foral and S.H. Langer, *Electrochim. Acta* 36, 299, 1991.
- [13] J. Willsau, J. Heitbaum, *J. Electroanal. Chem.* 194, 27, 1985.
- [14] A. Rodes, R. Gómez, J.M. Orts, J.M. Feliu, J.M. Pérez and A. Aldaz, *Langmuir* 11, 3549, 1995.
- [15] R. Gómez, A. Rodes, J.M. Orts, J.M. Feliu and J.M. Pérez, *Surf. Sci.* 342, L1104, 1995.
- [16] A. Rodes, R. Gómez, J.M. Pérez, J.M. Feliu and A. Aldaz, *Electrochim. Acta* 41, 729, 1996.
- [17] I. Villegas, R. Gómez and M.J. Weaver, *J. Phys. Chem.* 99, 14832, 1995.
- [18] S. Sugai, K. Takeuchi, T. Ban, H. Miki, K. Kawasaki and T. Kioka, *Surf. Sci.* 282, 67, 1993.
- [19] Y.O. Park, R.I. Masel and K. Stolt, *Surf. Sci.* 13, 385, 1993.
- [20] S. Sugai, H. Watanabe, H. Miki, T. Kioka and K. Kawasaki, *Vacuum* 41, 105, 1990.
- [21] W. Ranke, *Surf. Sci.* 209, 57, 1989.
- [22] C.M. Comrie, W.H. Weinberg and R.M. Lambert, *Surf. Sci.* 57, 619, 1976.
- [23] R.J. Gorte and J. Gland, *Surf. Sci.* 102, 348, 1981.
- [24] S. Sugai, K. Shimizu, H. Watanabe, H. Miki and K. Kawasaki, *Surf. Sci.* 287/288, 455, 1993.
- [25] H. Miki, T. Nagase, T. Kioka, S. Sugai and K. Kawasaki, *Surf. Sci.* 225, 1, 1990.
- [26] S. Sugai, H. Watanabe, T. Kioka, H. Miki and K. Kawasaki, *Surf. Sci.* 259, 109, 1990.

-
- [27] R.D. Ramsier, Q. Gao, H. Neergaard Waltenburg and J.T. Yates Jr., *J. Chem. Phys.* 100, 6837, 1994.
- [28] K. Nakamoto, *Infrared and Raman Spectra of Inorganic and Coordination Compounds*; John Wiley & Sons: New York, 1986.
- [29] P. Gardner, M. Tushaus, R. Martin and A.M. Bradshaw, *Surf. Sci.* 240, 112, 1990.
- [30] D.S. Corrigan and M.J. Weaver, *J. Electroanal. Chem.* 241, 143, 1988.
- [31] N. Furuya and S. Koide, *Surf. Sci.* 220, 18, 1989.
- [32] T.Ya. Safonova and O.A. Petrii, *Russ. J. Electrochem.* 31, 1373, 1995.
- [33] W.-F. Lin, S.-G. Sun, Z.-Q. Tian and Z.-W. Tian, *Electrochim. Acta* 38, 1107, 1993.
- [34] S. Zou and M.J. Weaver, *J. Phys. Chem.* 100, 4237, 1996.
- [35] D.K. Lambert, *J. Chem. Phys.* 89, 3847, 1988.
- [36] A. Wieckowski, P. Zelenay and K. Varga, *J. Chim. Phys.* 88, 1247, 1991.
- [37] F.C. Nart, T. Iwasita and M. Weber, *Electrochim. Acta* 39, 961, 1994.
- [38] K. Shimazu and H. Kita, *J. Electroanal. Chem.* 341, 361, 1992.
- [39] T. Frelink, W. Visscher and J.A.R. van Veen, submitted for publication

The electrocatalytic reduction of NO_3^- on Pt, Pd and Pt-Pd electrodes activated with Ge

Abstract

The electrocatalytic reduction of nitrate has been investigated on Pt, Pd and Pt-Pd electrodes covered with a submonolayer of germanium. Pt-Pd electrodes were prepared by electroless deposition of submonolayers Pd on Pt by exchange of PdCl_2 for preadsorbed copper. Underpotentially deposited germanium enhances the reduction rate of nitrate strongly. The reduction of nitrite is enhanced to a lesser extent, whereas germanium is inactive for NO and hydroxylamine reduction. Cyclic voltammetry further shows that the well known inhibition of the nitrate reduction at low potentials is absent for germanium modified electrodes. Amperometry shows that the current densities for nitrate reduction at 0.1 V depend strongly on the composition of the electrode surface. The activities increase in the order Pd, Pt and Pt-Pd and all electrodes display a proportional relation between the activity and the germanium coverage. This shows that germanium is involved in the rate determining step, which is the reduction of nitrate to nitrite and its role is to bind the oxygen atom of nitrate. The higher activities for Pt-Pd electrodes can be understood in terms of changes in the electronic structure of the metals as a result of alloying. Selectivity measurements with a rotating ring-disk electrode have shown for all electrodes that the hydroxylamine selectivity increases for increasing germanium coverage. Pd displays higher hydroxylamine selectivities than Pt and Pt-Pd electrodes. No gaseous products were observed for Pt, whereas for Pt-Pd and Pd N_2O selectivities up to 8% were found.

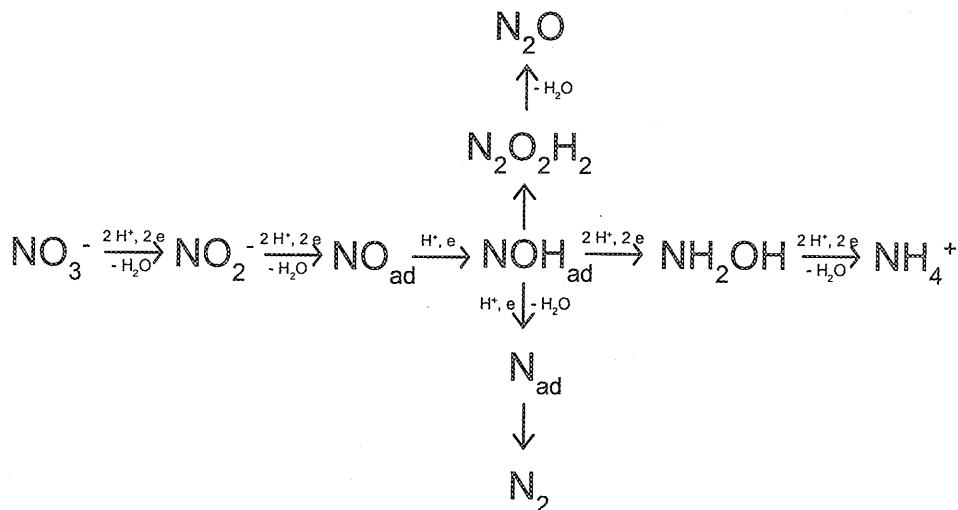
7.1 Introduction

The reduction of nitrate has recently gained renewed attention in view of its relevance to pollution control. Both the catalytic reduction [1-3] with hydrogen and the electrochemical reduction [4] can be applied to the treatment of industrial waste water, whereby nitrate is transformed into harmless nitrogen gas. Moreover, the reduction of nitrate to hydroxylamine is carried out industrially in the formation of caprolactam, the monomer of nylon [5].

The electrochemical reduction of nitrate has been investigated on a large number of metals and the half-wave potential has been established to vary periodically with the atomic number of the cathode material [6]. The same periodic dependence is known for the hydrogen evolution reaction. These data were later reinterpreted and the nitrate reduction activity on transition metals displayed a volcano relationship with the M-H and M-O interaction energies; moderate values of M-H and M-O bond energies result in the optimum activity [7]. A recent study on palladium [8] shows that it is equally active for nitrate reduction as platinum, whereas rhodium has been found to be much more active [8,9].

Several studies have been carried out with platinum, using different concentrations of the conducting electrolyte and nitrate [8,10-20]. For high nitrate concentrations in concentrated sulfuric acid electrolytes, the reduction was reported to be autocatalytic [10-16], based on the observation that the reaction was accelerated by nitrite and slowed down on stirring of the solution [10,11]. Several reaction mechanisms have been proposed to explain the autocatalytic behaviour. (i) A model with two cycles that comprise a reaction between HNO_3 and HNO_2 as the first step to form two NO_2 molecules [10,11,15], that are subsequently reduced to nitrite [6], or react with a single NO molecule via N_2O_3 to HNO_2 [10,11]. The NO molecule necessary in this step is formed by reduction of HNO_2 . (ii) Another model is based on autocatalytic cycles where HNO_3 reacts with HNO_2 to give N_2O_4 , that subsequently reacts with two NO molecules to HNO_2 [17]. (iii) Others proposed reactions between HNO_3 and NO to form NO_2 [14] and between HNO_3 and NH_2OH to form HNO_2 [14].

In contrast with this, no evidence was found for an autocatalytic mechanism in more dilute electrolytes, using moderate nitrate concentrations [8,18-20]. The reduction of nitrate in these media was observed at potentials where platinum is partially covered with hydrogen, both in acid and alkaline solutions. Therefore, it was concluded that adsorbed nitrate ions and adsorbed hydrogen atoms participate in the reduction reaction. Several studies concerning the electrochemical reduction of NO have been carried out and the most frequently proposed mechanism contains NOH_{ads} or NHO_{ads} as the key intermediate, which determines the selectivity by either reduction to NH_2OH and NH_4^+ or by dimerisation to form N_2O [21-28]. Based on the publications in the electrochemical literature on the reduction of nitrate, nitrite and NO in both dilute and concentrated electrolytes the most frequently reported mechanism



Scheme 1: Most frequently reported reaction mechanism in the electrochemical literature

can be drawn up in Scheme 1.

Competitive adsorption of electrolyte anions affects the nitrate reduction rate. A higher activity was found in perchloric acid than in sulfuric acid [20,29]. Both nitrate and nitrite reduction become inhibited at potentials that impose a high hydrogen coverage. This inhibition, which was also found for N₂O reduction [30], is observed in acid and alkaline solutions and originates from the competitive adsorption of hydrogen [8,18-20]. However, others have explained the passivation by breaking of the autocatalytic cycle [14].

No detailed information is available on the product distribution of nitrate reduction on platinum. DEMS measurements in 0.5 M H₂SO₄ on platinum have shown that no N₂ and N₂O are formed, indicating that NH₄⁺ and NH₂OH are the only possible products [31]. A combined rotating ring-disk and mass spectrometry study of the reduction of nitrite in perchloric acid on platinum found selectivities of 60 % for NH₂OH, 21 % for NH₃ and 19 % for N₂O [32]. For NO reduction maximum selectivities for hydroxylamine of 70% [22] and 78% [25] were found in concentrated sulfuric acid electrolyte.

Germanium is known to enhance the rate of the catalytic hydrogenation of nitrate on supported palladium and palladium/platinum catalysts [5]. Hardly any information is available in the electrochemical literature on the effect of submonolayers of germanium on platinum or

palladium electrodes for the electrocatalytic reduction of nitrate [33]. In this chapter we investigate the activating effect of submonolayers germanium on nitrate reduction with platinum, palladium and platinum-palladium surface-alloys. We will demonstrate that there is a strong effect of the electrode composition on the activity and selectivity of the reaction.

7.2 Experimental

Cyclic voltammetry, amperometry and rotating ring-disk electrode (RRDE) measurements were carried out with a Tacussel bipotentiostat and Wenking VSG 72 voltage scan generator, that were connected via an A/D interface to a personal computer. A home-made setup was used for the RRDE measurements. A Hg/Hg₂SO₄ electrode in saturated K₂SO₄ was used as a reference electrode, while all potentials in the text will be referred to the reversible hydrogen electrode (RHE). Platinized platinum electrodes were prepared by electrodeposition from a 0.05 M H₂PtCl₆ + 0.01 M HCl solution on smooth platinum. A deposition current of 10 mA/cm² was used. Platinized platinum was chosen in order to minimize the influence of impurities on the results. Two different methods were used to prepare platinum/palladium electrodes by the electroless deposition of a submonolayer palladium on platinized platinum. In the immersion method the electrode was first reduced in hydrogen saturated ultrapure water for 30 seconds and then transferred to an oxygen free 10⁻² M PdCl₂ solution, where it is left for 30 seconds. Then the electrode was washed with oxygen free ultrapure water and transferred to the electrochemical cell. The second method consists of the electroless exchange of underpotential deposited copper for palladium. The deposition of copper is carried out at 0.4 V in a 5x10⁻⁴ M CuSO₄ solution in 0.5 M H₂SO₄ and the coverage is determined directly from the deposition charge Q according to:

$$\theta_{\text{Cu}} = Q / 2 Q_{\text{H}}^0 \quad (1)$$

where Q_{H}^0 is the charge involved in the oxidation of a monolayer of hydrogen on the platinum substrate. After deposition, the copper solution was replaced by blank electrolyte, while the potential was held at 0.4 V. The electrolyte was then removed from the cell under argon atmosphere and an oxygen free palladium solution was subsequently admitted to the cell at open circuit potential, which rose as a result from 0.4 to 0.85 V. This indicates that copper is fully removed from the surface by exchange with palladium. Palladium electrodes were prepared by electrodeposition of Pd in a 0.05 M PdCl₂ + 0.01 M HCl solution on smooth or platinized platinum. Germanium deposition was carried out by deposition at 0.3 V in a 0.15 mM GeO₂ solution in 0.5 M H₂SO₄. Before each measurement, potential cycling between 0 en

1.5 V was carried out until a stable voltammogram was obtained. The electrode areas were determined from the oxidation charge for hydrogen desorption in a cyclic voltammogram in 0.5 M H₂SO₄. For palladium, the surface area was determined with adsorbed CO, taking a monolayer coverage of 0.65 [34]. All chemicals used were obtained from Merck, p.a. grade. Ultrapure water (18.2 MΩ), obtained with an Elga purifying system, was used for preparation of the 0.5 M H₂SO₄ electrolyte solutions. The selectivity of the reaction was determined with rotating ring disk electrode (RRDE) measurements. DEMS measurements were performed with a Leybold Quadruvac PGA 100 Mass Spectrometer. Details of the experimental setup are given elsewhere [35]. The products were examined for N₂ (m/z = 28) and N₂O (m/z = 44).

7.3 Results

7.3.1 Preparation of Platinum/Palladium electrodes

Platinum-palladium electrodes could easily be prepared with the immersion technique. The deposition of palladium takes place by exchange with adsorbed hydrogen according to:

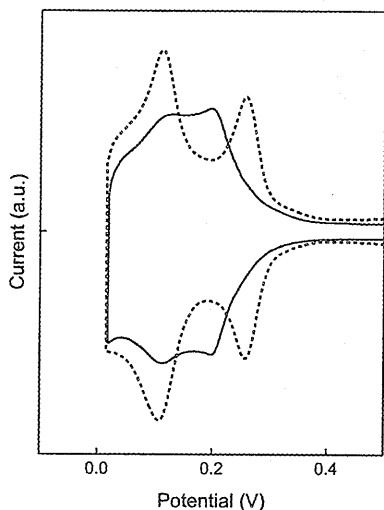
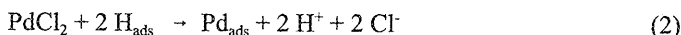


Figure 1a: Cyclic voltammogram after electroless Pd deposition by exchange of PdCl₂ with adsorbed hydrogen. Clean platinum (-----) and after one immersion (—), scan rate 20 mV/s, electrolyte 0.5 M HClO₄.

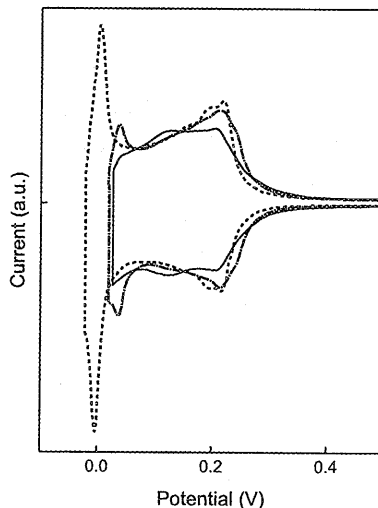
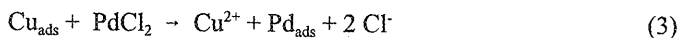


Figure 1b: Same procedure as in Figure 1a. After one (—), two (---) and three (.....) immersions.

It follows from this equation that only half a monolayer can be formed by using the immersion technique. By repeating this sequence, palladium coverages exceeding half a monolayer can be obtained. The cyclic voltammograms recorded after palladium deposition are depicted in Figure 1a and b. After a single immersion the hydrogen peak characteristic for platinum at 0.12 V and 0.27 V have decreased considerably and a new hydrogen peak appears at 0.21 V. It is noteworthy that the total charge involved in the hydrogen region as well as the double layer region has decreased slightly. After a second immersion the new hydrogen peak at 0.21 V increases further. The platinum peaks at 0.12 V decrease further and an additional small peak appears at 0.03 V. Surprisingly, this peak has grown considerably after the third immersion and has shifted to 0 V. After a fourth immersion, not shown here, the peak height is nearly doubled. Repeated immersions result in a further growth of this peak, while the peak at 0.21 V hardly changes. The peak at low potentials is connected to the presence of multilayer palladium and can therefore be assigned to the dissolution of hydrogen in the palladium bulk. The sudden increase of this peak after the third immersion indicates that during the second immersion palladium is predominantly adsorbed on the platinum substrate and only to a small extent on top of first layer palladium. Note that in a single immersion only half a monolayer of palladium can be deposited. The voltammogram for half a monolayer of palladium in Figure 1a is different from both platinum and multilayer palladium and this seems to indicate that palladium is evenly spread on the platinum substrate. However, we cannot exclude the possibility that small islands of palladium atoms are present on the platinum substrate or that part of the adsorbed palladium diffuses into subsurface positions. The platinum substrate used here contains a considerable number of steps and kinks and it is likely that layer growth occurs on these sites. A high density of steps and kinks is expected to favour the spreading of palladium on the platinum substrate. The voltammograms in Figure 1 are stable, indicating that palladium seems to remain on top of the platinum substrate and does not diffuse into the substrate. Only when the oxide region is entered in a cyclic voltammogram the characteristic hydrogen peaks change, due to reconstruction processes that occur during formation and removal of the oxide layer.

A disadvantage of this simple immersion technique is that it is not possible to tune the palladium coverage. Therefore we devised a method to obtain Pd coverages other than 0.5, that consists of the exchange of dissolved palladium with preadsorbed copper atoms according to:



In contrast with palladium, copper can be underpotentially deposited on platinum in submonolayer quantities. Since the exchange between copper and palladium occurs in a one to one ratio, also coverages higher than 0.5 can be obtained. The maximum obtainable copper coverage was 0.75 after deposition at 0.4 V. The PtPd electrodes obtained in this way display

essentially the same voltammetric response as the electrodes obtained through immersion.

7.3.2 Germanium underpotential deposition

Germanium was deposited for several minutes from a 0.15 mM GeO₂ solution in 0.5 M H₂SO₄ keeping the potential at 0.3 V. Since germanium displays under potential deposition at this potential, submonolayers can easily be obtained. After electrolyte exchange, a voltammogram is recorded starting in the negative direction; a characteristic diagram for platinum is shown in Figure 2. Besides the Pt-H peaks and the broad Pt-O oxidation wave, two oxidation waves occur at 0.7 V and 0.45 V, in accordance with literature results for germanium underpotential deposition on polycrystalline platinum [36]. At moderate coverages, the oxidation wave at -0.25 V broadens and starts to overlap slightly with the hydrogen area. If the upper limiting potential is set to -0.15 V, the reduction and oxidation waves at 0.45 V remain unchanged, indicating that adsorbed species are involved. Experiments performed with platinum single crystals [37] have shown that the redox behaviour of germanium on platinum is structure sensitive. On Pt(100) a transition occurs at 0.57 V from Ge to GeO, that resides on the surface. A second wave at 0.77 V is ascribed to the subsequent transition from GeO to GeO₂, which dissolves. In contrast with this, a direct transition from Ge to GeO₂ is reported on Pt(110) and Pt(111) around 0.7 V. On Pt(110) the oxidation broadens considerably at more negative potential for increasing coverages. On the basis of these single crystal studies it can be concluded that the oxidation peak at 0.45 V is connected with the formation of GeO, possibly on Pt(100)-related sites, whereas the second oxidation at 0.7 V is due to formation of GeO₂ from both Ge and GeO. The germanium coverage can be determined by evaluating the total charge involved in both germanium oxidation waves using the equation:

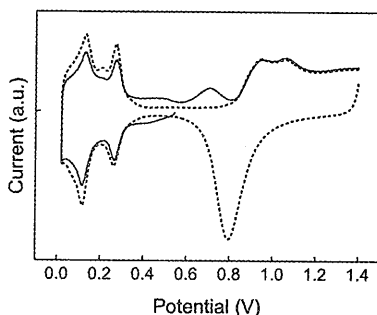


Figure 2: Cyclic voltammogram recorded after germanium deposition on platinized platinum in 0.5 M H₂SO₄ + 0.15 mM GeO₂ at 0.3 V, followed by electrolyte exchange. First (—) and second (---) cycle, scan rate 20 mV/s.

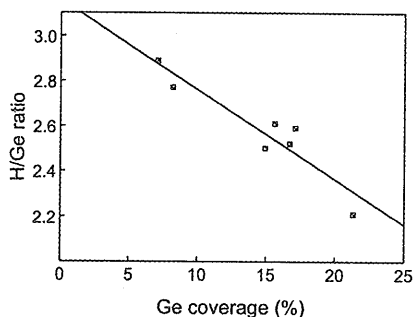


Figure 3: Displacement ratio H/Ge, expressing the number of hydrogen adatoms displaced by a single germanium adatom, as a function of the germanium coverage. The ratio H/Ge is determined from a cyclic voltammogram as shown in Figure 2.

$$\theta_{Ge} = \frac{Q_{ox, Ge}}{(n Q_H^0)} \quad (4)$$

where Q_H^0 is the charge involved in the hydrogen desorption in blank electrolyte. Four electrons are involved in the oxidation of germanium to dissolved germaniumdioxide. A maximum coverage of 0.25 was reported for Pt(100) with every germanium atom blocking four hydrogen atoms, whereas for Pt(110) a maximum coverage of 0.4 was found [37]. We found a maximum coverage of 0.35 on platinized platinum, a value which is intermediate between those for Pt(100) and Pt(110). Figure 2 shows that the coverage of adsorbed hydrogen decreases in the presence of adsorbed germanium, demonstrating that hydrogen does not adsorb on germanium. The ratio $4(Q_H^0 - Q_H)/Q_{Ge}$ represents the number of hydrogen atoms displaced by a single germanium atom and figure 3 shows this displacement ratio as a function of the germanium coverage for platinum. Germanium blocks approximately 3 hydrogen atoms for low coverages, while values around 2.4 are found for high coverage. It was found in a previous report that germanium displaces 2 hydrogen atoms on polycrystalline platinum, irrespective of the coverage [36]. For single crystals it was found that on Pt(100) every germanium blocks 4 hydrogen atoms, while on Pt(110) 2.5 hydrogen atoms are blocked. For low coverages the displacement is intermediate between Pt(100) and (110) and for higher coverages the displacement ratio equals the value for (110). The hydrogen blocking of germanium is different from that of underpotential deposited copper, which displaces a single hydrogen atom per Cu adatom, irrespective of the coverage. This implies that copper adsorbs on the same site as hydrogen does, whereas germanium takes in a different position. On palladium, only a single germanium oxidation wave was observed at 0.7 V, as shown in Figure 4, in agreement with previous results for polycrystalline palladium [38,39]. It is remarkable that the oxidation of germanium is not completed at the beginning of the oxide

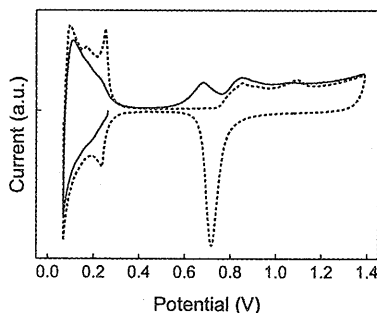


Figure 4: Cyclic voltammogram recorded after germanium deposition on electrodeposited palladium in 0.5 M H_2SO_4 + 0.15 mM GeO_2 at 0.25 V, followed by electrolyte exchange. First (—) and second (----) cycle, scan rate 20 mV/s.

region, but extends throughout the oxide region. Since no single crystal data are available in the literature for palladium we have no explanation for the difference with platinum. The maximum obtainable germanium coverage on palladium was 0.20, which is considerably lower than on platinum, 0.35. Bakos et al. [38] found higher coverages after deposition from germanium solutions exceeding 10 mM GeO₂, whereas we used 0.15 mM GeO₂. However, they found that rapid alloy formation occurs at the deposition potential of 0.15 V. In a future publication higher germanium on palladium will be investigated for the reduction of nitrate [40]. On the platinum electrodes covered with a submonolayer of palladium the germanium oxidation occurred in an intermediate fashion between platinum and palladium. For low coverages two separate peaks were observed at 0.7 V and 0.45 V, whereas at higher coverages these two peaks merge into one broad peak with a small shoulder.

7.3.3 Effect of adsorbed germanium on NO₃⁻, NO₂⁻ and NH₂OH reduction

Figure 5 shows the cyclic voltammograms for both clean and germanium covered platinum in the presence of 0.1 M KNO₃. The dashed curve represents the nitrate reduction on platinum in the absence of germanium, whereas the full line shows the curve for germanium covered platinum. The dotted curve represents a blank cyclic voltammogram recorded in 0.5 M H₂SO₄. The reaction is inhibited in the potential region below 0.05 V, which is ascribed to the blocking of the surface by adsorbed hydrogen [8,18,19]. It is remarkable that there is no

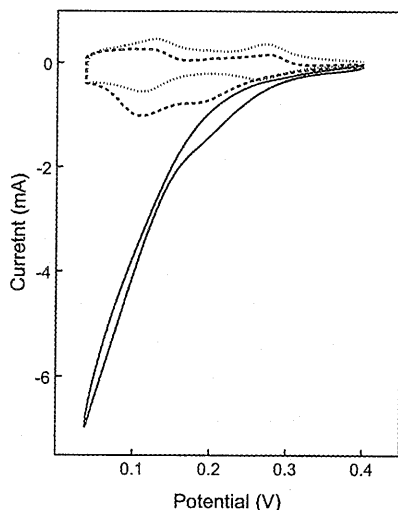


Figure 5: Cyclic voltammogram for clean platinum (----) and platinum covered with a submonolayer of germanium (—) in 0.5 M H₂SO₄ + 0.1 M KNO₃. Scan recorded in 0.5 M H₂SO₄ (.....), scan rate 20 mV/s.

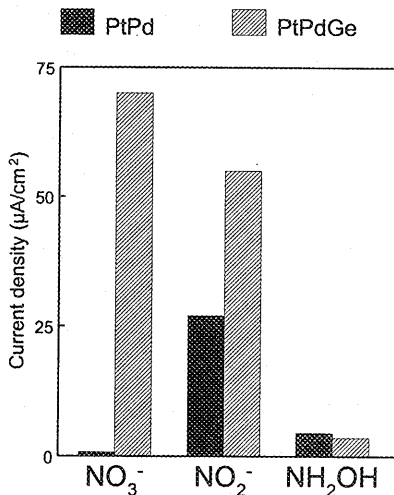


Figure 6: Current density for the reduction of 10 mM NO₃⁻, NO₂⁻ and NH₂OH in 0.5 M H₂SO₄ for a clean Pt-Pd electrode and a Pt-Pd electrode covered with a submonolayer of germanium. Current density measured at a constant potential of 0.1 V after waiting 2 minutes.

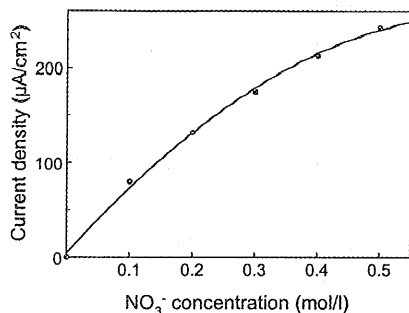


Figure 7a: Current density for Pt-Pd-Ge electrode at 0.1 V, as a function of the NO_3^- concentration in 0.5 M H_2SO_4 electrolyte.

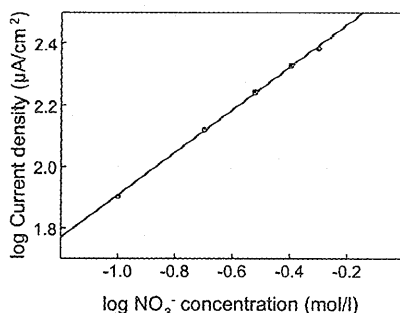


Figure 7b: The logarithm of the current density as a function of the logarithm of the NO_3^- concentration.

inhibition at all in the presence of adsorbed germanium and the current increases continuously with decreasing potential. The effect of adsorbed germanium on the reduction activity is very great, especially at low potentials. Convection of the solution was found to have no effect on the reaction rate, demonstrating that the rate is kinetically limited and not diffusion limited. The same features were observed for the platinum-palladium surface alloy and for pure palladium electrodes. As with platinum, the nitrate reduction is inhibited for low potentials, whereas the inhibition is absent in the presence of adsorbed germanium. A discussion of the quantitative aspects of the effect of germanium on the reaction rate will be given below.

Germanium also accelerates the reduction of nitrite. As reported earlier [8], this reaction is also inhibited at potentials below 0.05 V on platinum. Surprisingly, germanium has absolutely no activating effect on the reduction of hydroxylamine and as a result the inhibition at low potential is maintained. On the contrary, germanium acts as a site blocker, resulting in a decrease in activity. It has been found by others that germanium is also inactive for the reduction of NO [5].

To compare the effect of germanium on the mentioned reduction reactions in a more quantitative way, we performed experiments using 10 mM concentrations of the various compounds with and without germanium present on a platinum-palladium electrode. The steady state reduction activity was measured at 0.1 V after two minutes reaction time and the germanium coverage was 0.04. The results are presented in Figure 6 and the activating effect of germanium for nitrate reduction is clearly shown. The reduction current for NO_2^- on clean platinum is much higher than for nitrate. However, in the presence of germanium, the nitrite reduction current is smaller than for nitrate. It must be considered though that under these conditions the reduction of nitrite is mixed diffusion-kinetically limited, implying that higher rates are possible upon improved mass transport, while the reduction of nitrate and hydroxylamine are kinetically limited. In addition, the rates in Figure 6 are expressed as $\mu\text{A}/\text{cm}^2$, but it should be considered that a decreasing number of electrons is involved in the

order nitrate, nitrite, and hydroxylamine. Thus when the current densities are expressed as turnover frequencies, the rates for nitrate and nitrite would be approximately equal.

The I-E curves obtained for the various electrodes were investigated for Tafel behaviour. A plot of the log(I) vs E was found to be linear only for small current densities in the potential region above 0.2 V. However, for higher current densities, which are observed at potentials below 0.2 V, the curve deviates from the straight line that is expected for ideal behaviour.

The effect of the concentration on the reduction current was also investigated. Figure 7a shows that the steady state reduction current measured at 0.1 V, increases with the nitrate concentration. If log(I) is plotted versus log ($c_{NO_3^-}$), shown in Figure 7b, a straight line is found. From the slope of this line the reaction order is found to be 0.69 for nitrate according to;

$$I \sim (c_{NO_3^-})^{0.69} \quad (5)$$

The same reaction order in nitrate was found for catalytic experiments on carbon supported platinum catalysts in the pH range 5-8, whereas the reaction order in H⁺ was found to be 0.1 [2].

7.3.4 Effect of electrode composition on nitrate reduction rate

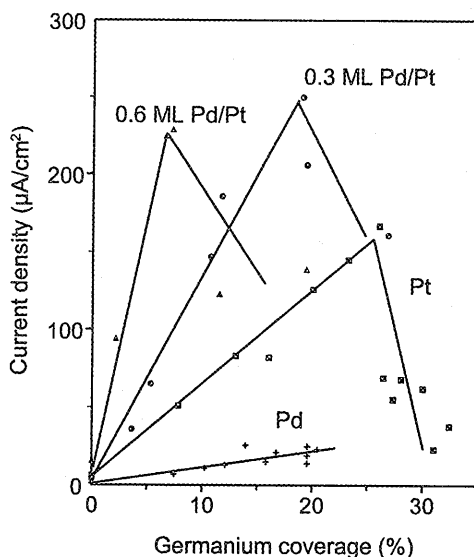


Figure 8: The current density in 0.5 M H₂SO₄ + 0.1 M KNO₃, at 0.1 V, as a function of the germanium coverage for Pd, Pt, and two different Pt-Pd electrodes.

The effect of the electrode material on the nitrate reduction activity is summarized in Figure 8 for Pt, Pd and PtPd as a function of the germanium coverage. Before the activity measurement, germanium was deposited on the surface at 0.3 V, followed by replacement of the germanium solution by a 0.1 M KNO_3 containing electrolyte, while keeping the potential at 0.3 V. The activity was determined at 0.1 V after 2 minutes waiting, to allow the current to reach a semi-steady state. The germanium coverage was determined after the nitrate reduction experiment in an anodic scan after electrolyte exchange. Figure 8 shows that the activity for platinum, expressed in $\mu\text{A}/\text{cm}^2$, is linearly related with the germanium coverage up to $\theta_{\text{Ge}} = 0.25$. For higher germanium coverages the activity drops rapidly to a much lower level. For palladium the rate likewise increased for increasing germanium coverage, however, the current densities observed for palladium are approximately four times lower than for platinum. In a future publication higher germanium coverages on palladium will also be investigated [40]. Surprisingly, the current densities on platinum-palladium electrodes are much higher than on platinum and palladium. The activity is linearly correlated with the germanium coverage in the low coverage region, reaches an optimum and then decreases. In the linear regime, the activity can be expressed as a turnover frequency per germanium adatom when the reduction is assumed to give 100% hydroxylamine with 6 electrons involved. For platinum, a turnover frequency of 0.5 NO_3^- molecules per germanium atoms per second is found, whereas for palladium a value of 0.1 is found. In the presence of submonolayers of palladium, turnover frequencies of 1.0 and 2.5 are found for palladium coverages of 0.3 and 0.6 respectively. However, as shown below the selectivity toward hydroxylamine deviates from 100% and therefore the true turnover frequencies will be somewhat lower.

7.3.5 Selectivity measurements with RRDE and DEMS

Rotating ring-disk (RRDE) experiments were performed to study the effect of the electrode material on the selectivity of the nitrate reduction toward hydroxylamine. From all possible products that are formed in the reduction of nitrate, only nitrite and hydroxylamine are sensitive towards oxidation at the platinum ring electrode, whereas other possible products like NH_4^+ , N_2 and N_2O are not susceptible toward oxidation at the platinum ring electrode. The measurements in Figure 6 have shown that the reduction rate of nitrite is higher than that of nitrate, so that it is unlikely that nitrite will be formed as a product. This opens the way for the direct detection of hydroxylamine by oxidation at the Pt ring electrode. However, a drawback is the non-ideal oxidation behaviour of hydroxylamine. A typical cyclic voltammogram for hydroxylamine is shown in Figure 9. The positive scan does not reach a limiting current, but contains a peak at 1.3 V, that originates from hydroxylamine adsorbates

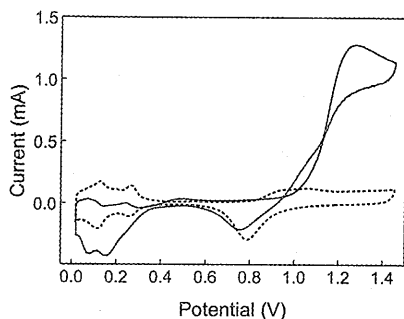


Figure 9: Cyclic voltammogram recorded at a Pt ring electrode. The Pt disk electrode, covered with a submonolayer germanium, was polarized at 0.1 V in 0.5 M H₂SO₄ + 0.1 M KNO₃. Rotation frequency 4 rev./s, scan rate 20 mV/s.

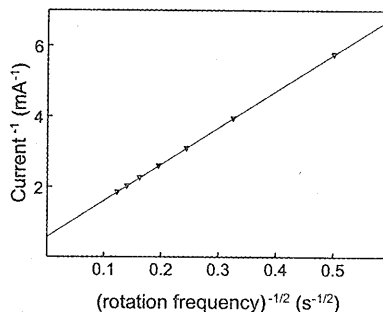


Figure 10: Inverse current density as a function of the inverse square root of the rotation frequency measured at a rotating Pt electrode in 0.5 M H₂SO₄ + 10 mM NH₂OH.

formed in the positive scan between 0.4 and 0.8 V. On the contrary, the negative scan does contain a limiting current, that was used for determination of the hydroxylamine selectivity. It is found that the hydroxylamine oxidation current is not proportional to the square root of the rotation frequency ω , indicating that the reaction rate is not diffusion limited, but that a kinetic limitation is involved. Indeed, a linear curve is found when $1/I$ is plotted versus $1/\sqrt{\omega}$ in Figure 10, as predicted by theory for a reaction rate that is mixed kinetic-diffusion limited. The reciprocal current can be represented by the following equation:

$$\frac{1}{I} = \frac{1}{I_{kin}} + \frac{1}{k\sqrt{\omega}} \quad (6)$$

From the slope of the curve k can be determined, enabling the reconstruction of the $I-\sqrt{\omega}$ plot that would have been obtained in the absence of kinetic hindrance. The deviation between the measured and the corrected curve can be substantial for higher current densities. The corrected value was taken to determine the ratio I_{ring}/I_{disk} of the ring and disk current. The molar selectivity for hydroxylamine can be obtained according to;

$$S_{NH_2OH} = \frac{1}{N} \frac{I_{ring} / n_{ring}}{I_{disk} / n_{disk}} \quad (7)$$

where $N=0.25$ is the collection factor, I_{ring} and I_{disk} the ring and disk current and n_{ring} and n_{disk} the number of electrons involved the reactions at the ring and the disk electrode. Several products can be formed at the disk electrode; N₂, N₂O, NH₂OH and NH₄⁺, each having a different number of electrons involved in the formation out of NO₃⁻. As a result n_{disk} is a weighed average of the values for the various products. However, the selectivities for the various products are not known in advance, and therefore the average value n_{disk} is unknown. An estimated hydroxylamine selectivity can be obtained by assuming that $n_{disk} = n_{ring}$. This

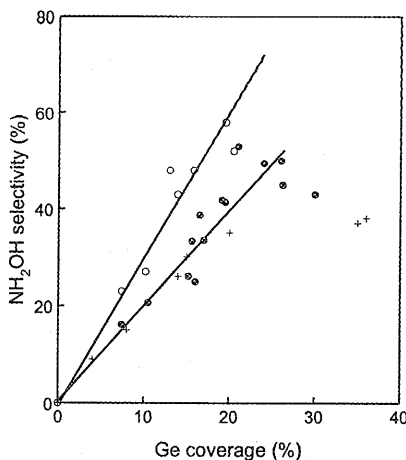


Figure 11: NH_2OH selectivity measured at a constant potential of -0.6 V as a function of the germanium coverage for Pt (\circ), Pd (\bullet) and Pt-Pd (0.5 ML) ($+$) electrodes measured with a rotating ring-disk electrode. Ring material was Pt. Electrolyte $0.5\text{ M H}_2\text{SO}_4 + 0.1\text{ M KNO}_3$.

would hold for the situation that the selectivity for hydroxylamine is 100%. In this case the molar selectivity can be written as:

$$S_{\text{NH}_2\text{OH}} = \frac{1}{N} \frac{I_{\text{ring}}}{I_{\text{disk}}} \quad (8)$$

As our measurements have shown, the major side product is NH_4^+ and therefore the selectivities indicated in Figure 11 are somewhat underestimated. Another difficulty in the measurement of the hydroxylamine selectivity was the fast deactivation of the ring electrode when it was held at a constant potential. This is probably caused by the slow formation of strongly bonded oxides on the platinum ring. To circumvent this problem the disk electrode was held at a constant potential of 0.1 V to reduce nitrate and a potential scan was made on the ring electrode to ensure that the hydroxylamine detection took place on a freshly activated surface.

Figure 11 shows the hydroxylamine selectivities obtained after correction of the measured ring currents as a function of the electrode composition. For all electrodes studied, it is found that the selectivity rises with the germanium coverage up to circa 0.25. For higher coverages, the selectivity remains more or less equal, in spite of a decreasing reduction activity. For platinum the selectivity reaches 50% for $\theta_{\text{Ge}} = 0.25$. In the case of platinum electrodes covered with a submonolayer of palladium approximately equal selectivities are observed. For

palladium the slope is higher, and a maximum selectivity of 60% is reached at $\theta_{\text{Ge}} = 0.20$. These results clearly demonstrate that the germanium coverage is a crucial factor for the selectivity and that palladium has a higher tendency to form hydroxylamine than platinum.

DEMS measurements were performed to establish the N₂ and N₂O selectivity as a function of electrode composition. The mass spectrometer was calibrated by oxidation of a monolayer of adsorbed CO to CO₂. For platinum, no gaseous products were found, indicating that only hydroxylamine and ammonia are formed. In the case of palladium and platinum-palladium electrodes N₂O was formed, whereas no N₂ was observed. A typical measurement for a PtPdGe electrode is shown in Figure 12; the N₂O production increases along with the reduction current. The maximum of the N₂O production is observed in the positive scan, but this originates from a retarded registration of the gaseous products by the mass spectrometer, as its response time is 3 seconds. The simultaneous change in current and N₂O response shows that N₂O is a true product of bulk NO₃⁻ reduction instead of being a product of reduction of an adspecies that is formed at higher potential as observed by Nishimura [32] for NO₃⁻ reduction on platinum. The selectivity for N₂O was determined after keeping the electrode potential at 0.1 V for 2 minutes, allowing the current to reach a semi-steady state. The N₂O selectivity was found to be slightly dependent on the reduction potential: decreasing toward higher potentials and remaining equal for lower potentials. Relatively low selectivities, up to 8%, were found for all electrodes studied. The N₂O selectivity was found to increase with germanium coverage.

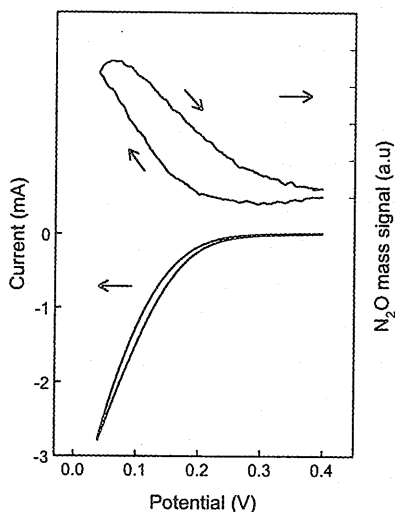


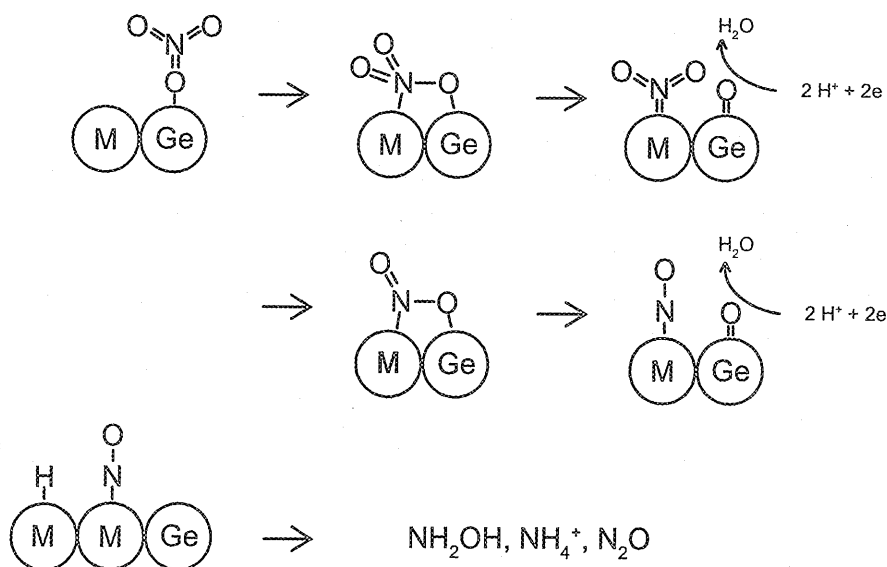
Figure 12: DEMS measurement on a Pt-Pd (0.5 ML) electrode covered with a submonolayer of germanium in 0.5 M H₂SO₄ + 0.1 M KNO₃ ($m/z = 44$ N₂O⁺). Scan rate 20 mV/s.

7.4 Discussion

Our measurements have shown that the activity of the nitrate reduction on non-activated Pt, Pd and PtPd electrodes is very low, as has been found earlier [8,18]. In addition, the reduction is inhibited at potentials that impose a high hydrogen coverage, which implies that the nitrate ion is unable to adsorb on the surface if covered with hydrogen, as was also concluded by Horanyi et al. [18,19]. This inhibition is caused by the low adsorption enthalpy of nitrate on platinum and palladium as compared to hydrogen. The adsorption strength of nitrate is comparable with that of phosphate, sulfate and perchlorate that all display weak reversible adsorption on these metals. A submonolayer germanium on the metal surface has a strong enhancing effect on the activity of the nitrate reduction and it is important to note that the inhibition by hydrogen no longer occurs in the presence of germanium, which does not adsorb hydrogen itself. This shows that germanium is directly involved in the adsorption of the nitrate ion on the catalyst surface. The enhancing effect of germanium is also observed for nitrite although to a lesser extent. The reduction activity on the PtPdGe electrode is lower for nitrate than for nitrite, which indicates that the reduction of nitrate to nitrite is the rate determining step. It is remarkable that germanium is not active for the reduction of NO [5] and NH_2OH and due to this inability of germanium it is possible to obtain high hydroxylamine selectivities upon activating the precious metal electrodes with germanium.

The proportional relation between the activity and the germanium coverage shows that germanium is involved in the rate determining step, which is the reduction of nitrate to nitrite. What might the specific action of the germanium atom be in catalyzing both the reduction of nitrate and nitrite? Our cyclic voltammograms demonstrate that germanium adatoms on platinum and palladium show oxygen uptake at lower potentials than platinum and palladium, which means that the adsorption energy of oxygen on germanium is considerably higher than on platinum and palladium. In analogy with the sulfate, chlorate and phosphate anions bonding of nitrate with the noble metal surface is expected to occur via interaction with an oxygen atom. On the basis of the cyclic voltammetry data, this interaction with oxygen is expected to be higher for germanium adatoms than for platinum and palladium.

The strong interaction between germanium and oxygen is important for the reduction of the nitrate molecule. For the dissociation of an N-O bond in a NO_3^- ion to occur, the bond has to be activated by interaction of both the N and O atom with the catalyst surface. Charge has to be transferred from the metal into an antibonding orbital of the nitrate molecule, enabling dissociation. The role of the electrode potential is to increase the Fermi level such that effective charge donation into these antibonding orbitals can occur. A stronger interaction of the catalyst surface with the oxygen atom of the nitrate molecule will automatically lead to a weakening of the N-O bond in the nitrate molecule and therefore facilitate dissociation. On



Scheme 2: Proposed reaction mechanism for the reduction of nitrate

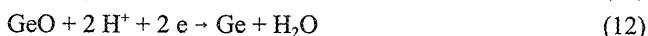
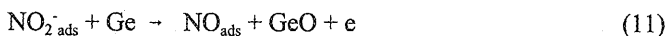
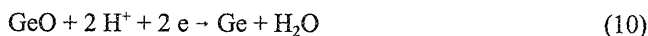
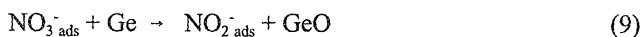
the basis of these arguments we believe that in the transition state of the dissociation reaction, the oxygen atom is bonded to the germanium atom and the nitrogen atom becomes bonded to a platinum or palladium atom as shown in Scheme 2. We must also consider that the nitrate ion contains negative charge on the oxygen atoms and a positive charge on the nitrogen atom, which may also influence the bonding of nitrate to the surface. The GeO species that is formed in the dissociation reaction is not stable at the potential of 0.1 V used in our experiments and will be reduced immediately to water. Because of the low potential, this regeneration reaction is not expected to be rate determining.

A similar effect of germanium has been proposed in the catalytic reduction of crotonaldehyde ($\text{CH}_3\text{-CH=CH-CHO}$) to crotyl alcohol on platinum catalysts with hydrogen as reductor [41]. As a result of its Lewis acidity germanium is proposed to interact with the lone pairs of the oxygen atom of crotonaldehyde, resulting in a weakening of the C=O bond and hence an increasing reactivity toward hydrogenation of this bond.

A second possible reaction mechanism for the nitrate reduction is dissociation of an N-OH bond in HNO_3 to form GeOH and NO_2^- . However, this possibility can be disregarded since we found that the hydrogenation of hydroxylamine to ammonium is not enhanced by germanium. The hydroxyl group of hydroxylamine is apparently not subject to the specific interaction of

the germanium adatom and therefore we expect the same inactivity towards N-OH bond breaking in nitrate.

After the first reduction step to form nitrite, the reaction can proceed in the same way; one of the oxygen atoms of nitrite interacts with the germanium atom, followed by dissociation of the N-O bond to form GeO and subsequently regeneration to Ge as shown in Scheme 2. After this reduction, NO_{ads} resides on the precious metal surface where it is subsequently hydrogenated. The reduction of nitrite to form adsorbed NO has recently been demonstrated with FTIRS to occur at 0.5 V on single crystal electrodes [42]. At this potential, in the double layer region, platinum is uncovered with adsorbed hydrogen, which indicates that this species is not necessary in the reduction of NO_2^- to NO_{ads} . As a consequence this reaction is certainly possible at lower potentials, as used in our reaction. The deoxygenation reactions on the germanium activated catalyst can be summarized as follows:



It seems somewhat surprising that NO dissociation is not enhanced by germanium. Several factors might explain the inactivity of germanium for this reaction. First, the N-O bond energy in NO is higher than in NO_3^- and NO_2^- , discouraging dissociation. Secondly, for dissociation to occur, the oxygen atom of the NO molecule has to interact with germanium, which is energetically unfavourable because of the high M-N-O angle, whereas for nitrate and nitrite this is not so much the case. Possibly germanium only interacts efficiently with negatively charged oxygen atoms as present on nitrate and nitrite. Another possibility is that the residence time of adsorbed NO is very short due to a fast follow-up hydrogenation reaction. The inactivity of germanium for the reduction of NH_2OH might be related to the formation of GeOH in this reaction, as no stable compounds of germanium containing OH groups are reported [43]. If NH_2OH reduction to NH_4^+ would proceed via dehydrogenation to NO, followed by dissociation of NO intermediate, the same inactivity of germanium is expected as for NO reduction itself.

Now we will discuss the effect of electrode composition on the activity pattern. It is remarkable that the highest turn over frequencies per germanium atom are found on platinum-palladium-germanium electrodes, whereas platinum and palladium display much lower TOF's. The question is what the characteristic properties of this alloy are that cause the higher turn over frequencies with respect to Pt and Pd. We should consider electronic effects as a possible cause for the observed activities of the alloy. Recent theoretical work has suggested

that electronic effects are present when mixing platinum and palladium. Density Functional Theory calculations were carried out for a Pt overlayer on Pd and vice versa as well as for a single Pt atom in a Pd matrix, and vice versa [44]. According to these authors, a good measure for the effect of alloying on the reactivity is the shift of the d-band center. For complete Pt and Pd overlayers hardly any electronic effect was found, whereas for the isolated atoms in the substrate matrix, shifts of the d band center of +0.19 and -0.17 eV, respectively, were found. This difference between a full overlayer and an isolated atom placed in a matrix suggests that the electronic effect on a metal as a result of alloying depends on its content in the alloy. A high electronic effect on a metal is expected when its content in the alloy is low and a small electronic effect is expected when its content in the alloy is high.

A shift of the d-band center caused by alloying has a clear effect on the reactivity; an upshift of the d-band center, as expected for Pt in a PtPd alloy, implies a stronger interaction of the metal atom with for instance adsorbed CO, due to an increased interaction between the metal d-band with the $2\pi^*$ orbitals of the CO molecule, that lie above the Fermi level [44,45]. For example, whereas theory found a d-band center shift of -0.47 eV for an overlayer of palladium on Ru [44], experimentally the CO desorption was found to shift 120 K to lower temperature for Pd on Ru(0001), corresponding to a decrease of the CO binding energy of 30 kJ/mol [45]. The calculated electronic effects in the case of Pt/Pd are lower [44], but are nevertheless expected to have a substantial effect on bonding properties.

However, one cannot straightforwardly translate these results to the germanium activated reduction of nitrate to nitrite, which is the rate determining step. The reaction rate of this step is determined by the activation Gibbs energy ΔG_{act} , the energy difference between the ground state and the transition state. The transition state that we have proposed in Scheme 2 is bonded with oxygen to germanium and with nitrogen to a precious metal atom in the surface. As a result the energetics of the reaction can be influenced via both the M-N bond and the Ge-O bond. The M-N interaction can be different for Pt and Pd and can therefore affect the activation energy and thus the reaction rate. In addition, the electronic effects on Pt and Pd due to alloying will also affect the metal-N interaction directly.

The predicted downshift of the d-band center for Pd in a PtPd alloy implies a weaker interaction of the Pd d-band with antibonding orbitals of the nitrate molecule just above the Fermi-level, like the situation for adsorbed CO [44]. This interaction results in a bond between the metal and the nitrogen atom, whereas filling of the antibonding nitrate orbital at the same time weakens the N-O bonds in the nitrate molecule. It is expected that this interaction is dominant in the bonding between the metal and the nitrate ion and more important in enabling breaking of the N-O bond in nitrate. Thus the downshift of the d-band center for Pd upon alloying results in a weaker interaction of Pd with the NO₃⁻ ion and therefore the activation energy for the reaction increases, resulting in a lower rate. In the case of platinum, the opposite holds; the predicted upshift of the d-band center for Pt implies a

stronger interaction between the d-band and the antibonding orbitals of the nitrate molecule. This strengthening of the M-N interaction in the ground state corresponds with a weakening of the N-O bond and therefore the activation energy for the reaction is lowered. As a result we would expect an increased activity of platinum upon alloying with palladium and a decreased activity of palladium upon alloying with platinum. Since both effects counteract, we might expect a zero effect on the reaction rate upon alloying of Pt and Pd. However, this is not necessarily true. We should recall that the reaction occurs on M-Ge pairs on the surface. Our experiments have shown that for increasing Pd coverage the current density per germanium adatom increases. Theory predicts that Pt becomes more active for increasing Pd content, whereas Pd itself recovers toward the value for pure Pd. This suggests that the observed increase of current density upon adding Pd to Pt originates from PtGe ensembles on the surface, since PdGe ensembles in the surface-alloy are expected to be less active than PdGe ensembles on pure Pd electrodes.

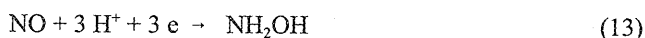
This model can also explain the shift of the observed activity optimum to lower Ge coverage for increasing Pd content. In the case of PtPd the Pt surface concentration decreases for increasing Pd coverage, resulting in a lower density of active sites on the surface. A Pt atom becomes activated in the presence of Ge adatom on a nearby site. With the surface compositions Pd:Pt=30:70 and 60:40 used in this study, a germanium atom that is randomly deposited on the surface will have one or more Pt neighbours that are activated for nitrate reduction as a result. However, since the Pt surface concentration is lower than for pure Pt less Ge will be needed to activate all Pt atoms in the surface and additional Ge deposition can block Pt sites, resulting in a decrease of the activity. This explains the shift of the optimum activity toward lower germanium coverages increasing Pd content in the surface. For a further increase in the palladium coverage than the coverages studied here, we expect a further shift of the optimum to lower germanium coverage.

The optimum that is observed in the activity curve for pure platinum at a germanium coverage of 0.25 has a different cause. The reduction of NO_3^- can be divided in two parts; first the successive deoxygenations of nitrate to nitrite and NO, which require germanium, and secondly the hydrogenation of NO to hydroxylamine that proceeds on the precious metal. In the case of platinum the activity is proportional to the germanium coverage up to $\theta_{\text{Ge}} = 0.25$ and drops for higher coverages. For increasing germanium coverage the amount of available precious metal surface for the reaction decreases. Both the deoxygenation reaction, as shown in Scheme 2, and the hydrogenation requires precious metal sites and one of these two reactions is the rate determining step above $\theta_{\text{Ge}} = 0.25$.

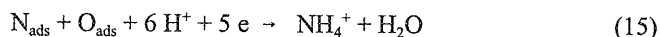
The composition of the precious metal surface can not only influence the M-N interaction but also the Ge-O interaction. Our experiments show that the interaction of germanium with platinum differs from that with palladium as indicated by the presence of an oxidation wave at lower potential in the cyclic voltammogram. The different interaction with germanium is also

expressed by the formation of intermetallic compounds after germanium deposition on palladium [38,39], whereas no alloy formation is known for platinum. As the interaction between Ge and the metal is different, this can also hold for the Ge-O interaction. It could be possible for example that whereas Pt is necessary for a beneficial interaction with the nitrogen atom of nitrate, Pd induces a beneficial interaction between germanium and the oxygen atom of nitrate. This might further enhance the activity of the PtPd alloy with respect to pure Pt and Pd.

The selectivity measurements for hydroxylamine give a different picture than the activity measurements. We found for all electrode compositions that the selectivity for hydroxylamine increases with increasing germanium coverage. The slope of the selectivity plots for low coverages in Figure 11 is about the same for Pt and PtPd and is higher for Pd. We do not have a good explanation why palladium is more selective for hydroxylamine. Apparently palladium is slightly less active in the dissociation of the N-O bond in order to form ammonium. Comparison of the activity plots in Figure 8 with the selectivity plots in Figure 11 shows that the selectivity remains constant for germanium coverage exceeding 0.25 while the activity decreases. There appears to be no clear correlation between the activity of the reaction and the selectivity for hydroxylamine. However, there seems to be a distinct correlation between the germanium coverage and the hydroxylamine selectivity. We can explain this correlation in the following way. The formation of hydroxylamine proceeds by hydrogenation of adsorbed NO intermediates to hydroxylamine according to:



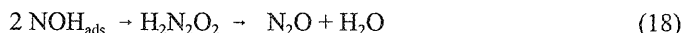
The formation of the other main product ammonia can proceed via different pathways; via dissociation of adsorbed NO or via dissociation of an adsorbed NH_xOH intermediate according to;



It is well known that dissociation of the N-O bond is strongly subject to the ensemble effect, thus requiring large metal ensembles for dissociation, while hydrogenations are not. Thus, with increasing germanium coverage dissociation of the N-O bond will be suppressed, leading to the observed increase in hydroxylamine selectivity. In fact, it is known that the selectivity for the catalytic hydrogenation of NO with hydrogen on precious metals is increased by the presence of carbonmonoxide or sulfur coadsorbates [23].

As to the production of N₂O, our DEMS measurements have shown that some N₂O is found

for palladium containing electrodes, whereas platinum does not display N_2O formation. The gaseous product N_2O can be formed via two possible reaction routes. The most frequently reported mechanism [21-28] consists of a single electron reduction of the NO molecule, followed by dimerization and N_2O formation according to:



Some authors have proposed HNO_{ads} instead of NOH_{ads} as an intermediate in the formation of N_2O [21-23,28]. So far, no direct evidence has been presented for the existence of NOH or HNO as an intermediate in the N_2O formation. However, we concluded in a previous paper [46] that in the potential region between 0.4 and 0.8 V, N_2O is formed via dissociation of NO, followed by recombination of NO with N. This conclusion was supported by the findings from Ultra High Vacuum experiments that NO dissociates at room temperature on Pt(100), Pt(310) and Pt(410) [47-49]. The NO dissociation mechanism is also possible at lower electrode potentials, since we expect that lower potentials further enhance NO dissociation, due to an increased donation of charge in the antibonding $2\pi^*$ orbitals of the NO adspecies.

The formation of N_2O can be influenced by several factors. Both NO_{ads} and N_{ads} have to be present on the surface in each others vicinity. There can be not only a difference in the dissociation ability of the two metals, but also in the rate of hydrogenation of adsorbed NO and N. Recent results which will be published elsewhere which confirm the idea that palladium is less active in the reduction of NO compared to platinum [40]. The low selectivity towards N_2O shows that the rate of hydrogenation is substantially larger than the association rate of N and NO to form N_2O . This might be related with the fact that the reduction of nitrate to nitrite is rate determining, which implies that the coverage of intermediates should be low. A low intermediate coverage suppresses N_2O formation. On the other hand the reduction potential of 0.1 V imposes a high hydrogen coverage, which enhances reduction of the intermediates that are necessary for N_2O formation. Previous work of Hörold et al. [1] on nitrite reduction at pH = 6 has shown that Pd gave a 99.9% selectivity to N_2 , whereas Pt gave approximately 60% N_2 and 40% NH_3 . This finding supports the idea that the rate of hydrogenation is higher for platinum than for palladium. In our situation this results in a lower coverage of NO and N intermediates and thus a lower N_2O selectivity. The increase in N_2O selectivity with increasing germanium coverage on PtPd electrodes is in accordance with this; an increasing germanium coverage results in a higher intermediate coverage due to an increased rate of nitrate reduction. As a result the N_2O selectivity will increase, as has been observed.

7.5 Conclusions

Underpotentially deposited germanium strongly enhances the reduction rate of nitrate on Pt, Pd and Pt electrodes modified with a submonolayer of Pd. The reduction of nitrite is also enhanced, whereas germanium is inactive for NO and hydroxylamine reduction. The inhibition of the reaction at low potentials that is known for Pt and Pd is completely absent for germanium modified electrodes. Germanium is involved in the rate determining step, which is the reduction of nitrate to nitrite and its role is to bind to the oxygen atom of nitrate.

The current densities for nitrate reduction strongly depend on the composition of the electrode surface. The activities increase in the order palladium, platinum and platinum-palladium. In all cases the activity increases with the germanium coverage. The higher activities for Pt-Pd electrodes can be understood in terms of changes in the electronic structure of the metals as a result of alloying. Pt-Ge sites become more active in the presence of palladium whereas Pd-Ge sites become less active in the presence of platinum.

The selectivity toward hydroxylamine increases for increasing germanium coverage. Palladium has a higher tendency to form hydroxylamine than platinum and platinum-palladium electrodes. For increasing germanium coverage the size of the available metal ensembles decreases, which suppresses N-O dissociative reactions that generate N₂O and NH₄⁺. No gaseous products were observed for Pt, whereas for Pt-Pd and Pd N₂O selectivities up to 8% were found.

References:

- [1] S. Hörold, K.-D. Vorlop, T. Tacke and M. Sell, *Catalysis Today* 17, 21, 1993.
- [2] T. Tacke and K.-D. Vorlop, *Chem.-Ing.-Tech.* 65, 1500, 1993.
- [3] T. Tacke, PhD Thesis Braunschweig University of Technology, 1991.
- [4] J.D. Genders, D. Hartsough and D.T. Hobbs, *J. Appl. Electrochem.* 26, 1, 1996.
- [5] C.G.M. van de Moesdijk, in J.R. Kosak (Ed.), *Catalysis of Organic Reactions in Chemical Industries*, Vol. 18, Marcel Dekker, New York, 379, 1984.
- [6] N.E. Khomutov and U.S. Stamkulov, *Sov. Electrochem.* 7, 312, 1971.
- [7] A.K. Vijh, *J. Catal.* 32, 230, 1974.
- [8] O.A. Petri and T.Y. Safonova, *J. Electroanal. Chem.* 331, 879, 1992.
- [9] M. Wasberg and G. Horányi, *Electrochim. Acta* 40, 615, 1995.
- [10] E. Abel and H. Schmid, *Z. Phys. Chem.* 132, 55, 1928.
- [11] E. Abel, H. Schmid, *Z. Phys. Chem.* 134, 279, 1928.
- [12] I.L. Rozenfeld and V.A. Kachanov, *Sov. Electrochem.* 5, 215, 1969.
- [13] G. Facsko and F. Golumbioschi, *Electrochim. Acta* 12, 1495, 1967.
- [14] V.P. Razygraev, M.V. Lebedeva and S.A. Kabakchi, *Dokl. Akad. Nauk USSR* 288, 1428, 1986.
- [15] K. Vetter, *Z. Phys. Chem.* 194, 199, 1950.
- [16] D. Dutta and D. Landolt, *J. Electrochem. Soc.* 119, 1320, 1972.
- [17] G. Schmid, *Ber. Bunsenges. Phys. Chem.* 63, 1183, 1959.

- [18] G. Horányi and E. M. Rizmayer, *J. Electroanal. Chem.* 188, 265, 1985.
- [19] G. Horányi and E. M. Rizmayer, *J. Electroanal. Chem.* 143, 323, 1983.
- [20] G. Horányi and E. M. Rizmayer, *J. Electroanal. Chem.* 140, 347, 1982.
- [21] S.H. Langer and K.T. Pate, *Ind. Eng. Chem. Process Des. Dev.* 22, 254, 1983.
- [22] L.J.J. Janssen, M.M.J. Pieterse and E. Barendrecht, *Electrochim. Acta* 22, 27, 1977.
- [23] S.H. Langer and K.T. Pate, *Nature* 284, 434, 1980.
- [24] J. A. Colucci, M.J. Foral and S.H. Langer, *Electrochim. Acta* 30, 521, 1985.
- [25] N.N. Savodnik, V.A. Shepelin and Ts.I. Zalkind, *Elektrokhimiya* 1, 564, 1971.
- [26] I. Paseka and J. Voňková, *Electrochim. Acta* 25, 1251, 1980.
- [27] I. Paseka and A. Hodinář, *Electrochim. Acta* 27, 1461, 1982.
- [28] P. Dutta, D. Landolt, *J. Electrochem. Soc.* 119, 1320, 1972.
- [29] I. Bakos and G. Horányi, *J. Electroanal. Chem.* 370, 309, 1994.
- [30] H. Ebert, R. Parsons, G. Ritzoulis and T. VanderNoot, *J. Electroanal. Chem.* 264, 181, 1989.
- [31] K. Nishimura, K. Machida and M. Enyo, *Electrochim. Acta* 36, 877, 1991.
- [32] R.R. Gadde and S. Bruckenstein, *J. Electroanal. Chem.* 50, 163, 1974.
- [33] J.F. van der Plas, PhD Thesis Eindhoven University of Technology 1978.
- [34] R. Gómez, A. Rodes, J.M. Pérez, J.M. Feliu, A. Aldaz, *Surf. Sci.* 344, 85, 1995.
- [35] O. Wolter and J. Heitbaum, *Ber. Bunsenges. Phys. Chem.* 88, 2, 1984.
- [36] N. Furuya and S. Motoo, *J. Electroanal. Chem.* 99, 19, 1979.
- [37] R. Gómez, M.J. Llorca, J.M. Feliu, A. Aldaz, *J. Electroanal. Chem.* 340, 349, 1992.
- [38] I. Bakos, S. Szabó and F. Nagy, *J. Electroanal. Chem.* 309, 293, 1991.
- [39] Z. Bodnar, T. Mallat and A. Baiker, *J. Electroanal. Chem.* 358, 327, 1993.
- [40] J.F.E. Gootzen, L. Lefferts J.A.R. van Veen, *in preparation*
- [41] M. Englisch, PhD Thesis University Twente 1996.
- [42] A. Rodes, R. Gómez, J.M. Pérez, J.M. Feliu and A. Aldaz, *Electrochim. Acta* 41, 729, 1996.
- [43] *Encyclopedia of Electrochemistry of the Elements*, vol. 5, ed. A.J. Bard, 1976.
- [44] A. Ruban, B. Hammer, P. Stoltze, H.L. Skriver and J.K. Nørskov, accepted *J. Mol. Catal.*
- [45] J.A. Rodriguez and D.W. Goodman, *Science* 257, 897, 1992.
- [46] J.F.E. Gootzen, R.M. van Hardeveld, W. Visscher, R.A. van Santen and J.A.R. van Veen, *Recl. de Trav. Chim. Pays-Bas* 115, 480, 1996.
- [47] S. Sugai, K. Takeuchi, T. Ban, H. Miki, K. Kawasaki and T. Kioka, *Surf. Sci.* 282, 67, 1993.
- [48] Y.O. Park, R.I. Masel and K. Stolt, *Surf. Sci.* 13, 385, 1993.
- [49] S. Sugai, H. Watanabe, H. Miki, T. Kioka and K. Kawasaki, *Vacuum* 41, 15, 1990.

Chapter 8

A DEMS and cyclic voltammetry study of NH_3 oxidation on platinized platinum

Abstract

The oxidation of ammonia on platinized platinum has been studied with cyclic voltammetry and DEMS. These techniques show the surface to be highly covered with adsorbates during the selective oxidation of ammonia to N_2 at potentials where platinum is free of oxides. These adsorbates are inactive in the formation of N_2 and consist of NH_x , probably N_{ads} , whereas no NO adsorbates are present among these adspecies. These adsorbates remain present on the surface after exchange of the ammonia solution for base electrolyte and in a negatively directed potential scan N_2 and NH_3 are formed. When this potential scan is interrupted by holding the potential at 0.55 V the current reverses from negative to positive, being accompanied by N_2 formation. These data support a mechanism in which NH_x species, proposedly NH_{ads} , are the active intermediates and N_{ads} acts as a poison.

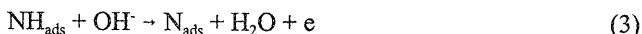
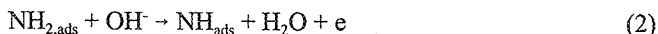
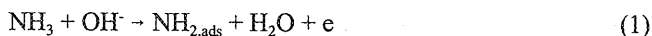
8.1 Introduction

The electrocatalytic oxidation of ammonia in alkaline solutions has received attention in the nineteenthies in the context of possible applications in fuel cells [1-7]. Later on, ammonia oxidation was also studied with a view to developing an electrochemical ammonia sensor [8], and for the treatment of waste water [9]. The latter has become a topic of current interest in industry, and especially catalytic routes using oxygen gas would be attractive to remove ammonia from waste water. Electrochemical studies can be very helpful in obtaining information that is relevant to catalytic ammonia oxidation.

A recent study [10] with Differential Electrochemical Mass Spectrometry (DEMS) has shown that ammonia is selectively oxidized on platinum to N_2 in the potential region where platinum is devoid of adsorbed oxygen, whereas oxygen containing products NO, N_2O , nitrite and nitrate are formed along with N_2 in the potential region where adsorbed oxygen is present. The reaction rate is higher in the potential region where N_2 is formed than in the potential region where platinum is partially covered with oxide.

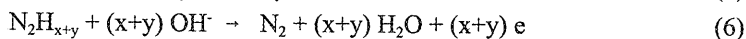
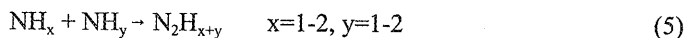
It has been found that the reaction rate in a cyclic voltammogram is much higher than in the potentiostatic mode, even when a very low scan rate of 1 mV/s is used [6], indicating that the reaction deactivates very fast at a constant potential. In addition to this fast deactivation, a slow deactivation was observed and after a few hours the current had decreased to a few percent of the initial current [3,6]. The activity can be restored after setting the potential to its open circuit value for a short time.

Two different mechanisms have been proposed in the literature for the oxidation of ammonia to nitrogen. The most widely accepted mechanism consists of a stepwise dehydrogenation of NH_3 , followed by recombination of adsorbed N_{ads} species, according to [1,3,4,9]:



On the basis of the Langmuir adsorption isotherm, that predicts the experimentally observed Tafel slope of 39 mV, it was concluded by Oswin and Solomon [1] that the oxidation of $NH_{2,ads}$ to NH_{ads} is the rate determining step for low current densities, whereas for high current densities nitrogen recombination was proposed as the rate determining step, since no dependence of the rate on the potential was observed. A second mechanism was proposed by Gerischer and Mauerer [6] in which the first steps are equal to equation 1-3, but now N_{ads} species block the surface and NH_2 and NH are the active intermediates that recombine to give

N_2H_x ($x=2-4$) adspecies, which subsequently dehydrogenate to form N_2 according to:



According to Gerischer and Mauerer the adsorption energy for N_{ads} is too high to enable N_2 formation by recombination of two nitrogen adatoms.

In this chapter we report on the results of a DEMS study of the ammonia oxidation on platinumized platinum. We are especially concerned with the adsorbates that are present on the surface during the reaction and their relation with the reported deactivation phenomena. The information that is obtained on the adsorbate properties will be discussed in view of the two mechanisms given above.

8.2 Experimental

DEMS measurements were performed with a Leybold Quadruvac PGA 100 mass spectrometer. The details of the experimental setup are given in a previous report [11]. The products were examined for nitrogen ($m/z = 28, N_2^+$), nitrous oxide ($m/z = 44, N_2O^+$), ammonia ($m/z = 15, NH^+$). Electrochemical measurements were performed with an Autolab PGSTAT 20 computer controlled potentiostat and a Wenking POS73 potentiostat coupled to an EG&G PARC Universal Programmer, which is connected via an A/D interface to a personal computer. A Hg/HgO electrode was used as a reference-electrode. All potentials will be referred to RHE. All measurements were performed with platinumized platinum, that was obtained by electrodeposition from a 0.05 M H_2PtCl_6 + 0.01 M HCl solution on smooth platinum. A deposition current of 10 mA/cm² was used for the DEMS gauze-electrode. The electrode area of the DEMS electrode was varied between 100 and 300 cm² and the electrode used for cyclic voltammetry was 50 cm², as determined from the hydrogen desorption region in the cyclic voltammogram. Platinumized platinum was chosen in order to minimize the influence of impurities on the adsorption process as well as to increase the mass signals in the DEMS technique. Potential cycling between 0 and 1.5 V was carried out until a stable voltammogram was obtained. Electrolytes were prepared using ultrapure water (18.2 M Ω) obtained with an Elga water purification system. In the DEMS experiments 0.5 M KOH (Merck p.a.) was used and for cyclic voltammetry 0.1 M KOH was used. Oxygen was removed from the electrolyte with Argon 4.6. Ammonia was obtained from Lamers and Pleuger.

8.3 Results

8.3.1 Cyclic Voltammetry

In the first part of this section we will present cyclic voltammetry results on the ammonia oxidation and in particular its deactivation. In the second part we use DEMS in combination with cyclic voltammetry to study in-situ the extent to which the surface is covered with adsorbates during the selective ammonia oxidation and to obtain information on the N_2 selectivity as a function of the potential. In the third part these techniques are also used to study the redox properties and the composition of the irreversible adspecies that are present during selective ammonia oxidation. Finally we will present some results on the properties of irreversible nitrite adsorbates in order to compare them with those for ammonia adsorbates.

A cyclic voltammogram recorded in a 0.1 M NH_3 solution in 0.1 M KOH is shown as the solid line in Figure 1. The dotted line represents a voltammogram recorded in the absence of ammonia in solution. The oxidation of ammonia starts at 0.45 V, reaches a maximum at 0.75 V followed by a decrease to a rather constant current at potentials above 0.95 V. Wasmus et al. [10] have shown with DEMS that the oxidation peak at 0.75 V is connected with the formation of N_2 with 100% selectivity. The oxidation profile for ammonia resembles that of methanol, which also reaches an optimum activity at a potential where formation of platinum oxides starts. In the reverse scan hardly any oxidation of ammonia is observed and no reduction of platinum oxide is visible at the potential where usually reduction of

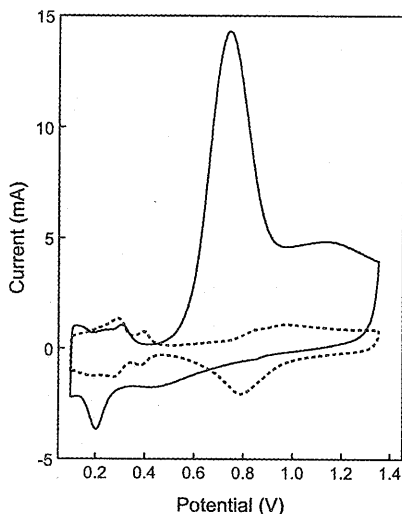


Figure 1: Cyclic voltammogram recorded for platinumized platinum in 0.1 M NH_3 in 0.1 M KOH (—) and in 0.1 M KOH (---). Scan rate 20 mV/s.

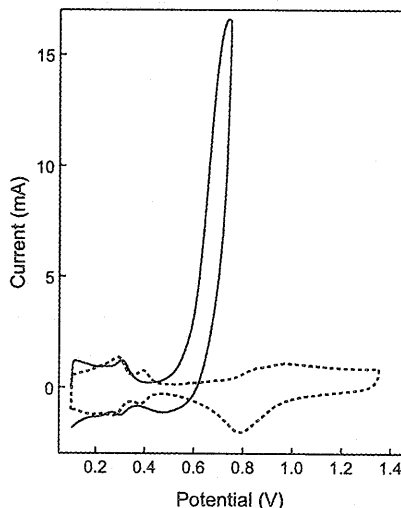


Figure 2: Cyclic voltammogram recorded for platinumized platinum in 0.1 M NH_3 in 0.1 M KOH (—) and in 0.1 M KOH (---). Scan rate 20 mV/s.

platinumoxide occurs. A broad reduction wave, however, is present at 0.45 V, followed by a clear reduction peak at -0.75 V. Figure 2 shows that when the forward scan is reversed at 0.7 V, where oxide formation has not yet occurred, the peak at 0.2 V in the backward scan has disappeared but a clear reduction remains present at 0.5 V, demonstrating that this reaction does not consist of the reduction of platinumoxides. This reduction is not influenced by convection of the solution, which shows that adsorbed species are involved. The disappearance of the reduction peak at 0.2 V indicates that the reaction is associated with a product that is formed in the potential region where platinum is covered with oxide. In previous reports this peak has been assigned to reduction of nitrite formed during oxidation of ammonia in the forward scan [10]. It is also clear from Figure 1 and 2 that the hydrogen adsorption/desorption peaks have changed in the presence of ammonia with respect to the cyclic voltammogram recorded in blank electrolyte.

When the forward potentialscan is stopped at 0.75 V, the oxidation current falls off very rapidly. When a potential step was made from 0.15 to 0.75 V, as shown in Figure 3, the reaction is also found to deactivate very rapidly in the first 20 seconds, followed by a slower deactivation. The current has decreased to 5% of its initial value after 15 minutes. The steady state current can be translated to a turnover frequency using the relation:

$$\text{TOF} = i / (n F A N_{\text{Pt}}) \quad (7)$$

with n the number of electrons involved in the formation of a single N_2 molecule, A the real area of the electrode and N_{Pt} the number of moles Pt per cm^2 ; $2.33 \cdot 10^{-9}$. By using this relation a turnover frequency of 0.011 N_2 molecules per Pt atom per second is found after 15 minutes, indicating that the reaction is very slow. According to Spahrber and Wolf [3], the reaction rate is independent of the ammonia concentration under these conditions.

We found that after holding the potential at 0.75 V for various times in the presence of

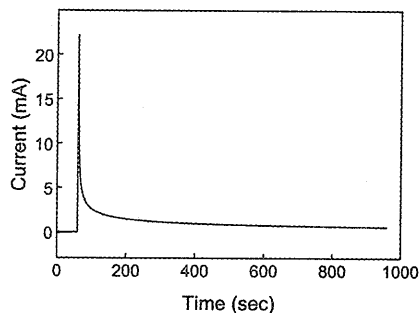


Figure 3: Current-time response obtained after a potential step from -0.85 V to -0.2 V in 0.1 M NH_3 in 0.1 M KOH.

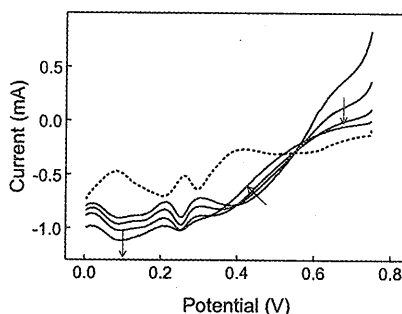


Figure 4: Cyclic voltammograms recorded after 1, 5, 15 and 90 minutes at -0.2 V in 0.1 M NH_3 in 1 M KOH (—). Scan in base electrolyte (---). Scan rate 5 mV/s.

Table 1: Current density for ammonia oxidation in 0.1 M NH₃ in 1 M KOH and Reduction Charge involved in the backward scan in Figure 4.

Reaction Time (min)	Current Density (uA/cm ²)	Reduction Charge (uC/cm ²)
1	31	252
5	14	288
15	5	325
90	1	325

ammonia, the broad reduction wave in the backward scan slowly increased and shifted in the cathodic direction as shown in Figure 4. Table 1 gives the current density for the ammonia oxidation at 0.75 V and the charge involved in the subsequent reduction of the adsorbed species for various reaction times. Table 1 clearly shows that the initial strong decrease of the ammonia oxidation current is accompanied by an increase of the reduction charge. An increase of the reduction charge suggests that either the coverage of adsorbates has increased or that the coverage has remained the same but that the oxidation state of these particular adsorbates has changed. For longer reaction times the decreasing ammonia oxidation current is no longer accompanied by an increasing reduction charge in the backward scan, although Figure 4 indicates that the reduction profile still changes for long reaction times.

8.3.2 Combined DEMS and cyclic voltammetry

Combined DEMS and cyclic voltammetry can be used to determine in-situ the extent to which the surface is covered with adsorbates during the selective oxidation of ammonia to N₂. Figure 5 shows the potential, current and N₂ mass signal versus time for an experiment that was carried out in a solution of 10 mM NH₃ in 0.5 M KOH. A scan was started at 0.1 V with 5 mV/s in the anodic direction, and N₂ formation starts at 0.45 V and increases along with the oxidation current. The potential scan was stopped at 0.65 V after which the current falls off immediately and converges slowly to a constant level. In contrast with this, the N₂ production shows no decline at all, but remains at a constant level. It follows then from Figure 5 that during the potential scan charge is transferred that does not result in the formation of N₂. This charge is used for the oxidation of ammonia to adspecies which remain present on the electrode surface. A quantitative analysis of these data can give information on the coverage of these adsorbates. After some time the current becomes constant and a calibration factor for the mass signal can be calculated according to:

$$K_{N_2} = \frac{i}{i_{mass,N_2}} \quad (8)$$

By using this calibration factor we can transform the measured N₂ evolution profile into a

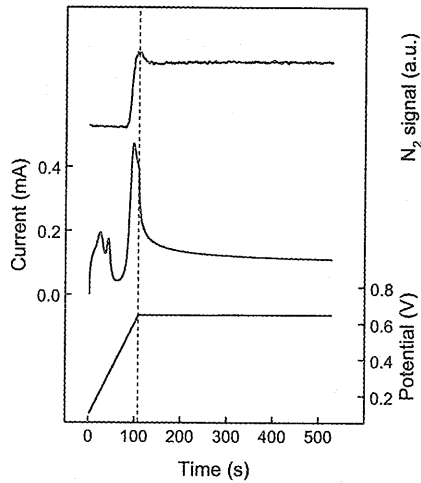


Figure 5: Current and N_2 mass current ($m/z = 28$) as a function of time, corresponding to the potential program indicated in the figure. The DEMS measurement was carried out in 10 mM NH_3 in 0.5 M KOH. Scan rate 5 mV/s.

current profile. By subtracting this calculated current-time curve from the measured current-time curve, ΔQ_{ox} can be determined, which stands for the charge that is transferred during the experiment that has not resulted in the formation of N_2 , but in the formation of adsorbed species. The adsorbate coverage can then be calculated according to:

$$\theta = \Delta Q_{ox} / n Q_H^0 \quad (9)$$

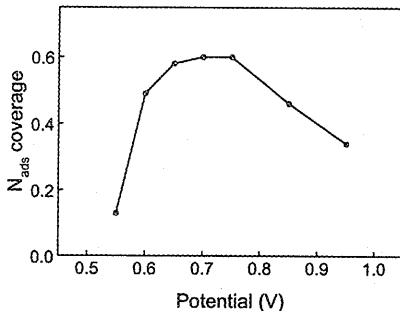


Figure 6: Calculated N_{ads} coverage for various electrodepotentials. The procedure was the same as described in Figure 5.

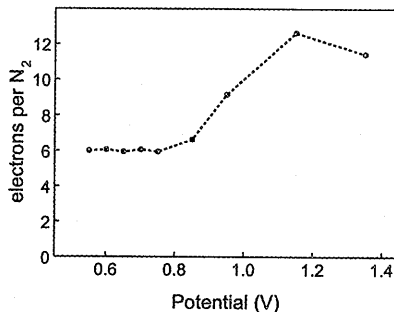
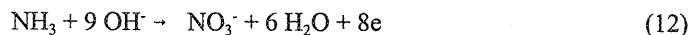
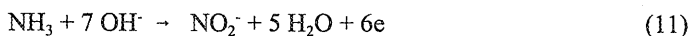


Figure 7: Number of electrons per N_2 molecule, calculated from $i/i_{mass, N_2}$ during oxidation of 0.1 M NH_3 in 1 M KOH for various electrodepotentials.

where n is the number of electrons involved in the oxidation of NH_3 to the corresponding adsorbate and Q_{H}^0 is the charge involved in the desorption of a monolayer of adsorbed hydrogen. If we assume that the adsorbate consists of N_{ads} , then $n=3$, whereas $n=2$ for NH and $n=1$ for NH_2 . This procedure was performed for several potentials and the calculated coverages, assuming that the adsorbate is N_{ads} , are given in Figure 6. It is clear that the coverage increases with increasing potential and reaches a plateau around 0.6 V. For higher potentials a decrease is observed. We should consider though that these results are to a certain extent qualitative. It is very well possible that at low potentials, the adsorbate is dehydrogenated to a lesser extent than at higher potentials, resulting in an underestimation of the coverage, whereas at potentials higher than 0.75 V it is reported in the literature [10] that other products are formed next to N_2 and thus n exceeds 3.

Combined DEMS and cyclic voltammetry can also be used to obtain semi-quantitative information concerning the N_2 selectivity of the reaction as a function of the electrode potential. Therefore, we have measured the $i/i_{\text{mass},N_2}$ values as a function of potential and at potentials below 0.75 V we found the ratio $i/i_{\text{mass},N_2}$ to be constant. According to the DEMS measurements of Wasmus et al. [10] the reaction is 100 % selective to N_2 in this potential region and therefore we normalized the measured $i/i_{\text{mass},N_2}$ to 6 electrons per N_2 , as shown in Figure 7. For potentials above 0.75 V the number of electrons per N_2 increases to approximately 13 electrons per N_2 , which can be explained in the following way. When the N_2 selectivity decreases charge is transferred that is used for the formation of products other than N_2 and as a result the ratio $i/i_{\text{mass},N_2}$ and thus the number of electrons per N_2 increases. A quantitative analysis of the data gives information on the selectivity of the reaction at high potentials. In the formation of N_2 from NH_3 6 electrons are involved per nitrogen molecule, whereas in the formation of NO_2^- or NO_3^- respectively 6 and 8 electrons are involved according to:



The measured value of 13 electrons per N_2 for high potentials can correspond for example with selectivities of 50% for N_2 , 25% NO_2^- and 25% NO_3^- ; then in total 13 electrons are transferred per formed N_2 molecule. No gaseous compounds like NO , N_2O or NO_2 are mentioned here since it was observed by Wasmus et al [10] that these products are formed in very low quantities.

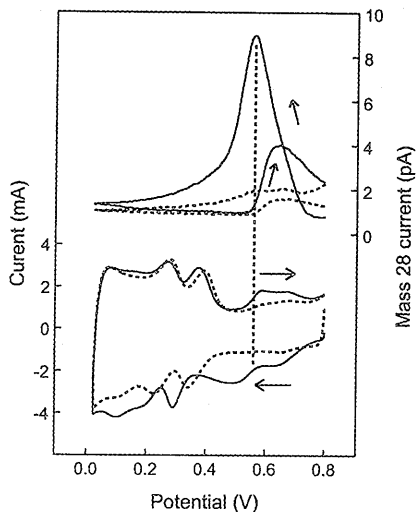


Figure 8: DEMS measurement after ammonia oxidation in 0.1 M NH_3 and 1 M KOH at -0.2 V, followed by electrolyte exchange. First cycle (—) and second cycle (---). Scan rate 5 mV/s, $m/z = 28$ (N_2^+).

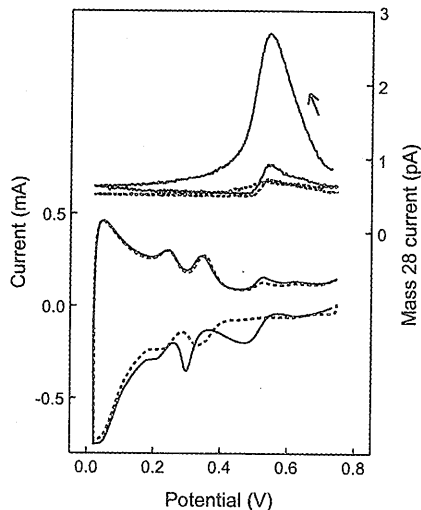


Figure 9: DEMS measurement after ammonia oxidation in 0.1 M NH_3 and 1 M KOH at -0.2 V, followed by electrolyte exchange. First cycle (—) and second cycle (---). Scan rate 1 mV/s, $m/z = 28$ (N_2^+).

8.3.3 Combined DEMS and cyclic voltammetry study of irreversible ammonia adsorbates

Combined DEMS and cyclic voltammetry gives information on the composition and properties of the adsorbates that are present during selective ammonia oxidation. Therefore these adspecies are isolated by exchange of the ammonia containing electrolyte for base electrolyte, after which the redox properties can be studied with cyclic voltammetry and DEMS.

To investigate whether the adsorbates present during reaction are irreversibly adsorbed, the ammonia containing electrolyte was exchanged for fresh KOH electrolyte while keeping the potential at 0.75 V. This potential was chosen since the experiments presented in the previous section indicated that the reaction is 100% selective for N_2 at 0.75 V. After exchange of the electrolyte a scan was started in the cathodic direction, simultaneously recording the mass signal for nitrogen, as shown in Figure 8. A broad reduction wave starts at 0.7 V and extends throughout the double layer region and hydrogen region to 0.02 V. The mass response shows that N_2 formation starts at 0.7 V with a maximum at 0.53 V and falls off rapidly for lower potentials. No N_2O was formed during the cathodic scan. The cell design used in our DEMS experiments causes some tailing of the N_2 peak, so that it is difficult to establish where nitrogen formation stops. The profile of the N_2 mass signal differs from that of the reduction current, which indicates that ammonia is probably formed next to N_2 . We were not able to

observe the formation of NH_3 with the mass spectrometer due to the interference of the various ammonia mass signals with those of water.

The oxidation between 0.4 and 0.75 V in Figure 8, which results in the formation of nitrogen, originates from dissolved ammonia that is formed in the first negative potential scan. This was confirmed by an experiment in which the electrolyte was exchanged for base electrolyte at 0.02 V after the first negative potential scan. In the subsequent anodic scan from 0.02 V to 0.75 V, neither an oxidation current nor N_2 was observed.

Insight in the product selectivity during adsorbate reduction can be obtained by analyzing the intensity of the N_2 mass signal and the reduction charge involved. The amount of nitrogen that is formed can be expressed as the number of monolayers N_2 , using the K_{N_2} calibration constant according to:

$$\theta_{\text{N}_2} = \frac{K_{\text{N}_2} Q_{\text{mass},\text{N}_2}}{n Q_{\text{H}}^0} \quad (13)$$

where $Q_{\text{mass},\text{N}_2} = \int i_{\text{mass},\text{N}_2} dt$, K is the calibration factor, $n=6$ the number of electrons involved in the formation of a single N_2 molecule and Q_{H}^0 is the charge involved in the desorption of a monolayer hydrogen. We found the amount of nitrogen formed in the cathodic scan to vary between 0.01 and 0.02 monolayers, demonstrating that the amount of nitrogen formed is rather low. This amount of N_2 corresponds with the removal of 0.02 to 0.04 monolayers of N containing adspecies, since two adspecies are involved in the formation of a single nitrogen molecule. The total charge involved in the reduction in Figure 8 was $148 \mu\text{C}/\text{cm}^2$, which indicates that the total coverage of adspecies is higher than 0.04 and that the selectivity toward N_2 is low.

The scan rate is found to have an effect on the the reduction profile of the irreversible ammonia adsorbates and the amount of N_2 formed during such a scan. When the cyclic voltammogram was recorded with a scan rate of 1 mV/s instead of 5 mV/s, a different cyclic voltammogram was obtained, as shown in Figure 9. Again an N_2 peak is observed at 0.53 V in the cathodic scan. However, no clear reduction current is visible this time at the initial stage of N_2 formation that could be responsible for its formation, of which the amount is a factor of three higher than at a scan rate of 5 mV/s. We will return to this point in the Discussion section.

The same experiment was repeated, but instead of starting the cyclic voltammogram in the cathodic direction, the scan was started in the anodic direction. The corresponding current and N_2 mass signal are presented in Figure 10, whereas no N_2O was observed. An oxidation reaction is present in the first anodic scan between 0.95 and 1.35 V. The reduction of platinum oxides in the backward scan has diminished with respect to a cyclic voltammogram in blank electrolyte and a reduction occurs between 0.65 and 0.15 V, which is accompanied by formation of N_2 . This reduction is the same reaction that was observed when scanning in the

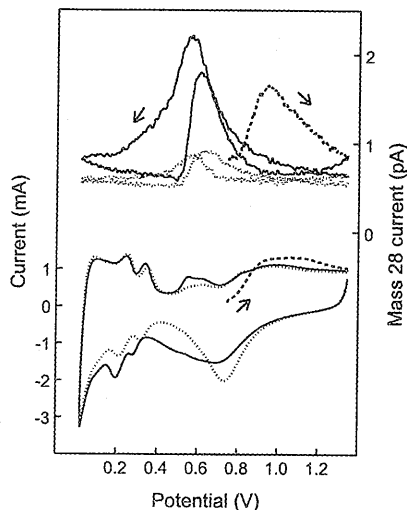


Figure 10: DEMS measurement after ammonia oxidation in 0.1 M NH_3 and 1 M KOH at -0.2 V, followed by electrolyte exchange. First (---), second (—) and third cycle (.....). Scan rate 5 mV/s, $m/z = 28$ (N_2^+).

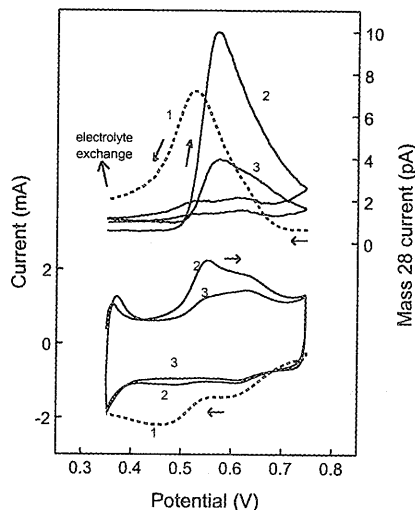


Figure 11: DEMS measurement after ammonia oxidation in 0.1 M NH_3 and 1 M KOH at -0.2 V, followed by electrolyte exchange. Scan rate 5 mV/s, $m/z = 28$ (N_2^+).

negative direction after adsorption and electrolyte exchange and it shows that in the forward scan the adsorbate layer was only partially removed. A small oxidation of ammonia is present in the subsequent anodic scan at 0.6 V, which also generates N_2 .

We also investigated the effect of the adsorption potential on the irreversible adsorbates. We found that the charge involved in the reduction of the adsorbate after adsorption at 0.85 V, $254 \mu\text{C}/\text{cm}^2$, is considerably higher than for adsorption at 0.75 V. The DEMS measurement demonstrates that the N_2 formation profile has slightly changed with respect to adsorption at 0.85 V. A second shoulder is visible 0.45 V, whereas the peak at 0.53 V is not so pronounced. No N_2O could be observed.

We performed some experiments to show that ammonia is not only formed at very low potentials but is also formed in the same potential region as N_2 . Some irreversible adsorbates are present after interrupting the negatively directed potential scan at 0.35 V followed by electrolyte exchange. These adspecies have to consist of NH_2 or NH , since reversibly adsorbed NH_3 is removed during electrolyte exchange. As shown in Figure 11, they can be oxidized in a positive going potential scan between 0.5 and 0.7 V, involving $26 \mu\text{C}/\text{cm}^2$, accompanied by formation of N_2 . The charge involved in the reduction in negatively directed scan; $78 \mu\text{C}/\text{cm}^2$, is much higher than the oxidation charge, demonstrating that a considerable amount of ammonia has already been formed. If the experiment was repeated in the absence of electrolyte exchange, the charges in the negative and positive going scans are approximately

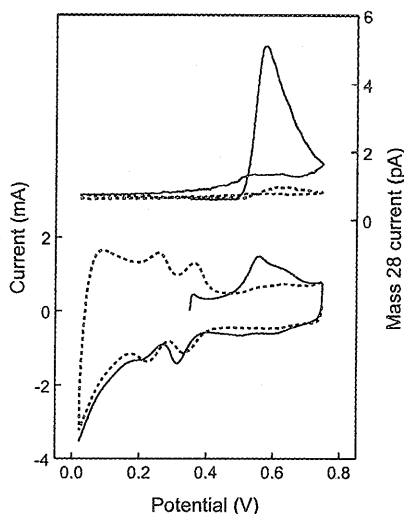


Figure 12: DEMS measurement after ammonia adsorption in 0.1 M NH_3 and 1 M KOH at -0.2 V, followed by electrolyte exchange. First cycle (—) and second cycle (---). Scan rate 5 mV/s, $m/z = 28$ (N_2^+).

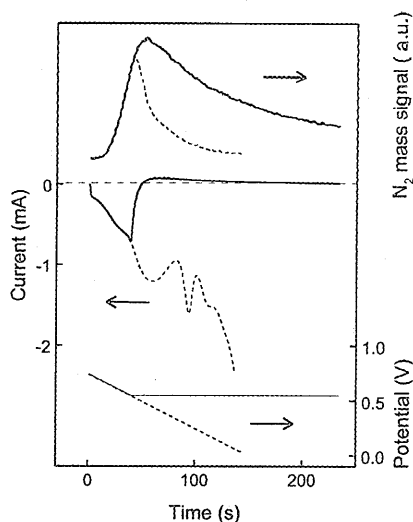


Figure 13: DEMS measurement after ammonia oxidation in 0.1 M NH_3 and 1 M KOH at -0.2 V, followed by electrolyte exchange. Scan interrupted at -0.4 V (—) and normal scan (---). Scan rate 5 mV/s, $m/z = 28$ (N_2^+).

equal, because ammonia formed during reduction remains present near the electrode and can be oxidized to N_2 . It is remarkable that after the initial N_2 formation in the negatively directed scan N_2 is also formed in the positive going scan and even to a higher extent, as can be seen in Figure 11.

To obtain information on the composition of the adspecies that were present on the surface at 0.35 V, we performed an adsorption experiment at this potential in 0.5 M KOH + 0.1 M NH_3 for 10 minutes, followed by electrolyte exchange. The charge transferred during adsorption was $33 \mu\text{C}/\text{cm}^2$. The subsequent oxidation of the adsorbates is shown in Figure 12 and a peak is observed at 0.55 V, involving $38 \mu\text{C}/\text{cm}^2$, which is accompanied by the formation of 0.025 monolayers N_2 . The presence of adsorbate reduction of $43 \mu\text{C}/\text{cm}^2$ in the negatively directed scan demonstrates that a large fraction of the adsorbates remains on the surface after oxidation. These charge data will be further analysed in the Discussion section.

A remarkable observation was made when the negatively directed scan recorded after NH_3 adsorption at 0.75 V and electrolyte exchange, was stopped at 0.55 V. Immediately after holding the potential at 0.55 V the negative reduction current decreased and reversed sign, becoming an oxidation current which slowly converges to zero. The potential, current and N_2 mass signal are plotted versus time in Figure 13. Surprisingly, the nitrogen signal increases for a while after holding the potential at 0.55 V and reaches a maximum after 15 seconds, followed by a slow decrease. So, Figure 10 clearly shows that N_2 formation can be

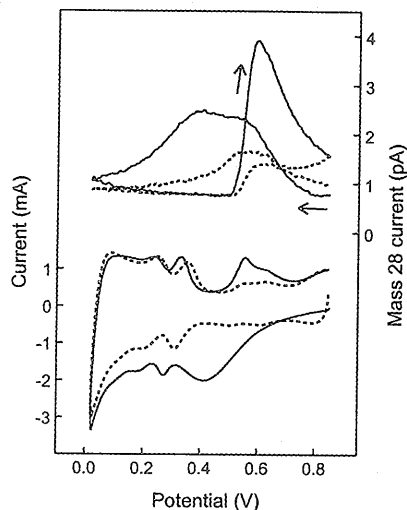


Figure 14: DEMS measurement after ammonia oxidation in 0.1 M NH_3 and 1 M KOH at -0.1 V, followed by electrolyte exchange. First cycle (—) and second cycle (---). Scan rate 5 mV/s, $m/z = 28$ (N_2^+).

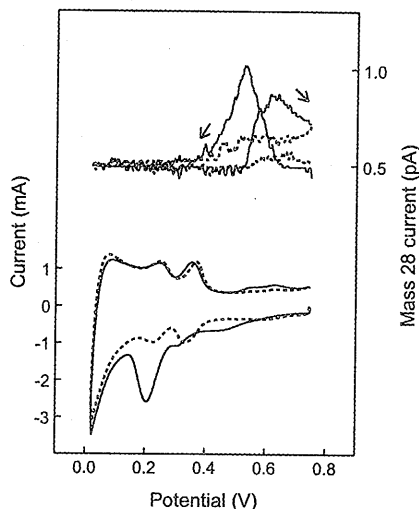


Figure 15: DEMS measurement after nitrite adsorption at -0.2 V in 10 mM NaNO_2 , followed by electrolyte exchange. First cycle (—) and second cycle (---). Scan rate 5 mV/s, $m/z = 28$ (N_2^+).

accompanied by a negative as well as a positive current. The dashed line represents the current and mass signal for a normal cathodic scan from 0.75 to 0.02 V without interruption at 0.55 V. It is clearly shown in Figure 10 that the amount of N_2 formed is considerably higher when the scan is stopped at 0.55 V, with respect to a normal cathodic scan; a factor 4 is found here. The charge involved in the reduction process, $49 \mu\text{C}/\text{cm}^2$, is higher than the charge involved in the oxidation after holding the potential at 0.55 V; $19 \mu\text{C}/\text{cm}^2$.

8.3.4 Combined DEMS and cyclic voltammetry of nitrite adsorbates

To investigate whether NO adsorbates can be present among the ammonia adsorbates, we performed some experiments with nitrite in order to compare the results with those of ammonia. The adsorption was carried out for 10 minutes at 0.75 V and the charge involved in the adsorption was $62 \mu\text{C}/\text{cm}^2$. After adsorption the electrolyte was exchanged for fresh 0.5 M KOH and a scan was started in the cathodic direction, as shown in Figure 12. A small reduction wave is present at 0.45 V, at the same potential where reduction of ammonia adsorbates occurs. This reduction is accompanied by formation of N_2 , although the amount is very low; about 0.002 monolayers N_2 . A clear reduction peak, that was reminiscent for ammonia adsorbates, is present at 0.2 V, that does not result in N_2 formation. The total charge involved in the reduction was $145 \mu\text{C}/\text{cm}^2$, and for the ratio $Q_{\text{ads}}/Q_{\text{red}}$ we find 0.43. The interpretation of this value for $Q_{\text{ads}}/Q_{\text{red}}$ will be discussed in the next section. In the backward

scan an oxidation is present between 0.5 V and 0.7 V that can be ascribed to the oxidation of NH_3 , that was formed during reduction.

8.4 Discussion

Our measurements have shown that the surface is highly covered with adsorbates during the oxidation of ammonia on platinum. The DEMS experiments that were carried out in the presence of ammonia in solution indicated a coverage of 0.6 when assuming the adsorbate to consist of N_{ads} . This value seems somewhat too high as the maximal coverages for NO_{ads} found on Pt(110) and Pt(100) electrodes was 0.46 and 0.51 respectively [12]. If we would assume that the adsorbates in our case consists of NH or NH_2 , then coverages of 0.9 or 1.8 are found, which are much higher than the coverage of 0.5 found in UHV. On the basis of this argument N_{ads} is the most likely adsorbate. The coverage of adspecies that are present during reaction can also be determined from the charge involved in the adsorbate reduction below 0.75 V, as shown in Figure 2, assuming the adsorbate to consist of N_{ads} . The reduction charge of $325 \mu\text{C}/\text{cm}^2$ measured after waiting for 15 minutes at 0.75 V, given in Table 1, implies an N_{ads} coverage of 0.5 using the relation $\theta = Q_{\text{red}}/(3 Q_{\text{H}}^0)$.

A considerable part of the adspecies remains on the surface after exchange of the ammonia containing electrolyte at 0.75 V or 0.85 V for base electrolyte, indicating that these species are irreversibly adsorbed and thus bonded so strongly that they are inactive in N_2 formation. Therefore, they can be regarded as site blockers. If N_{ads} is taken as the adspecies, coverages between 0.20 and 0.25 are found for $E = 0.75 \text{ V}$ and a coverage of 0.4 is found for $E = 0.85 \text{ V}$. These coverages show that a another part of the adsorbates have reacted to nitrogen during electrolyte exchange as compared to the coverage of 0.5 found without electrolyte exchange, indicating that this fraction of the adspecies displays some reactivity towards N_2 formation.

The irreversible adsorbates of nitrite display a different reduction profile in the cyclic voltammogram than the irreversible adsorbates of ammonia and thus the adspecies formed in both cases are different. In the case of nitrite, previous experiments on single crystal electrodes in acid electrolyte have shown that high coverages of adsorbed NO are formed in the potential region where platinum is devoid of both adsorbed oxygen and hydrogen [12]. It is reasonable then to expect that this is also the case in alkaline electrolyte. The different reduction profiles for the ammonia and nitrite adsorbates then show that hardly any NO is formed during ammonia oxidation at 0.75 V, thus implying adsorbed NH_x or N to be predominant. In a previous report we have concluded for NO adsorbate layers on platinized platinum in acid electrolyte that NO dissociation occurs to a certain extent, resulting in the presence of some N_{ads} in addition to NO_{ads} [13]. If the dissociation of NO_{ads} also occurs in

alkaline electrolyte we might expect a reduction in combination with N_2 formation in the cyclic voltammogram at the same potential as for the N-containing adsorbates formed from ammonia. Indeed a small reduction accompanied by nitrogen formation is observed for the nitrite adsorbates around -0.5 V in Figure 14, indicating that some N_{ads} might have been formed as a result of NO dissociation.

An important observation in Figure 8 is that reduction of the adsorbates, which were isolated at 0.75 V by electrolyte exchange, results in the formation of some N_2 next to ammonia. The question is why these adsorbates suddenly become activated to form nitrogen after lowering the electrode potential. We can discuss this observation in the light of the two mechanisms that have been proposed in the literature for the oxidation of ammonia to molecular nitrogen. The most widely accepted mechanism consists of a stepwise dehydrogenation of NH_3 to N_{ads} , followed by recombination of these adatoms to N_2 . In the context of this mechanism we can explain the N_2 formation in Figure 8 only by assuming that lowering the electrode potential results in a lower adsorption energy for N_{ads} , which triggers N_2 formation. Upon lowering the electrode potential the Fermi level of the platinum metal increases which results in the filling of antibonding platinum-nitrogen orbitals.

The opposing mechanism of Gerischer and Mauerer [6] also consists of a stepwise dehydrogenation of NH_3 to N_{ads} , although in this mechanism N_{ads} acts as a site blocker whereas NH and NH_2 adspecies can dimerize to N_2H_x and subsequently dehydrogenate to N_2 . The observation that N_2 is formed from the irreversible ammonia adsorbates after lowering the potential can also be explained by this mechanism. The potential scan in negative direction causes reduction of N_{ads} to NH_{ads} and $NH_{2,ads}$, which can recombine to N_2H_x and dehydrogenate to N_2 . However, the net current for this reaction is zero, whereas clearly a reduction current is present in our cyclic voltammogram. This is easily understood when it is considered that the amount of molecular nitrogen formed is actually low and that the majority of the adspecies is reduced to ammonia. This explains that in the cyclic voltammogram a net reduction current is visible. It is remarkable in this context that a scan with 5 mV/s shows a reduction current at the early stages of the potential scan whereas the scan with 1 mV/s gave a no clear reduction current in this potential region. This observation can also be explained by the mechanism of Gerischer and Mauerer. When scanning very slowly, the reduction rate of N to NH and NH_2 adspecies is equal to the oxidation rate to form N_2 , resulting in a net zero current, whereas for higher scan rates the N_2 formation rate does not keep up with the reduction rate, resulting in a net reduction current. This view is supported by the fact that the amount of N_2 formed in the slow scan is about three times higher.

A crucial observation, which can only be explained with the mechanism of Gerischer and Mauerer, is shown in Figure 10. The reduction current reverses into an oxidation current, when the potential scan was stopped at 0.55 V. It is impossible that the reduction reaction suddenly reverses after stopping the potential scan at 0.55 V, thus being responsible for the

oxidation. Therefore, two different reactions must be involved in the reduction and oxidation. Note that the oxidation current in Figure 10 is accompanied by formation of N_2 , demonstrating that the formation of molecular nitrogen is actually an oxidation reaction. This is perfectly in line with the Gerischer and Mauerer mechanism which states that the actual N_2 formation consist of the oxidation of N_2H_x species, which are formed from recombination of NH_x species. The reduction current in Figure 10 originates from the formation of NH_x out of N_{ads} species.

The original argument of Gerischer and Mauerer for their theory was that adsorbed nitrogen atoms are adsorbed too strongly to be able to recombine to form N_2 . They supported their theory with an experiment in which the adspecies during reaction were isolated and studied in the gas phase by thermal desorption spectrometry. In the temperature range between 400 and 600°C, nitrogen gas was found to desorb whereas no hydrogen gas was detected. Recent experimental [14] and theoretical work [15] has shown that N_{ads} is indeed more strongly bound than NH and NH_2 adspecies with adsorption energies of -116, -71 and -42 kcal/mol [14], respectively. The theoretical study further showed that N_{ads} will bond in a threefold geometry, whereas NH is most likely bonded onefold or twofold and NH_2 favours 2-fold bonding [15]. We should consider that these data hold for relatively low coverages. For increasing coverages the adsorption energy of N , NH and NH_2 is expected to decrease as is generally observed in UHV studies for various adsorbates. A lower adsorption energy will favour the recombination of these adspecies to form N_2 .

The mechanism of Gerischer and Mauerer can explain the deactivation phenomena that are described by us and by others very well. Our experiments have clearly shown that the decrease of the activity for ammonia oxidation is accompanied by an increase of charge involved in the reduction of adspecies as shown in Figure 4. This implies that the coverage with adsorbed inactive nitrogen adatoms slowly increases in time, which further decreases the available area for NH_3 to adsorb and dehydrogenate to the active NH_x intermediate. It has been reported by Spahrber and Wolf [3] and Gerischer and Mauerer [6] that the deactivation can be largely removed by keeping the electrode at open circuit potential for a short time. Our experiments indicated that the inactive nitrogen adatoms are reduced at potentials which are equivalent with the open circuit potential in ammonia solution reported in the literature [3,6]. The disappearance of the inactive nitrogen adatoms nicely explains the reactivation of the electrode surface upon treatment of the electrode at open circuit potential.

In the context of the Gerischer and Mauerer mechanism [6], our adsorption experiments of ammonia at 0.35 V seem to indicate that $NH_{2,ads}$ species are not active in the formation of N_2 , leaving NH as the only active intermediate. The experimentally observed ratio Q_{ads}/Q_{ox} of 0.70 indicates that of the three electrons transferred in the oxidation of NH_3 to N , 1.3 electrons are transferred during the adsorption and 1.7 electrons are transferred during oxidation. This indicates that the adsorbates formed at 0.35 V, consist mainly of NH_2 , though we should

consider that this refers to the average composition. From the total charge involved in the adsorption and oxidation, the coverage of adspecies can be calculated to be 0.12 using the relation $\theta = Q/(n Q_H^0)$, with $n=3$, the number of electrons involved in the oxidation of NH_3 to N. Hardly any N_2 was formed during adsorption, implying that the NH_2 adspecies are not active in the formation of N_2 . However, N_2 formation does occur when the potential is increased and oxidation of the adspecies occurs. After increasing the potential to 0.75 V only a part of the adsorbates has been removed from the surface as N_2 , as indicated by the presence of a reduction in the subsequent cathodic scan to 0.02 V. From the charge involved in the reduction, the coverage at 0.75 V was calculated to be 0.07, which indicates that a NH_x coverage of 0.05 has been removed as N_2 during the first anodic scan. The amount of nitrogen observed with the mass spectrometer was in good agreement with this calculation. As both NH_2 and N adspecies are inactive our results would appear to indicate that NH is an active adspecies in the formation of N_2 . The adsorbate NH has also been proposed to be the active intermediate in nitrogen formation on the basis of a Field Emission Spectroscopy (FEM) study of the $NO + H_2$ reaction on polycrystalline Rh [16].

Electrochemical versus gasphase oxidation of ammonia

In the gasphase ammonia is unreactive in the absence of adsorbed oxygen. Thermal Desorption Spectrometry [17] has shown that a (sub)monolayer ammonia desorbs intact at temperatures below 400 K at Pt (111). Only in the presence of adsorbed oxygen, ammonia is activated to form N_2 and NO [17, 18]. On Pt(111), N_2 is only formed at temperatures above 380 K [17], whereas on Pt(100) N_2 can be formed at temperatures below room temperature [18], demonstrating that Pt(100) is much more reactive than Pt(111). Recent Density Functional calculations are in line with these experimental observations [15], confirming that adsorbed oxygen atoms are necessary to stabilize the hydrogen atom during N-H bond dissociation.

In contrast with gasphase experiments, electrochemical oxidation of ammonia occurs at potentials where adsorbed oxygen is hardly present. An important difference between gasphase and electrochemical ammonia oxidation is that the electrode surface is polarized, containing excess positive charge. Increasing the electrode potential and thus lowering the Fermi level of the metal results in a decrease of the electron density in the ammonia orbitals and as a result the Pt-N bond strengthens the N-H bonds weaken, making them more prone to dissociation. A second important difference between gasphase and electrochemical ammonia oxidation is the presence of the aqueous solvent in the latter. The stabilizing role that is played by adsorbed oxygen in the gasphase ammonia oxidation can be played by H_2O or OH^- during dissociation of the N-H bond in the electrochemical process.

8.5 Conclusions

The present study has shown that the surface is highly covered with adsorbates during the oxidation of ammonia on platinized platinum in the potential region where platinum is devoid of adsorbed oxygen. The ammonia oxidation is selective to N_2 at potentials where adsorbed oxygen is absent whereas other products are formed in addition to N_2 at potentials where adsorbed oxygen is present. A large part of the adsorbates present during selective ammonia oxidation is inactive in the formation of N_2 and these adspecies remain present on the surface after electrolyte exchange. They consist of NH_x , probably N_{ads} whereas no NO adsorbates are present among the adsorbates. During a potential scan in negative direction they react to N_2 and NH_3 . When this scan is interrupted by holding the potential at 0.55 V the current reverses from negative to positive, being accompanied by N_2 formation. These data support the mechanism proposed by Gerischer and Mauerer [6], in which NH_x species are the active intermediates and N_{ads} acts as a poison.

References:

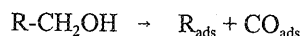
- [1] H.G. Oswin, M. Salomon, *Canad. J. Chem.* 41, 1686, 1963.
- [2] D. Katan, R.J. Galiotto, *J. Electrochem. Soc.* 110, 1022, 1963.
- [3] D. Spahrbier, G. Wolf, *Z. Naturforsch.* 19a, 614, 1964.
- [4] A.R. Despić, D.M. Dražić, P.M. Rakin, *Electrochim. Acta* 11, 997, 1966.
- [5] D.W. McKee, A.J. Scarpellino, Jr., I.F. Danzig, M.S. Pak, *J. Electrochem. Soc.* 116, 562, 1969.
- [6] H. Gerischer, A. Mauerer, *J. Electroanal. Chem.* 25, 421, 1970.
- [7] K. Sasaki, Y. Hisatomi, *J. Electrochem. Soc.* 117, 761, 1970.
- [8] D.-M. Pfenning, J. Deprez, D. Kittelmann, *Ber. Bunsenges. Phys. Chem.* 94, 988, 1990.
- [9] L. Marinčić, F.B. Leitz, *J. Appl. Electrochem.* 8, 333, 1978.
- [10] S. Wasmus, E.J. Vasini, M. Krausa, H.T. Mishima, W. Vielstich, *Electrochim. Acta* 39, 23, 1994.
- [11] O. Wolter, J. Heitbaum, *Ber. Bunsenges. Phys. Chem.* 88, 6, 1984.
- [12] A. Rodes, R. Gómez, J.M. Pérez, J.M. Feliu, A. Aldaz, *Electrochim. Acta* 41, 729, 1996.
- [13] J.F.E. Gootzen, R.M. van Hardeveld, W. Visscher, R.A. van Santen, J.A.R. van Veen, *Recl. Trav. Chim. Pays-Bas* 115, 480, 1996.
- [14] E. Shustorovich, A.T. Bell, *Surf. Sci.* 268, 397, 1992.
- [15] A. Fahmi, R.A. van Santen, *Z. Phys. Chem.* 197, 203, 1996.
- [16] A.R. Cholach, M.F.H. van Tol, B.E. Nieuwenhuys, *Surf. Sci.* 320, 281, 1994.
- [17] W.D. Mieber, W. Ho, *Surf. Sci.* 322, 151, 1995.
- [18] J.M. Bradley, A. Hopkinson, D.A. King, *J. Phys. Chem.* 99, 17032, 1995.
- [19] J.M. Orts, R. Gómez, J.M. Feliu, A. Aldaz, J. Clavilier, *Electrochim. Acta* 39, 1519, 1994.

Summary

Catalysis is highly relevant to chemical industry as the majority of chemical products is nowadays produced with the aid of catalysts. The recent progress in the study of heterogeneous catalysis has relied strongly on spectroscopic techniques that can provide in-situ or ex-situ information of the events that occur on the catalyst surface. A drawback in the research on liquid phase heterogeneous catalysis is that hardly any in-situ spectroscopic techniques are available. Employing an electrochemical approach to liquid phase heterogeneous catalysis offers new possibilities to use in-situ surface spectroscopy. Heterogeneously catalyzed oxidations or hydrogenations in the liquid phase can also be carried out electrochemically by application of a potential difference between the catalyst and the solution in the absence of hydrogen or oxygen. In this way recently developed combined in-situ electrochemical and spectroscopic techniques can help to generate a molecular picture of electrocatalytic and thus catalytic reactions.

This thesis describes the use of two of such techniques which have been developed during the last two decades and that consist of combinations of electrochemical tools and respectively reflection-absorption Fourier Transform IR spectroscopy and mass spectrometry. Pure electrochemical techniques like cyclic voltammetry can also be used to generate useful information. Several electrocatalytic reactions were investigated in this thesis; (i) the electrocatalytic oxidation of alcohols on platinum, (ii) the reduction of nitrate on platinum, palladium and platinum-palladium and related to that the redox behaviour of NO adlayers on platinum and (iii) the oxidation of ammonia.

The first part of this thesis treats the (electro)catalytic oxidation of alcohols on platinum. Chapter 3 and 4 deal with the composition of irreversible adsorbates of small primary and secondary alcohols and polyols in 0.1 M HClO₄. It has been shown with FTIRS en DEMS that both primary alcohols and polyols adsorb C-C(OH) dissociatively and dehydrogenate at 0.4 V, where platinum is free of adsorbed oxygen and hydrogen. It was found that 1,2-ethanediol and 1,2,3-propanetriol dehydrogenate fully to CO. For primary alcohols like ethanol, 1-propanol and 1-butanol the alcohol group dehydrogenates fully to CO and in addition a coadsorbate R is formed;



No further C-C dissociation occurs in R_{ads} species, which are strongly dehydrogenated. In the case of ethanol the C₁ species partially oxidizes to CO. It can be concluded that C-C dissociation only occurs when CO is formed as a result. The hydrocarbon adspecies R can be partly hydrogenated at low potential to gaseous compounds. The non-hydrogenable part has probably

grafitized.

In contrast to the primary alcohols and polyols, 2-propanol and ethene display no C-C dissociation accompanied by CO formation but they do show dehydrogenation.

It was found in Chapter 5 that the C-C(OH) dissociative adsorption also occurs at high pH for ethanol and 1,2-ethanediol. Even for a polyol like methyl- α -D-glucopyranoside CO formation was dominant during adsorption. Moreover, the composition of the catalyst surface was studied during (electro)catalytic alcohol oxidation. It was established that the catalytic alcohol oxidation can be seen as an electrochemical process existing of two independent halfreactions that determine the open circuit potential. This open circuit potential is low in the O₂ diffusion limited regime and high in the kinetic regime. During ethanol and MGP oxidation in the kinetic regime the surface is highly covered with adsorbed oxygen or hydroxyl. However, in the O₂ diffusion limited regime the surface is covered with CO and C species, which have been formed by C-C(OH) dissociative adsorption. The catalyst deactivates during oxidation of MGP in both regimes. Whereas in the diffusion limited regime deactivation is caused by accumulation of carbon residue, in the kinetic regime it is caused by changes in the oxygen adlayer instead of by a plain increase in oxygen coverage.

The second part of this thesis deals with reactions of nitrogen containing species as NO, NO₃⁻ and NH₃. Chapter 6 treats the composition of adlayers on platinum obtained by exposure to NO containing aqueous H₂SO₄ solutions. FTIRS demonstrated the presence of high coverages of NO on (100) and (110) sites of platinum, in accordance with two separate reduction peaks in the cyclic voltammogram. Evaluation of the charges involved in both the oxidation and reduction of the adsorbate layer leads to the conclusion that nitrogen adatoms are present in addition to adsorbed NO. We therefore propose that the electrochemical reduction of NO to N₂O [1-12] proceeds through dissociation of NO, followed by recombination of NO with N. This contrasts with the general view in the electrochemical literature that N₂O formation proceeds through dimerization of adsorbed NOH or HNO species to H₂N₂O₂ followed by N₂O formation.

The reduction rate of nitrate, described in Chapter 7, is strongly enhanced by underpotentially deposited germanium on Pt, Pd and Pt-Pd electrodes. The reduction of nitrite is also enhanced, whereas germanium is inactive for NO and hydroxylamine reduction. The inhibition of the reaction at low potentials that is known for Pt and Pd is completely absent for germanium modified electrodes. Germanium is involved in the rate determining step, which is the reduction of nitrate to nitrite and its role is to bind to the oxygen atom of nitrate.

The current densities for nitrate reduction strongly depend on the composition of the electrode surface. The activities increase in the order palladium, platinum and platinum-palladium. In all cases the activity increases with the germanium coverage. The higher activities for Pt-Pd electrodes can be understood in terms of changes in the electronic structure of the metals as a result of alloying. Pt-Ge sites become more active in the presence of palladium whereas Pd-Ge sites become less active in the presence of platinum.

The selectivity toward hydroxylamine increases for increasing germanium coverage. Palladium has a higher tendency to form hydroxylamine than platinum and platinum-palladium electrodes. For increasing germanium coverage the size of the available metal ensembles decreases, which suppresses N-O dissociative reactions that generate N_2O and NH_4^+ . No gaseous products were observed for Pt, whereas for Pt-Pd and Pd N_2O selectivities up to 8% were found.

In Chapter 8 it is shown that the surface is highly covered with adsorbates during the oxidation of ammonia on platinized platinum in the potential region where platinum is devoid of adsorbed oxygen. The ammonia oxidation is selective to N_2 in this potential region whereas other products are formed in addition to N_2 when adsorbed oxygen is present. These adsorbates are strongly bound and therefore quite inactive in the formation of N_2 . They consist of NH_x , probably N_{ads} whereas no NO adsorbates are present among the adsorbates. During a potential scan in negative direction they react to N_2 and NH_3 . When this scan is stopped at 0.55 V the current reverses from negative to positive, continuously accompanied by N_2 formation. These data support a mechanism as proposed by Gerischer and Mauerer [6], in which NH_x species are the active intermediates and N_{ads} acts as a poison.

Samenvatting

Katalyse is erg belangrijk voor de chemische industrie daar het merendeel van de producten tegenwoordig wordt geproduceerd met behulp van katalysatoren. De recente vooruitgang in de studie van heterogene katalyse steunt op spectroscopische technieken, die in-situ en ex-situ informatie verschaffen aangaande de processen die zich afspelen op het oppervlak van de katalysator. Een beperking in het onderzoek naar heterogene katalyse in de vloeistoffase is het feit dat daarvoor nauwelijks geschikte in-situ technieken voorhanden zijn.

Een electrochemische benadering van vloeistoffase heterogene katalyse biedt nieuwe mogelijkheden om in-situ spectroscopie te gebruiken. Heterogeen gekatalyseerde oxidaties of hydrogenerings-reacties in de vloeistoffase kunnen namelijk ook electrochemisch worden uitgevoerd zonder waterstof of zuurstof door enkel het aanleggen van een electrochemische potentiaal. Recent ontwikkelde gecombineerde electrochemische en spectroscopische technieken kunnen bijdragen aan het verwerven van een moleculair begrip van elektrokatalytische en dus katalytische reacties.

Dit proefschrift beschrijft de toepassing van twee van zulke technieken die de afgelopen twee decennia zijn ontwikkeld en die bestaan uit combinaties van electrochemische en respectievelijk Fourier Transform IR spectroscopie en massaspectrometrie. Daarnaast kunnen ook puur electrochemische technieken zoals cyclische voltammetrie worden toegepast. Verscheidene elektrokatalytische reacties zijn in dit proefschrift bestudeerd; (i) de oxidatie van alcoholen op platina, (ii) de reductie van nitraat op platina, palladium en platina-palladium, waaraan gerelateerd de reductie van geadsorbeerd NO en (iii) de oxidatie van ammonia op platina.

Het eerste deel van het proefschrift behandelt de elektrokatalytische oxidatie van alcoholen op platina. Hoofdstukken 3 en 4 beschrijven de compositie van irreversibele adsorbaten van kleine primaire en secundaire alcoholen en polyolen in 0.1 M HClO₄. Het is aangetoond met FTIRS en DEMS dat zowel primaire alcoholen en polyolen C-C(OH) dissociatief adsorberen en dehydrogeneren bij 0.4 V, een potentiaal waarbij platina vrij is van geadsorbeerd zuurstof en waterstof. Het bleek dat 1,2-ethaandiol en 1,2,3-propaantriol volledig dehydrogeneren naar CO. Tijdens de adsorptie van primaire alcohol zoals ethanol, 1-propanol en 1-butanol dehydrogeneert de alcohol groep volledig naar CO en wordt er een restgroep R gevormd;



Er treedt geen verdere C-C dissociatie op in de R_{ads} species die sterk gedehydrogeneerd zijn. In het geval van ethanol oxideert het C₁ species gedeeltelijk naar CO. C-C dissociatie treedt dus

alleen op indien daarbij CO wordt gevormd. De koolwaterstof adsorbaten R kunnen gedeeltelijk worden gehydrogeneerd bij lage potentiaal tot de overeenkomstige gasvormige componenten. Het niet hydrogeneerbare deel is waarschijnlijk geëgrafitseerd. In tegenstelling tot de primaire alcoholen en de onderzochte polyolen vertonen 2-propanol en etheen geen C-C dissociatie vergezeld van CO vorming maar wel sterke dehydrogenering.

In hoofdstuk 5 werd gevonden dat de C-C(OH) dissociatieve adsorptie eveneens bij hoge pH optreedt voor ethanol en 1,2-ethaandiol. Zelfs voor een polyol zoals methyl- α -D-glucopyranoside was CO vorming dominant tijdens adsorptie. Daarnaast werd de toestand van het katalysatoroppervlak bestudeerd tijdens (electro)katalytische alcohol oxidatie. Er werd gevonden dat de katalytische alcohol oxidatie kan worden beschouwd als een electrochemisch proces dat bestaat uit twee onafhankelijke halfreacties die samen de evenwichtspotentiaal bepalen. De evenwichtspotentiaal is laag in het O₂ diffusiegelimiterde regime en hoog in het kinetische regime. Tijdens oxidatie van ethanol en MGP in het kinetische regime is het oppervlak in hoge mate bedekt met geadsorbeerd zuurstof of hydroxyl. In het O₂ diffusiegelimiterde regime daarentegen is het oppervlak bedekt met CO en C species, die zijn gevormd door C-C(OH) dissociatieve adsorptie. De katalysator deactiveert tijdens oxidatie van MGP zowel in de diffusiegelimiterde als in het kinetische regime. Terwijl de deactivering in het diffusiegelimiterde regime wordt veroorzaakt door accumulatie van koolstofresidu, wordt deze in de kinetische regime niet veroorzaakt door een toename van de zuurstof bedekking maar door veranderingen in de zuurstof adsorbaatlaag.

Het tweede deel van dit proefschrift heeft betrekking op reacties van stikstofhoudende moleculen zoals NO, NO₃⁻ en NH₃. Hoofdstuk 6 behandelt de samenstelling van adsorbaten op platina na blootstelling aan een NO bevattende oplossing van zwavelzuur. FTIRS heeft de aanwezigheid van NO op (100) en (110) sites van platina aangetoond, corresponderend met twee afzonderlijke reducties in het cyclisch voltammogram. Uit de analyse van de ladingen die zijn betrokken bij de oxidatie en de reductie van deze adsorbaten volgt dat N_{ads} aanwezig is naast NO. Op basis hiervan wordt voorgesteld dat de electrochemische reductie van NO naar N₂O verloopt via dissociatie van NO, gevolgd door recombinatie van N met NO. Dit mechanisme is in tegenspraak met het algemeen geaccepteerde beeld in de electrochemische literatuur dat N₂O vorming verloopt via dimerisatie van NOH of NHO species to H₂N₂O₂, gevolgd door N₂O afsplitsing.

De reductiesnelheid van nitraat, beschreven in hoofdstuk 7, wordt sterk versneld door onderpotentiaal afgezet germanium op Pt, Pd en Pt-Pd electrodes. De reductie van nitriet wordt eveneens versneld, terwijl germanium inactief is voor reductie van NO en NH₂OH. De inhibitie van de reactie bij lage potentiaal die bekend is voor platina en palladium is afwezig bij germanium gemodificeerde electrodes. Germanium is betrokken in de snelheidsbepalende stap, de reductie van nitraat naar nitriet, en diens rol is het binden van het zuurstofatoom van nitraat. De stroomdichtheden voor nitraat reductie hangen sterk af van de samenstelling van het electrode-oppervlak. De activiteiten nemen toe in de volgorde Pd, Pt en PtPd. Voor alle

electrodes neemt de activiteit toe met de germanium bedekking. De hogere activiteiten voor PtPd electrodes kunnen worden verklaard in termen van veranderingen in de elektronische structuur van de metaal atomen in de legering. PtGe sites worden actiever in de aanwezigheid van palladium terwijl PdGe sites minder actief worden in aanwezigheid van platina.

De selectiviteit naar hydroxylamine neemt toe voor toenemende germanium bedekking. Palladium is iets selectiever voor hydroxylamine dan platina en platina/palladium electrodes. Voor toenemende germanium bedekking neemt de grootte van de metaalensembles af waardoor N-O dissociatie wordt onderdrukt die leidt tot N_2O en NH_4^+ . Er wordt geen N_2O gevormd op platina terwijl voor PtPd en Pd N_2O selectiviteiten tot 8% zijn gevonden.

In hoofdstuk 8 wordt aangetoond dat het katalysator oppervlak tijdens de oxidatie van ammonia in het potentiaalgebied waarbij geadsorbeerd zuurstof ontbreekt is bedekt met adsorbaten. In dit potentiaalgebied is de reactie selectief naar N_2 terwijl in aanwezigheid van geadsorbeerd zuurstof ook andere zuurstofhoudende producten worden gevormd. Deze adsorbaten zijn sterk gebonden en tamelijk inactief in de N_2 vorming. Ze bestaan uit NH_x , waarschijnlijk N_{ads} terwijl NO afwezig is. Tijdens een potentiaalscan in negatieve richting wordt hieruit N_2 en NH_3 gevormd. Als deze potentiaalscan wordt gestopt bij 0.55 V keert de stroom om van negatief naar positief, continu vergezeld door N_2 productie. Deze waarnemingen ondersteunen een mechanisme zoals voorgesteld door Gerischer en Maurer waarin NH_x een actief intermediair is en N inactief.

List of publications

- Chapter 3 J.F.E. Gootzen, W. Visscher, J.A.R. van Veen, *Langmuir* 12, 5076, 1996.
- Chapter 4 J.F.E. Gootzen, A.H. Wonders, W. Visscher, J.A.R. van Veen, *Langmuir* 13, 1659, 1997.
- Chapter 5 J.F.E. Gootzen, A.H. Wonders, A.P. Cox, W. Visscher, J.A.R. van Veen, to appear in *J. Mol. Catal.*
- Chapter 6 J.F.E. Gootzen, R.M. van Hardeveld, W. Visscher, R.A. van Santen, J.A.R. van Veen, *Recl. Trav. Chim. Pays-Bas* 115, 480, 1996.
- Chapter 7 J.F.E. Gootzen, P.G.J.M. Peeters, J.M.B. Dukers, L. Lefferts, W. Visscher, J.A.R. van Veen, to appear in *J. Electroanal. Chem.*
- Chapter 8 J.F.E. Gootzen, A.H. Wonders, W. Visscher, J.A.R. van Veen, to appear in *Electrochim. Acta.*

J.F.E. Gootzen, L. Lefferts, J.A.R. van Veen, *in preparation*. "The electrocatalytic reduction of NO_3^- on palladium based electrodes activated with germanium"

W. Visscher, J.F.E. Gootzen, A.P. Cox, J.A.R. van Veen, to appear in *Electrochim. Acta*. "Electrochemical Quartz Crystal Microbalance measurements of adsorbed layers on Pt."

Dankwoord

Via deze weg wil ik iedereen bedanken die heeft bijgedragen aan de totstandkoming van dit boekje. In de eerste plaats Rob van Veen en Wil Visscher, die altijd nauw betrokken waren bij het uitstippelen van de te volgen koers, het bediscussiëren van de verkregen resultaten en het nauwgezet corrigeren van alle manuscripten.

In het kader van het STW project waren ook Guy Marin, Ben Kuster en Frank de Bruijn van de vakgroep Chemische Technologie nauw betrokken bij het onderzoek en 'gebruiker' DSM Research heeft in de persoon van Leon Lefferts zowel financieel als wetenschappelijk het nodige bijgedragen.

Daarnaast wil ik Ad Wonders en Anton Cox bedanken voor hun bijdrage. Jullie hebben een groot aantal waardevolle metingen verricht voor dit proefschrift, maar tevens hebben jullie het nodige ondersteunende werk verricht, wat essentieel is om een groep draaiende te houden.

'Mijn' afstudeerders, Patrick Peeters en Pascal Dukers, en research stagiaires Freek Ulkeman en Hans de Rooy hebben grote inspanningen geleverd wat geresulteerd heeft in een groot deel van hoofdstukken 5, 6 en 7.

Mijn kamergenoten Timoer Frelink en Arnoud de Vooy wil ik bedanken voor de hulp op velerlei gebied; Martijn van Hardeveld voor de prettige samenwerking die geleid heeft tot hoofdstuk 6 en alle leden van de vakgroep wil ik bedanken voor de prettige sfeer in de koffiekamer en daaromheen.

Tot slot wil ik Ariadne bedanken voor alle ondersteuning op het mentale vlak.

Curriculum Vitae

Albert Gootzen werd geboren op 16 april 1970 in Maasbracht. Na het behalen van het VWO diploma aan het Bisschoppelijk College te Echt ging hij scheikunde studeren aan de Katholieke Universiteit Nijmegen. Tijdens de hoofdvakstage, uitgevoerd in de vakgroep Anorganische Chemie o.l.v. van prof. J.J. Steggerda en dr. J.G.M. van der Linden, werd de vorming van superclusters uit $\text{Au}_{55}(\text{PPh}_3)_{12}\text{Cl}_6$ onderzocht m.b.v. X-ray diffractie en electrochemische methoden. In een uitgebreide bijvakstage, in de vakgroep Anorganische Chemie en Katalyse aan de TU Eindhoven o.l.v. prof. R.A. van Santen en dr. J.W. Niemantsverdriet, werd de interactie van zuurstof met een zilver éénkristal oppervlak onderzocht m.b.v. oppervlakte-spectroscopie. In mei 1993 trad hij in dienst bij SON/NWO in het kader van een STW-project. Het onderzoek werd verricht in de vakgroep Anorganische Chemie en Katalyse van de TU Eindhoven onder leiding van prof. J.A.R. van Veen en dr. W.H.M. Visscher. De resultaten van dit onderzoek zijn beschreven in dit proefschrift.

Stellingen behorende bij het proefschrift:

**In-situ spectroscopic and electrochemical studies
related to
liquid phase heterogeneous catalysis**

door J.F.E. Gootzen

1. Zowel de katalytische oxidatie van alcoholen met zuurstof als de reductie van nitraat met waterstof in waterig milieu verlopen volgens een electrochemisch mechanisme bestaande uit twee onafhankelijke halfreacties.
Hoofdstukken 5 en 7 van dit proefschrift.
2. Het optreden van zuurstofgas diffusielimitering in platina gekatalyseerde oxidatiereacties in waterig milieu leidt tot elektronen-transport door de koolstofdrager.
Hoofdstuk 5 van dit proefschrift.
3. Het functioneringsgesprek moet vaker gebruikt worden als instrument om het persoonlijk functioneren van de promovendus los van de voortgang van het onderzoek te beoordelen.
4. De C-H vibraties die worden gedetecteerd door Pastor et al. zijn afkomstig van koolwaterstof verontreiniging op de spiegels van de IR-spectrometer.
T. Iwasita, E. Pastor, Electrochim. Acta 39, 531, 1994.
E. Pastor et al., J. Electroanal. Chem. 350, 97, 1993.
5. Het dreigende tekort aan chemici is als het naderen van de regentijd in de Afrikaanse savanne.
6. In de platina gekatalyseerde alcohol oxidatie met zuurstofgas in waterig milieu wordt de reactant zuurstof niet ingebouwd in het uiteindelijk product maar wordt daarentegen omgezet in water.
Hoofdstuk 5 dit proefschrift.

7. De door het international climate conference getrokken conclusie dat de stijging van de gemiddelde temperatuur ontegenzeggelijk kan worden toegeschreven aan het broeikaseffect is helaas voorbarig.
8. De hedendaagse controverse tussen klassieke egyptologen en enkele niet-egyptologen omtrent de oorsprong en het doel van de Egyptische piramides laten zien dat het theorema van de 'scientific revolution' volgens Thomas Kuhn nog steeds opgeld doet.
9. De treffende gelijkenis tussen de adsorptieproducten van stikstofmonoxide, alcoholen en aldehyden op platina in ultrahoogvacuüm enerzijds en in de vloeistoffase anderzijds, toont aan dat ultrahoogvacuüm-literatuur verplichte kost zou moeten zijn voor elektrokatalytici.
Hoofdstukken 3,4 en 6 van dit proefschrift.
10. Het is ontstellend dat electrochemici de meest ingewikkelde reactiemechanismes bedenken voor de reductie van NO naar N₂O (via NOH en H₂N₂O₂ intermediären), terwijl de dissociatie van NO gevolgd door recombinitie van N met NO tot N₂O niet eens wordt overwogen.
N.N. Savodnik et al. Elektrokhimiya 1, 564, 1971.
11. De invloed van theoretische methoden in de elektrokatalyse is nu gering. Deze invloed zal moeten toenemen wil een beter begrip van elektrokatalytische processen worden verkregen.
12. Werkgevers zouden wettelijk verplicht moeten worden om dicht bij de werkplek kinderopvang aan te bieden.
13. Het beschrijven van een elektrokatalytische reactie met de parameter E₀ is betekenisloos daar deze parameter wordt voortgebracht door een theorie die adsorbaat interacties evenals het verbreken en vormen van chemische bindingen niet beschrijft.